

NECROBIOME SUCCESSION IN MUSCLE TISSUE AS A POTENTIAL INDICATOR OF
POSTMORTEM INTERVAL

By

Anna K. Wacker

A THESIS

Submitted to

Northern Michigan University

in partial fulfillment of the requirements

for the degree of

MASTER OF SCIENCE

2021

SIGNATURE APPROVAL FORM

Necrobiome Succession in Muscle Tissue as a Potential Indicator of Postmortem Interval

This thesis by Anna Wacker is recommended for approval by the student's Thesis Committee and Department Head in the Department of Biology and by the Dean of Graduate Education and Research.

Committee Chair:

Date

First Reader:

Date

Second Reader (if required):

Date

Department Head:

Date

Dr. Lisa Schade Eckert
Dean of Graduate Education and Research

Date

ABSTRACT

NECROBIOME SUCCESSION IN MUSCLE TISSUE AS A POTENTIAL INDICATOR OF POSTMORTEM INTERVAL

By

Anna K Wacker

Human decomposition is a complex and variable process influenced by innumerable factors such as the weather, innate microbiome, environmental microbes, and a myriad of other factors. The purpose of this study is to illuminate how the aforementioned factors influence necrobiome succession and how it relates to postmortem interval through the use of buccal swab and muscle tissue sampling from the arm (deltoid) and thigh (vastus lateralis). The use of muscle tissue samples is a novel means to study bacterial succession during human decomposition. Utilization of 16s rRNA sequencing provided information used to assess the overall diversity and variability of the necrobiome community composition over the course of the decomposition process for three donors. Human remains were donated to Forensic Research Outdoor Station (FROST) through the Northern Michigan University Body Donation Program. Analysis of the results using next generation metagenomic sequencing successfully showed patterns relating to time, temperature, accumulated degree-days, bacterial markers for sample site location, bacterial markers for donor identification, and as a whole, potential indications of postmortem interval.

I would like to dedicate this document to the donors' friends and family. Your loved ones believed in this study and thus gave me the confidence and inspiration to do so as well.

ACKNOWLEDGEMENTS

I am having a very difficult time putting into words how grateful I am to each and every person who has helped me throughout this process. I never expected nor strived to get a masters degree after completing my bachelors degree. Dr. Sharp, working in your lab via the McNair program inspired me to continue working in the research field and pursue a masters degree- an experience I cherish and has taught me so much. Dr. Harris, working with you and Rachel Smith at FROST is what ultimately inspired this research project and I am forever grateful for the opportunity you have given me. Thank you to the NMU PRIME grant, which funded this project. A massive thank you to Joe Receveur for all of your work with sequencing, data interpretation, and answering all of the mundane questions I posed. Without you, this thesis would not have even been possible. All of the undergraduates who have helped on this project, Molly Cormier, Bailey Gomes, and Lauren Blosser, it was wonderful working with you in the lab and out at the FROST site. You made the days enjoyable and filled them with smiles. To my fellow graduate students, Rachael Nelson and Alex Markle, sharing the office with you both was the absolute best. You kept me sane and have made a friend for life. To my two best friends, Nikki Ziegler and Bailey Barthel, I could not have survived any of this without you two. You made me laugh, you listened to my frustrations, and you were always there for me. Finally, I would love to thank my mom, dad, stepdad, and brother. The support you all have given me throughout my life makes everything I do possible no matter the undertaking.

Without all of you, this project would not have been possible and I wholeheartedly thank each and every one of you for the contribution, support, and time you have contributed.

Table of Contents:

[LIST OF TABLES](#)

[LIST OF FIGURES](#)

[LIST OF ABBREVIATIONS, ACRONYMS, AND COMMONLY USED TERMS](#)

[Chapter 1: History and Background](#)

[Postmortem Interval](#)

[Microbiome and Necrobiome](#)

[Warm Weather Decomposition](#)

[Cold Weather Decomposition](#)

[The Gut Microbiome Influence on Decomposition](#)

[Environmental Microbes](#)

[Muscle Tissue Decomposition](#)

[Previous Decomposition Studies](#)

[Previous Decomposition Studies at FROST](#)

[Accumulated Degree-Days](#)

[16s Ribosomal RNA Sequencing:](#)

[Previous Decomposition Studies Using 16s Ribosomal RNA sequencing:](#)

[Chapter 2: Research Questions, Goals, and Hypothesis](#)

[Goal of this Study](#)

[Hypotheses](#)

[Chapter 3: Materials and Methods](#)

[Acquisition of Donors](#)

[Methods](#)

[Samples](#)

[DNA Isolation and Purification](#)

[Preliminary Testing: Polymerase Chain Reaction and Gel Electrophoresis](#)

[Next Generation 16s rRNA Sequencing](#)

[Chapter 4: Proof of Concept](#)

[Purpose](#)

[Proof of Concept Experimental Setup](#)

[DNA Isolation and Purification](#)

[Polymerase Chain Reaction and Gel Electrophoresis](#)

[Results](#)

[Chapter 5: Results](#)

[Purpose and justification](#)

[Temperature Data](#)

[DNA Isolation and Purification](#)
[Polymerase Chain Reaction and Gel Electrophoresis](#)
[Next Generation 16s rRNA Sequencing](#)

[Chapter 6: Discussion](#)

[DNA Isolation and Purification](#)
[Polymerase Chain Reaction and Gel Electrophoresis](#)
[Next Generation 16s rRNA Sequencing](#)

[APPENDICES](#)

[Appendix A: General Cadaver Information](#)
[Appendix B: Full Sample Data Sheets](#)
[Appendix C: DNA Isolation and Purification Sample Data Sheets](#)

Table of Contents:

LIST OF TABLES.....	vi
LIST OF FIGURES.....	vii
LIST OF ABBREVIATIONS, ACRONYMS, AND COMMONLY USED TERMS.....	ix
CHAPTER 1	
HISTORY AND BACKGROUND.....	1
Postmortem interval.....	1
Microbiome and necrobiome.....	1
Warm weather decomposition.....	2
Cold weather decomposition.....	3
The gut microbiome influence on decomposition.....	3
Environmental microbes.....	4
Muscle tissue decomposition.....	6
Previous decomposition studies.....	7
Previous decomposition studies at FROST.....	8
Weather influence on decomposition.....	9
Accumulated degree-days.....	9
16s ribosomal RNA sequencing.....	10
Previous decomposition studies using 16s ribosomal RNA sequencing.....	11
CHAPTER 2	
RESEARCH QUESTIONS, GOALS, AND HYPOTHESIS.....	14
Goal of this study.....	14
Hypotheses.....	14
CHAPTER 3	
MATERIALS AND METHODS	16

Acquisition of donors.....	16
Timeline for sample acquisition.....	16
Samples.....	16
DNA isolation and purification.....	18
Preliminary Testing: Polymerase Chain Reaction and Gel Electrophoresis.....	18
Next generation 16s rRNA sequencing.....	19
CHAPTER 4	
PROOF OF CONCEPT.....	21
Purpose.....	21
Proof of concept experimental setup.....	21
DNA isolation and purification.....	22
Polymerase chain reaction and gel electrophoresis.....	22
Results.....	23
Discussion.....	25
CHAPTER 5	
RESULTS.....	26
Purpose.....	26
Temperature Data.....	27
DNA isolation and purification.....	28
Polymerase chain reaction and gel electrophoresis.....	28
Next generation 16s rRNA sequencing.....	32
CHAPTER 6	
DISCUSSION.....	66
DNA isolation and purification.....	66
Polymerase chain reaction and gel electrophoresis.....	66

Next generation 16s rRNA sequencing.....	67
By time, temperature, and ADD.....	67
By sample site location.....	68
By donor.....	69
General sample information.....	71
In conclusion.....	73
Future directions.....	73

APPENDICES

Appendix A: Cadaver information.....	75
Appendix B: Full sample data sheets.....	76
Appendix C: DNA isolation and purification data sheets.....	79
REFERENCES.....	82

LIST OF TABLES

Table 1: Proof of concept polymerase chain reaction and gel electrophoresis results.....23

LIST OF FIGURES

Figure 1: 16S ribosomal RNA sequencing.....	11
Figure 2: Proof of concept polymerase chain reaction results.....	24
Figure 3: Temperature throughout the study period.....	27
Figure 4: Polymerase chain reaction and gel electrophoresis results for donor 1.....	30
Figure 5: Polymerase chain reaction and gel electrophoresis results for donor 2 (muscle tissue samples).....	30
Figure 6: Polymerase chain reaction and gel electrophoresis results for donor 2 (buccal swab samples).....	31
Figure 7: Polymerase chain reaction and gel electrophoresis results for donor 3.....	31
Figure 8: Sample overview.....	32
Figure 9: Richness of bacterial species over ADD.....	34
Figure 10: Taxa plot - phylum level.....	36
Figure 11: Taxa plot - family level.....	39
Figure 12: Taxa plot - genus level.....	41
Figure 13: Relative abundance of major phyla by sample location (2019).....	43
Figure 14: Relative abundance of major phyla by sample location (2020).....	44
Figure 15: Relative variation of bacterial organisms at the family level by sample location.....	46
Figure 16: Relative variation of bacterial organisms at the genus level by sample location.....	47
Figure 17: Relative variation of bacterial organisms at the family level by donor.....	49
Figure 18: Relative variation of bacterial organisms at the genus level by donor.....	50
Figure 19: Relative variation of bacterial organisms at the family level by date.....	52
Figure 20: Relative variation of bacterial organisms at the genus level by date.....	53
Figure 21: Principal coordinates analysis (PCoA plot) of samples by date and tissue type (family level).....	55
Figure 22: Principal coordinates analysis (PCoA plot) of samples by date and tissue type (genus level).....	56

Figure 23: Most important genera for classifying samples by tissue type.....	58
Figure 24: Most important genera for classifying samples by donor.....	59
Figure 25: Relative abundance of bacterial genera by tissue type.....	62
Figure 26: Relative abundance of bacterial genera by donor.....	65

LIST OF ABBREVIATIONS, ACRONYMS, AND COMMONLY USED TERMS

PMI postmortem interval

Necrobiome the species and quantity of bacteria present in an organism after death.

FROST Forensic Research Outdoor Station

FIRS Forensic Investigation Research Station

CMU Colorado Mesa University

TBS total body score; the sum of a series of quantified categories of change during decomposition to specific body regions.

UV ultraviolet

Donor deceased individuals whose remains have been donated, either by themselves or by an individual who has legal authority to make funeral decisions, in accordance with the Michigan Uniform Anatomical Gift Act, MCL 700. 3206, and NMU FROST/FARL policies.

ADD accumulated degree-days

rRNA ribosomal ribonucleic acid

BP base pair

V4 region variable 4 region

DNA deoxyribonucleic acid

OTU operational taxonomic unit

PCR polymerase chain reaction

NMU Northern Michigan University

IRB Institutional Review Board; group designated to review and monitor biomedical research involving human subjects.

HIPAA Health Insurance Portability and Accountability Act; United States privacy law to protect personal medical information and patient privacy.

PBS phosphate-buffered saline

MSU Michigan State University

E. coli *Escherichia coli*

S. aureus *Staphylococcus aureus*

B. subtilis *Bacillus subtilis*

ASVs Amplicon sequencing variants; single DNA sequences resultant from a high throughput marker gene analysis.

IQR interquartile range

PCoA Plot Principal coordinates analysis plot

SEM structural equation modeling

GI gastrointestinal

Chapter 1: History and Background

Human decomposition is a complex and variable process influenced by intrinsic and extrinsic factors. Each factor plays a key role in how decomposition progresses in terms of time spent in each stage, physical appearance, and microbial community composition in and around the body. Intrinsic factors, such as the living microbiome and extrinsic factors such as temperature, humidity, insect activity, and scavenging can drastically affect the rate of decomposition and thus, the estimation of time since death (1).

Postmortem Interval

Time since death, or postmortem interval (PMI), can be an important factor in determining the identity of a decedent and/or the manner of death, which are often critical in medicolegal death investigations. Most often, investigators turn to entomological evidence for the estimation of PMI; however, methods exist for PMI estimation based on a number of variables, such as the condition of the body, biological and chemical analyses of the soil surrounding the body and botanical data (2). In practice, these methods result in high variability among individual investigators in their estimates of the PMI (3). Sequential changes in the gut bacterial composition of decomposing organisms can provide a timeline allowing for a more reliable, unbiased, and reproducible means to determine PMI (4,5).

Microbiome and Necrobiome

An organism's microbiome is the species and quantity of the bacteria present in or on the organism while it is living (6). After death, the living microbiome can change drastically as

decomposition progresses, this is termed as the organism's necrobiome. Shifts in the necrobiome can be tracked through each stage of decomposition (7). These shifts occur in a predictable manner through a series of specific stages, otherwise referred to as succession.

Warm Weather Decomposition

Necrobiome succession has been well studied in warm climates. However, very little is known about how cold weather influences this process. Warm weather studies have shown that there are five main stages of decomposition, each with morphologically distinct appearances (8). Early stages are wet, concomitant with skin discoloration and the beginning and ending of the bloat period (9). During the bloat stage, a shift from aerobic to anaerobic bacteria produce a buildup of gasses, causing a distended appearance seen most prominently in the abdomen (1,3).

This is likely due to the large quantity and diversity of gut microbes present in the human digestive tract (5). Although bloat is most noticeable in the abdomen, it can occur anywhere anaerobic bacteria are present.

Anaerobic bacteria use a process known as anaerobic respiration in order to yield the energy they need to survive and reproduce. This is accomplished through one of two possible means: fermentation and glycolysis. The byproduct from both of these processes is carbon dioxide gas (10). The buildup of carbon dioxide gas within the body, especially seen around the abdominal cavity, causes the distended appearance seen during the bloat stage (9).

The shift from early to late stage decomposition is marked by a purging event. The increased pressure resulting from the buildup of gasses forces fluids out of the decedent and the abdominal cavity can become exposed to the environment. Once this occurs, rapid decomposition

predictably ensues followed by the final decomposition stage. The final stages are characterized as dry decomposition. During this stage, mummification, partial skeletonization, or complete skeletonization may occur (9).

Cold Weather Decomposition

Researchers at the Forensic Research Outdoor Station (FROST) have observed, anecdotally, that decedents exposed to cold or refrigeration do not predictably progress through the five typical stages of decomposition. Instead, the skin becomes dry and sometimes blisters, the viscera frequently mummify, and there is little or no bloat stage.

Connor et al. (2019) also observed atypical trends in decomposition resultant from cold weather patterns. The Forensic Investigation Research Station (FIRS) in Colorado Mesa University (CMU) located in Grand Junction, Colorado is a semiarid steppe environment that receives about 19 cm of snow annually. This study noted significant color, tissue quality, moisture quality, and tissue thickness deviations from the typical total body scores (TBS) model (11). This study also noted long, sustained periods of stasis in the progression of TBS scores in this cold weather environment. All of these factors lead this study to conclude that more reliable and accurate means for determining PMI in cold weather environments is needed (11).

The Gut Microbiome Influence on Decomposition

The gut microbiome plays a key role in decomposition (3). In the early stages, the aerobic bacteria present in the gut start the process of decomposition. As decomposition progresses, a shift from aerobic bacteria to anaerobic bacteria occurs. The shift to anaerobic bacteria produces the characteristic bloat stage. As these bacteria decompose adjacent tissues, they travel out of the

gut and start decomposing adjacent organs, adipose tissue, muscle tissue, and skin (3). I hypothesize that exposure to cold or refrigeration alters the initial necrobiome present in the gut, which leads to the atypical decomposition processes that researchers at FROST have observed.

Environmental Microbes

Through the process of decomposition, environmental microbes are quickly introduced to the decedent. The species of these microbes vary widely depending on the location of the cadaver and the environmental conditions. The specific bacterial species introduced to the decedent can drastically alter the course of decomposition in terms of time and physical characteristics. Overall, there are four general categories of environmental microbes: soil microbes, insect microbes, scavenger microbes, and air microbes.

Soil Microbes

Soil microbes are bacteria present in the soil or substrate surrounding the decedent. The species of microbes present in soil samples is highly dependent on geographic location, weather conditions, and many other factors. A common soil microbe associated with human decomposition is *Acinetobacter*, which is typically present during the skeletonization phase (4).

Insect Microbes

Insects, particularly several species of flies and beetles, and their accompanying bacteria, are a crucial component in studying decomposition. Again, the bacterial species composition associated with insects is highly dependent on geographic location as well as the species of insect. Common bacteria associated with flies are *Ignatzschineria* and *Wohlfahrtimonas* (4).

Scavenger Microbes

While, technically, insects are scavengers, “scavenger” in this context refers to vertebrates that feed on the insects and/or human tissue (e.g., rodents, canids, and other carrion feeders). Scavenger activity is also a very important factor in decomposition (12). There are countless microbes associated with each individual scavenger and is highly dependent on geographical location and the animals present in that specific region. In our preliminary research at FROST, we have found that skunks (*Mephitis mephitis*) and red foxes (*Vulpes vulpes*) are the main scavengers at this site.

Air Microbes

Aeromicrobiology is a relatively new field of study in microbiology. Airborne bacteria are ubiquitous constituents of the atmosphere and are hypothesized to influence many processes such as cloud formation and ice nucleation (13).

There are several studies detailing the metabolic properties (14), species composition (13,15) potential human health implications (13,15), and applications for use of airborne bacteria in fields such as climate change and biotechnology (13). Although, there are no previous studies on how these airborne microbes can affect decomposition processes.

Womack (2010) found that most airborne bacteria come from aerosolized bacteria from the surrounding environment such as from the soil. Aerosolized bacterial community composition is dependent on numerous factors such as sun exposure (ultraviolet (UV) radiation) and precipitation, but most importantly, temperature, the adjacent environment, and humidity (14).

Aerosolized bacteria have been found in various layers of the atmosphere including the boundary layer (1.5 km altitude), the upper troposphere (up to 12 km altitude), and even the stratosphere (20-40 km altitude). Further, common mold (*Penicillium notatum*) and the bacteria *Micrococcus albus* have been collected at altitudes of 77 km and 70 km, respectively. This indicates that the aerosolized bacterial community composition is not only influenced by the nearby environment, it can also be influenced by faraway environmental microbes as well (15).

Given the previous findings, it is imperative to take all four of the categories of environmental microbes; soil, insect, scavenger, and aeromicrobes into consideration when evaluating bacterial community succession during decomposition.

Muscle Tissue Decomposition

Based on known information regarding the human microbiome and environmental microbes, this research seeks to identify what is responsible for the decay of specific tissues within the body. In the past, researchers at FROST have observed interesting trends in the decay of muscle tissue.

Muscle tissue and skin that have been exposed to cold or refrigeration tend to decompose abnormally (16). Previous research at FROST has indicated, anecdotally, that frozen remains tend to decompose from the outside-in as thawing occurs. Further, freezing disrupts cellular membranes and leads to an atypical manner of decomposition in terms of soft tissues (Harris, Northern Michigan University, personal communication, 2021).

I hypothesize that there is also a decrease in populations of specific types of bacteria due to mass die-offs resulting from exposure to cold temperatures, whereas under warmer environmental conditions, these bacteria would be responsible for the decomposition of soft tissues in an inside-

out manner. Understanding these differences can be extremely important for determining a systematic and non-biased determination of PMI for cold weather environments.

Previous Decomposition Studies

An Austrian research group has shown that several muscle-associated proteins decay in a time and condition-dependent fashion (Pittner, University of Salzburg, Austria, personal communication, 2019). A recent study from this same group showed that both porcine and mouse muscle (17) as well as human muscle (18) protein degradation follows a specific and predictable pattern that can be used as a marker for PMI.

There have been multiple recent studies detailing the bacterial species composition turnover throughout the decomposition process. Damann et al. (2015) focused on correlating PMI with bacterial community succession, specifically in decomposition of bone tissue. This study showed that gut-associated microbes were found in samples taken from decomposing human bone tissue throughout and until partial skeletonization. Indicating that gut-associated microbe migration to peripheral tissues is responsible for much of the decomposition process (19).

In contrast, samples taken after complete skeletonization showed that the bacterial community profile more closely resembled samples taken from adjacent soil samples. This indicates that environmental microbes also play an important role in the decomposition process (19).

Dibner et al. (2019) pursued to categorize the decomposer community throughout pig (*Sus scrofa domesticus*) decomposition. This study found that on the island of Oahu, Hawaii, the warm temperatures, averaging 26 °C [~ 220 accumulated degree-days (ADD)], allowed about 80 % of decomposition to be completed within 8 days. They found that scavengers such as fly larvae and

the Indian Mongoose (*Herpestes javanicus*) were the main extrinsic factors affecting the decomposition process (20).

The study went one step further and sampled the fly larval masses to determine the species of bacteria present. Results showed that there were two main phyla present in these samples- Firmicutes [family: *Clostridiaceae*, *Enterococcaceae*, and *Planococcaceae*] and Proteobacteria [family: *Enterobacteriaceae*]. Bacteria from Firmicutes were most commonly found. Although they noted a shift from aerobic to anaerobic bacterial species throughout the early stages of decomposition, they noted that a clear microbial succession pattern was not observed (20).

Burcham et al. (2019) also utilized postmortem microbial metatranscriptomic analyses to detail the community structure and functional data of bacterial community succession and associated metabolic pathways throughout decomposition in pursuit of correlating this information with PMI (21).

This study found that there was an initial abundance of strict anaerobic bacterial families such as *Lachnospiraceae* and *Ruminococcaceae* within the murine intestine shortly after death. Following the bloat stage and purging, the researchers discovered a shift to more aerotolerant anaerobic bacterial families such as *Lactobacillaceae* and *Clostridiaceae* as oxygen was being introduced into this environment (21).

Previous Decomposition Studies at FROST

Previous necrobiome studies at FROST have focused on sampling the cecum (large intestine) and oral cavity for identification of bacterial species present. Less is known about muscle tissue

decomposition and the role of bacteria in this process. This study aims to add to these previous findings and to expand the number of sample sites that are studied.

Weather Influence on Decomposition

As previously noted, weather plays a crucial role in the decomposition process. Not only are the differences between warm and cold weather decomposition important, other environmental factors contribute to the rate of decomposition. Temperature, sun exposure, humidity, and precipitation are some examples among the countless variables weather conditions can reveal.

Although specific effects of each of the aforementioned conditions have not been studied independently, as these studies are located outdoors, all work together to influence decomposition processes (9).

While there are countless variables in terms of weather, temperature is the most important factor influencing the manner, characteristics, and overall rate of decomposition (9). Data from a weather station located at the FROST site will be utilized to account for weather conditions over the course of this study.

Accumulated Degree-Days

Accumulated degree-days are a measure of heat energy units that constitute the accumulation of thermal energy over a period of time (22). ADDs are calculated by averaging the highest and lowest temperature within all consecutive 24-hour periods that the subject was exposed to. This represents the heat energy the subject was exposed to over a specific period of time. Thermal energy is needed to allow for biological and biochemical processes to take place that, in turn, drives the decomposition process (23).

Although accumulated degree-days are a very useful tool for determining PMI, previous research has shown that microclimates exist between weather recording stations where temperatures and other climatological characteristics can be drastically different (24). For this reason, this study will be utilizing a weather station located at the FROST site for acquisition of temperature data used for calculating ADDs.

16s Ribosomal RNA Sequencing:

Central to this research will be the use of 16s ribosomal RNA (rRNA) sequencing to determine the identity and quantity of bacterial species present throughout decomposition. Every living cell needs ribosomes for protein synthesis. The 16s portion of the rRNA gene has conserved and variable regions present throughout the ~1500 base pair (bp) segment. The variable regions can be used as an indicator specific for identifying each different bacterial species (25).

The identity of the bacterial species present in the isolated DNA samples can be determined by sequencing the 16s rRNA gene alone, instead of using the more time-consuming and costlier whole-genome sequencing method (26). A simplified description of 16s rRNA sequencing can be seen in Figure 1 (25).

The sequencing most commonly used for bacterial species lies within the fourth variable (V4) region. The V4 region is flanked on either side by a highly conserved region; the target for the sequencing primers. The middle variable portion is specific to different bacterial species, allowing us to determine which microbes are present. This region is amplified thousands of times throughout the sequencing process, yielding a large amount of DNA fragments. Highly similar sets of fragments (97% similarity or higher) are grouped together, forming an operational taxonomic unit (OTU) (26).

The relative number of OTUs combined with the corresponding taxonomic information will reveal the species and quantity of bacteria present during each stage of decomposition and from each sample site. This information will allow us to form a timeline correlating bacterial population composition shifts in relation to decomposition time and conditions effectively revealing another method to determine PMI.

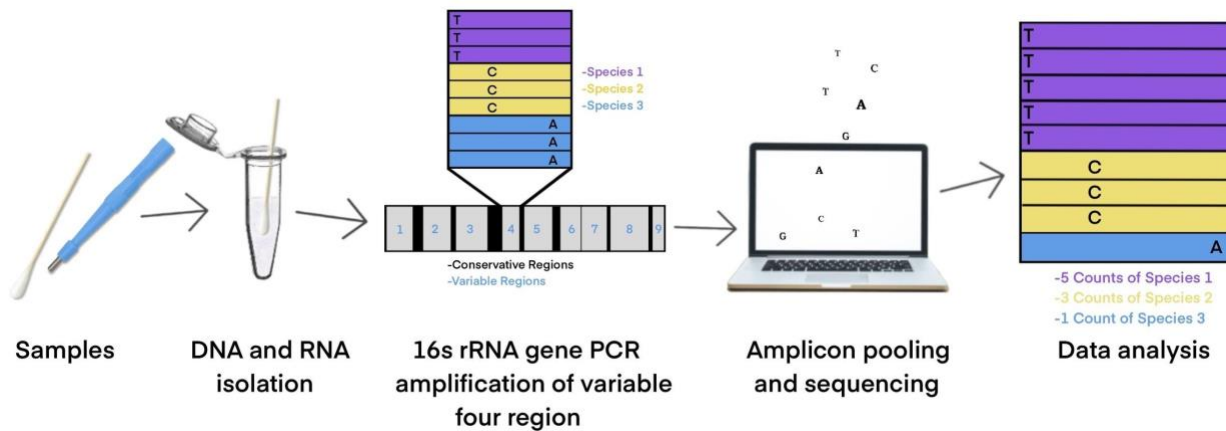


Figure 1: 16s Ribosomal RNA Sequencing. Sequencing using this method involves sample collection followed by DNA isolation. From the isolated DNA, a highly variable region [grey segments] flanked by highly conserved regions [black segments; targets for primer binding] will be amplified using polymerase chain reaction (PCR) and sequenced. Once sequenced, similar taxonomic groups (about 97 % similarity and higher) will be clustered together, forming operational taxonomic units (OTUs) [purple, yellow, and blue bars in the final picture]. Data analysis on the relative abundance of OTUs in conjunction with sequencing information, will reveal the quantity and diversity of the bacterial organisms present during each stage of decomposition.

Previous Decomposition Studies Using 16s Ribosomal RNA sequencing:

There are multiple previous studies that have utilized next-generation metagenomic sequencing techniques in order to quantify and categorize microbial communities associated with

decomposition and PMI. Finley et al. (2015) summarized multiple studies utilizing this technique for identifying and quantifying microbial community succession in soil samples, mouse model samples, human microbial samples, and cadaver samples (27).

One such study from Metcalf et al. utilized high throughput sequencing of the 16s rRNA gene in a mouse model system to determine the presence of certain microbial organisms throughout decomposition. This study obtained a total of 223 samples from locations in or around the abdominal cavity, skin, and of soil samples (grave soil) adjacent to the decomposing mice. The mouse model allowed the researchers to control the microbiome of the soil and the mice so there were no inherent differences in microbial community composition at the beginning of the study (28). To correlate the microbial findings with PMI, the researchers used the total body visual scoring system by Megyesi et al. (2005) to determine the stage of decomposition the mice were in when samples were taken. The decomposition process from start to skeletonization lasted 48 days (28).

After filtering the samples for quality readings, the study used 167 samples (samples with insufficient 16s rRNA reads were removed from the data analysis set) that gave 2,931,901 16s rRNA reads, and yielded 4505 OTUs. Most samples that had too few reads were from days 0-3 (fresh stage). On days 6-9 (bloat stage), endogenous anaerobes such as Firmicutes and Proteobacteria were common. Around day 9 (purging stage), the abdominal cavities became exposed to air and the abundance of these phyla significantly decreased. While these organisms decreased, other families of aerobic bacteria increased over this time such as *Bacteroidaceae* and *Enterobacteriaceae*. Up until advanced decomposition and subsequently skeletonization, the aerobic bacteria abundance stayed relatively consistent and then fell as skeletonization progressed (28).

The use of variable regions within the 16s rRNA gene, in particular, has been used for its ability to accurately identify between bacterial species without the need for costly and time-consuming whole genome sequencing methods. Hyde et al. (2015) used this approach to study bacterial community succession in human decomposition using samples taken from the mouth, skin, and rectum. This study found that bacterial community composition is variable at placement and during and after the bloat stages. However, as time progressed, bacteria associated with flies became increasingly more common as well as bacteria associated with soil (9).

Chapter 2: Research Questions, Goals, and Hypothesis

Goal of this Study

The goal of this study is to determine if there is bacterial DNA present in specific tissue samples using DNA isolation techniques, polymerase chain reaction (PCR), and next generation 16S rRNA sequencing and to use this information to determine changes in the necrobiome community during the decomposition process. These data may be useful to determine if specific microbes present during decomposition or specific changes in the necrobiome during decomposition can be used to form a timeline for PMI.

Hypotheses

Hypothesis 1

If changes in the necrobiome occur in a predictable pattern over time, then these changes can be used to determine PMI.

Expectation: The presence and quantity of specific bacterial phyla, classes, orders, families, genus, or species of microbes can act as “markers” for indicating a pattern of succession that can be used to determine PMI.

Hypothesis 2

If certain bacterial species (i.e. human microbes vs environmental microbes) are the cause of rapid decomposition in muscle tissue samples, then these microbes can be associated with PMI.

Expectation: It is possible to determine whether specific bacterial phyla, classes, orders, families, genus, or species that are responsible for rapid decomposition in muscle and indicate a pattern of succession useful for PMI estimation are of human or environmental origin.

Hypothesis 3

If changes in the necrobiome occur due to cold weather conditions, these changes can be compared to previous knowledge on warm weather studies and be used to determine PMI.

Expectation: When compared, data from warm weather decomposition studies and cold weather decomposition studies will show that the estimation of PMI is directly related to the environmental conditions.

Chapter 3: Materials and Methods

Acquisition of Donors

All human tissue included in this study is sampled from human remains donated to FROST through the NMU Body Donation Program according to guidelines established by the Michigan Public Health Code Act 368 of 1978, Part 1: Revised Uniform Anatomical Gift Law (29). All human tissue used for this study is from deceased individuals and therefore does not require IRB approval and is not subject to HIPAA.

Each FROST donor is given a donor number that protects their confidentiality and separates their living identities from the research and data collection that are performed postmortem. For the purpose f this study, the donors' identities are further protected by referring to them as "Donor 1," "Donor 2," and "Donor 3." Details of specific donors, including age-at-death, sex, approximate body size, time interval between date-of-death and date-of-placement, and temperature at which they were stored during that time can be found in Appendix A.

Methods

Timeline for Sample Acquisition:

Daily sampling took place for 14 days following donor placement. Afterwards, weekly or bi-weekly sampling was done unless affected by freezing, snow accumulation, insect activity, or later stages of decomposition. Following snow melt in the spring, additional samples were taken at regular intervals.

Samples

Arm muscle (Deltoid) Sampling

Prior to making any incisions, each time samples were collected, the incision site was disinfected using 70% isopropyl alcohol followed with 10% povidone-iodine solution. A 2-3 cm incision was made in the superior, medial aspect of the deltoid using a number 15 scalpel. The incision extended through the subcutaneous fat until muscle was reached. A Robbins Instruments® 8 mm, single use biopsy punch was inserted into the incision to retrieve the sample. The muscle sample was put into a 15 mL conical tube and stored at - 80 °C. The incision site was covered with Tegaderm® Film sterile surgical dressing to prevent environmental contamination. One sample was taken each day, using a new incision site for every new sample.

Thigh Muscle (*Vastus Lateralis*) Sampling

Prior to making any incisions, each time samples were collected, the incision site was disinfected using 70% isopropyl alcohol followed with a 10% povidone-iodine solution. A 2 - 3 cm incision was made in the lateral thigh starting proximal and, for future sampling, moving distally toward the knee. The incision was made using a number 15 scalpel and extended through the skin and subcutaneous fat until the muscle was accessed. A biopsy needle was inserted into the muscle to retrieve a sample. The muscle sample was put into a 15 mL conical tube and stored at - 80 °C. The incision site was covered with Tegaderm® Film sterile surgical dressing to prevent environmental contamination. Two samples were taken daily, extending the existing incision site each day. Duplicate samples were taken to be sent to an Austrian group studying changes in muscle protein degradation during decomposition. This study will also be useful for determining PMI.

Buccal Sampling

A sterile, cotton tipped swab (VWR® Scientific) was used to swab the inside of the decedent's right cheek. The swab was placed into a 1.7 mL centrifuge tube containing 0.5 mL of phosphate-buffered saline (PBS) and stored at - 80 °C. Two samples were taken each sampling day until it was no longer possible to obtain more samples. Donor 2 was the only donor from which buccal swab could be taken. Other donors in this study had confounding factors that prevented buccal swab collection.

DNA Isolation and Purification

DNA Isolation

DNA was isolated from the buccal swabs and muscle tissue samples following the QIAGEN QIAamp Fast DNA Tissue Kit protocol.

Determining Concentration and Purity of the DNA

The concentration and purity of the extracted DNA was measured using a NanoDrop spectrophotometer from ThermoScientific® using the final reagent (eluting buffer "ATE") as the blank. Pure DNA absorbs UV light at 260 nm. This measurement can be used to determine DNA concentration. Pure DNA also has an absorbance 260 nm / 280 nm ratio of 1.8 - 2.0. Samples that have low concentrations or 260 / 280 ratio higher/lower than 1.8 - 2.0 may be repurified.

Preliminary Testing: Polymerase Chain Reaction and Gel Electrophoresis

Polymerase Chain Reaction

The presence of bacterial DNA was determined using polymerase chain reaction (PCR) targeting the conserved 16s ribosomal RNA (rRNA) gene found in all bacterial species.

R: 5'- GAC TAC HVG GGT ATC TAA TCC - 3' F: 5' - CCT ACG GGN GGC WGC AG - 3'

Gel Electrophoresis

A 1% agarose gel was used for separation of the PCR product. Once the samples were loaded, the BIO-RAD® PowerPac Basic Electrophoresis Power Supply was started at 100 V and then increased to 135 V for about 1 hour. The gel was imaged using the BIO-RAD® Molecular Imager, Gel Doc XR+ imaging system. The presence of a band at 360 bp indicated that bacterial species were present in that sample.

Next Generation 16s rRNA Sequencing

All purified DNA samples were stored at - 20 °C until sequencing. DNA samples were sent to Michigan State University (MSU) for analysis using next generation 16S sequencing. Bioinformatic analysis was partially done at MSU and “R” was used to sort the data into graphical formats to show the necrobiome composition at various time points. Statistical analysis was used to determine if the changes in the necrobiomes at different times are significant.

Sequencing

The V4 hypervariable region of the 16S rRNA gene was amplified using dual indexed Illumina compatible primers 515f/806r. PCR products were batch normalized using Invitrogen SequalPrep DNA Normalization plates and the products recovered from the plates pooled. The pool was cleaned up and concentrated using AmpureXP magnetic beads; it was QC'd and quantified using a combination of Qubit dsDNA HS, Agilent 4200 TapeStation HS DNA1000

and Kapa Illumina Library Quantification qPCR assays. The pool was loaded onto an Illumina MiSeq v2 standard flow cell and sequencing was performed in a 2x250 bp paired end format using a MiSeq v2 500 cycle reagent cartridge. Base calling was done by Illumina Real Time Analysis (RTA) v1.18.54 and output of RTA was demultiplexed and converted to FastQ format with Illumina Bcl2fastq v2.19.1.

Data processing

Initial processing of sequencing files was conducted using QIIME 2 (v 2020.11). Sequences were demultiplexed and quality filtered using the q2-demux plugin before denoising with DADA2. Singletons were removed before alignment (mafft) and building of a phylogenetic tree (fasttree). Samples were rarefied to 3,000 reads based on rarefaction plots (see figure). A naïve Bayes taxonomy classifier (classify-sklearn) trained against the SILVA (13.8, 99%) reference database was used to assign taxonomy to amplicon sequence variants (ASVs).

Acknowledgements:

Data processing and analysis was supported in part through computational resources provided by the Institute for Cyber-Enabled Research at Michigan State University. Costs associated with this analysis were paid for through an NMU PRIME grant awarded to Sharp, Froelich and Wankmiller in 2019.

Chapter 4: Proof of Concept

Purpose

The purpose of this proof-of-concept experiment was to determine if prokaryotic DNA could be isolated from muscle tissue samples. If prokaryotic DNA was found using the aforementioned DNA isolation and purification techniques and confirmed using PCR, then this would support use of these methods to isolate and purify microbial DNA from human muscle tissue samples.

Proof of Concept Experimental Setup

Samples

A beef steak was used as a trial to determine the efficacy of obtaining bacterial DNA from muscle tissue samples. In the first trial, samples were taken from a steak that had been refrigerated at 4 °C for three months. Based on visual assessment of the steak at that time, it was presumed to have sufficient bacterial contamination to use as a representative for decaying human muscle tissue samples. Swabs were taken of the liquids surrounding the steak and of the steak itself. Then muscle tissue samples were taken from various parts of the steak.

In the second trial, a fresh steak was used. Muscle tissue samples were taken and then inoculated with an overnight culture of *Escherichia coli* (*E. coli*) using a 10-fold dilution range from undiluted to 10^{-6} , separately.

DNA Isolation and Purification

DNA extraction was completed by following the QIAGEN QIAamp Fast DNA Tissue Kit protocol. The concentration and purity of the extracted DNA was determined using the ThermoScientific® NanoDrop Spectrophotometer. The results can be seen in Table 1.

Polymerase Chain Reaction and Gel Electrophoresis

Polymerase chain reaction

Following DNA extraction and purification, PCR targeting the 16s rRNA gene was done for all of the samples listed in Table 1. Water was added as a negative control and DNA from *Staphylococcus aureus* [*S. aureus*], *Bacillus subtilis* [*B. subtilis*], & *Escherichia coli* [*E. coli*] all at a dilution of 3 ng/µL of DNA, were used as positive controls.

Gel Electrophoresis

Following PCR targeting the 16s rRNA gene, the PCR products were loaded into a 1% agarose gel and imaged using the BIO-RAD® Molecular Imager, Gel Doc XR+ imaging system. The results of this can be seen in Figure 2.

Results

Table 1: Proof of Concept NanoDrop Results. The concentration and purity of the steak samples from the proof of concept experiments 1 and 2. Experiment 1 consisted of samples from various parts of a decomposing steak. Swabs of the fluid surrounding the steak and of the steak itself as well as two muscle tissue samples from the “white” portion and the “brown” portion of the steak were sampled (the color distinctions “white” and “brown” refer to visual assessment of different parts of the steak). Experiment 2 consisted of samples taken from a fresh steak inoculated with overnight cultures of *E. coli* in a 10-fold dilution range from undiluted to 10^{-6} , choosing certain dilutions to represent the results.

Experiment 1			Experiment 2				
Sample	Concentration (ng/ μ L)	260/280	260/230	Sample	Concentration (ng/ μ L)	260/280	260/230
Swab (steak "juice")	17.7	1.91	1.97	<i>E. coli</i> Undiluted (steak)	31.6	1.96	2.63
Swab (steak)	113.3	1.89	1.07	<i>E. coli</i> -1 (steak)	33.5	1.82	3.44
Muscle Sample "white"	36.1	1.85	1.68	<i>E. coli</i> -4 (steak)	33.7	1.82	2.42
Muscle Sample "brown"	16	1.86	0.13	<i>E. coli</i> -5 (steak)	10.8	1.73	0.22
				<i>E. coli</i> -6 (steak)	41	1.83	2.18

Table 1 shows the results from isolating and purifying DNA from (1) a decomposing steak and (2) from a fresh steak inoculated with serial dilutions of *E. coli*. The concentration of DNA isolated from the 16s rRNA gene ranged from (1) 16 ng/ μ L to 113.3 ng/ μ L and (2) from 10.8 ng/ μ L to 41 ng/ μ L. For both experiments, the 260/280 ratio averaged about 1.85 and the 260/230 ratio was variable, ranging from 0.13 to 3.44.

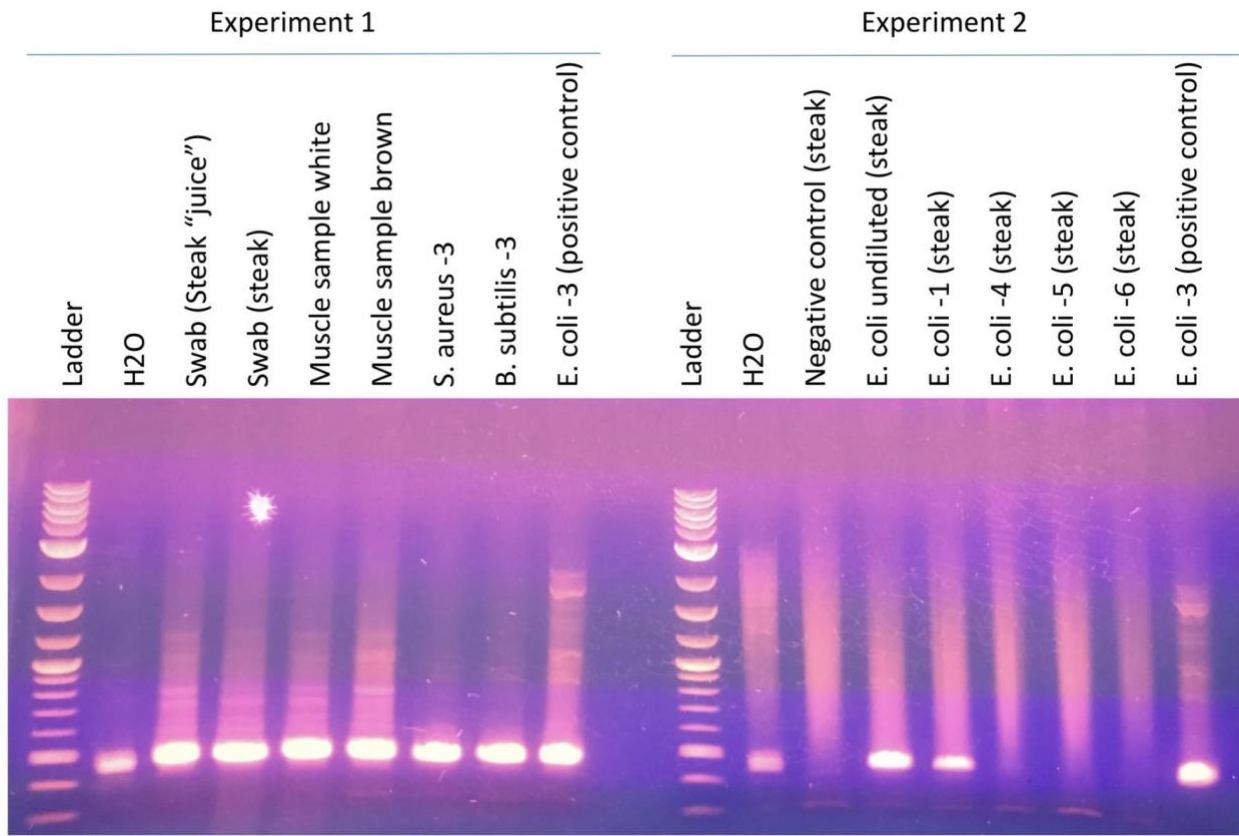


Figure 2: Proof of concept polymerase chain reaction and gel electrophoresis results. PCR and gel electrophoresis results for trials 1 and 2. Water was used as a negative control for both experiments. For experiment 1, *S. aureus*, *B. subtilis*, and *E. coli* DNA were used for positive controls (no muscle tissue present in the samples). Swabs of the fluid surrounding the steak, swabs of the steak itself, as well as two muscle tissue samples from the “white” portion and the “brown” portion of the steak were sampled (the color distinctions “white” and “brown” refer to visual assessment of different parts of the steak). For trial 2, uninoculated steak and water were used as negative controls and *E. coli* DNA was used as a positive control (no muscle tissue present in the sample). Finally, fresh steak was inoculated with overnight cultures of *E. Coli* in a 10-fold dilution range from undiluted to 10^{-6} , choosing certain dilutions to represent the results.

Discussion

For trial 1, DNA concentration varied significantly based on the location of the swab or muscle tissue sample. The swab of the surface of the steak proved to have the highest concentration of amplified DNA from the 16s rRNA gene at 113.3 ng/µL. The two muscle tissue samples had similar concentrations of 36.1 ng/µL [“white sample”] and 16 ng/µL [“brown sample”]. Finally, the liquid surrounding the steak had a DNA concentration of 17.7 ng/µL.

For trial 2, the concentration of isolated DNA remained fairly stable throughout. With the exception of the 10^{-5} ng/µL dilution of *E. coli* which had a concentration of 10.8 ng/µL. This was likely due to a discrepancy during the DNA isolation stage.

For both trials, the 260/280 ratio (purity ratio for nucleic acids) was well within the normal range of about 1.8. However, the 260/230 ratio (indicates presence or absence of unwanted organic compounds and contamination) was highly variable, ranging from 0.13 to 3.44. This is postulated to be due to the presence of muscle tissue proteins that were not adequately filtered out during the purification step.

Figure 2 shows strong bands at 360 bp for all of the samples taken from the steak as well as the positive controls in the first trial. The second trial showed 16s rRNA detection in the positive control as well as in the inoculated steak samples up to the *E. coli* 10^{-1} ng/µL dilution. The negative control (uncontaminated steak) showed no detection. These results indicate that prokaryotic or bacterial DNA could be isolated from muscle tissue samples.

The results from the proof of concept experiment supports the feasibility of isolating microbial DNA from donor muscle tissue throughout decomposition and would allow us to study necrobiome shifts that could be indicative of PMI.

Chapter 5: Results

Purpose and justification

The undermentioned addresses the results from preliminary testing and the 16s rRNA sequencing data. This information will be used to assess the overall diversity and variability of the necrobiome community composition over the course of the decomposition process for all three donors. The bacterial community composition will be assessed for patterns relating to time, temperature, ADD, bacterial markers for sample site location and donor identification, and PMI. This information will be critical in the evaluation of necrobiome succession as it relates to PMI.

Temperature Data

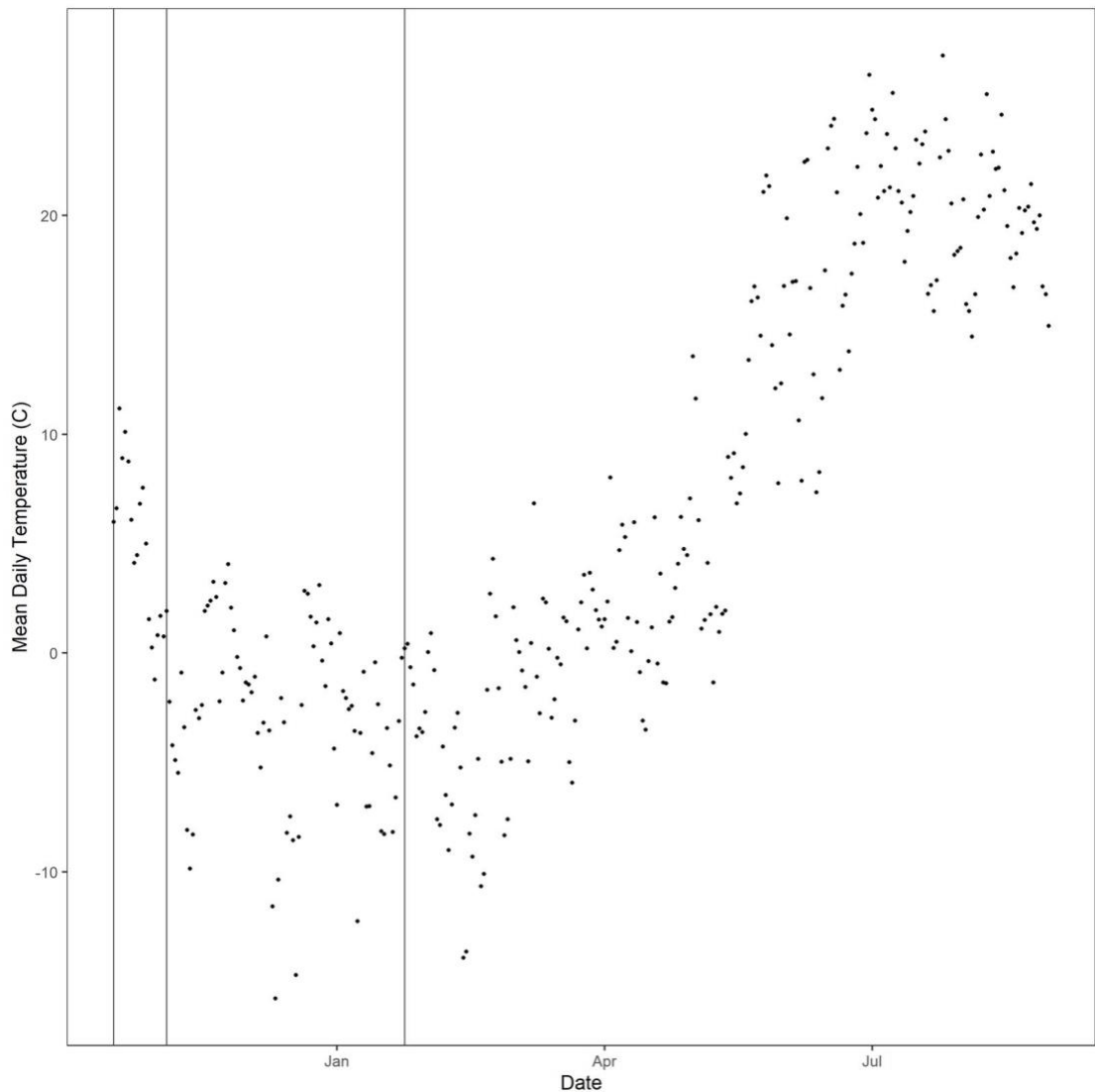


Figure 3: Temperature throughout the study period. Daily temperature recordings were taken from the weather station located at the FROST site. The means of the daily readings were calculated and graphed in accordance with the dates within the study period. The vertical lines represent when a donor was initially placed at the FROST site (first line is when donor one was placed, second is donor 2, and the third line is when donor 3 was placed).

DNA Isolation and Purification

DNA isolation and purification were performed as previously described in the “DNA Isolation and Purification” methods section. NanoDrop Spectrophotometer analysis of the concentration and purity of the extracted DNA yielded concentrations ranging from 28.7 to 222.0 ng/ μ L (donor 1; deltoid samples [MD-1]) and 47.3 to 271.5 ng/ μ L (thigh muscle samples [MT-1]). Results from donor 2 showed a range from 9.2 to 190.5 ng/ μ L (MD-2), 69.1 to 164.2 ng/ μ L (MT-2), and 2.3 to 16.3 ng/ μ L (buccal swab samples [B-2]). Finally, results from donor 3 showed DNA concentration ranges from 31.6 to 120.0 ng/ μ L (MD-3) and 25.8 to 217.2 ng/ μ L (MT-3). DNA purity results showed a similar trend to the proof of concept experiments where the 260/280 ratio averaged about 1.81 for all of the muscle tissue samples; being slightly more variable for the buccal swabs, ranging from 1.05 to 1.76 with an average of 1.6. The 260/230 ratio for all samples was variable ranging from 0.07 at the lowest and 2.91 at the highest. The full set of data detailing the DNA isolation and purification information can be seen in appendix C.

Polymerase Chain Reaction and Gel Electrophoresis

Following PCR targeting the 16s rRNA gene, the PCR product was loaded into a 1 % agarose gel and imaged as described in the “Preliminary Testing: Polymerase Chain Reaction and Gel Electrophoresis” methods section. The results of this can be seen for each donor in figures 4 - 7.

Figures 4, 5, and 7 show the results specifically from the two muscle groups that were sampled from each donor. All show prokaryotic DNA detection for each of the samples taken. Interestingly, a trend emerged revealing that as time progresses the strength of the band

increases, which is especially apparent in samples from donor 1. Figure 6 shows the PCR results from DNA isolation from buccal swabs. In contrast to the muscle samples, the buccal swab samples did not show a trend of increased detection of prokaryotic DNA. The water samples for each do show a small amount of prokaryotic DNA detection based on the gel images.

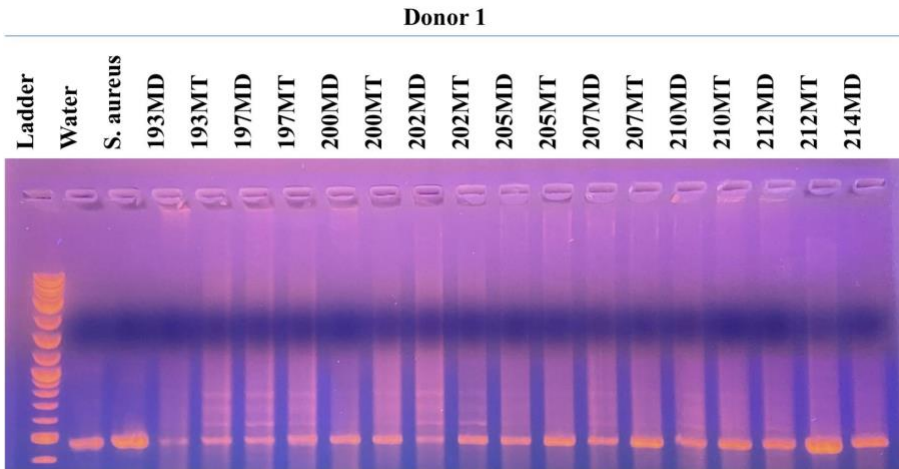


Figure 4: Polymerase chain reaction and gel electrophoresis results for donor 1. PCR and gel electrophoresis results for the muscle tissue samples collected from donor 1. Water was used as a negative control and *S. aureus* was used as a positive control (no muscle tissue present in these samples). The samples were named based on the location of the muscle tissue sample (MD indicates muscle from the deltoid and MT indicates muscle from the thigh) and the number of days following donor placement the sample was collected.

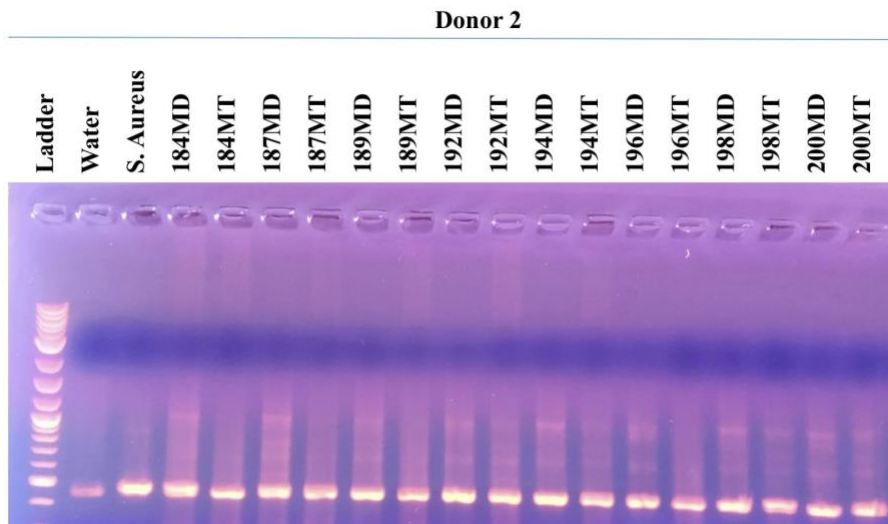


Figure 5: Polymerase chain reaction and gel electrophoresis results for donor 2 (muscle tissue samples). PCR and gel electrophoresis results for the muscle tissue samples collected from donor 2. Water was used as a negative control and *S. aureus* was used as a positive control (no muscle tissue present in these samples). The samples were named based on the location of the muscle tissue sample (MD indicates muscle from the deltoid and MT indicates muscle from the thigh) and the number of days following donor placement the sample was collected.

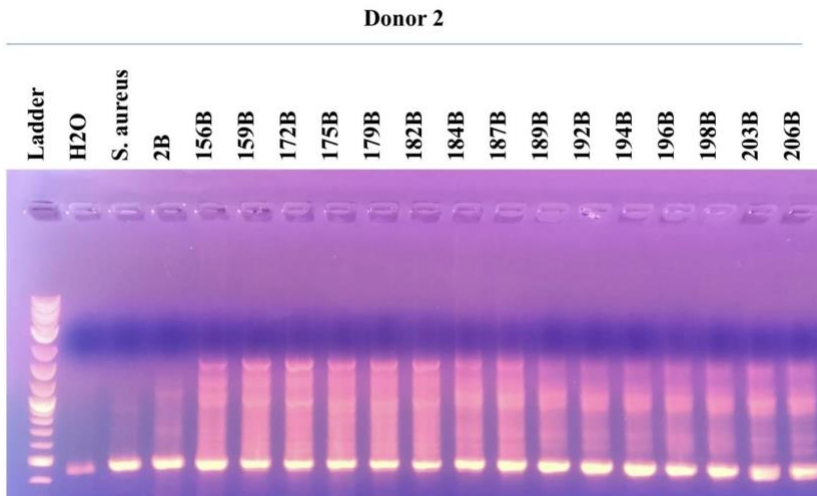


Figure 6: Polymerase chain reaction and gel electrophoresis results for donor 2 (buccal swab samples). PCR and gel electrophoresis results for the buccal swab samples collected from donor 2. Water was used as a negative control and *S. aureus* was used as a positive control (no muscle tissue present in these samples). The samples were named based on the location of the sample (B indicates a buccal swab) and the number of days following donor placement the sample was collected.

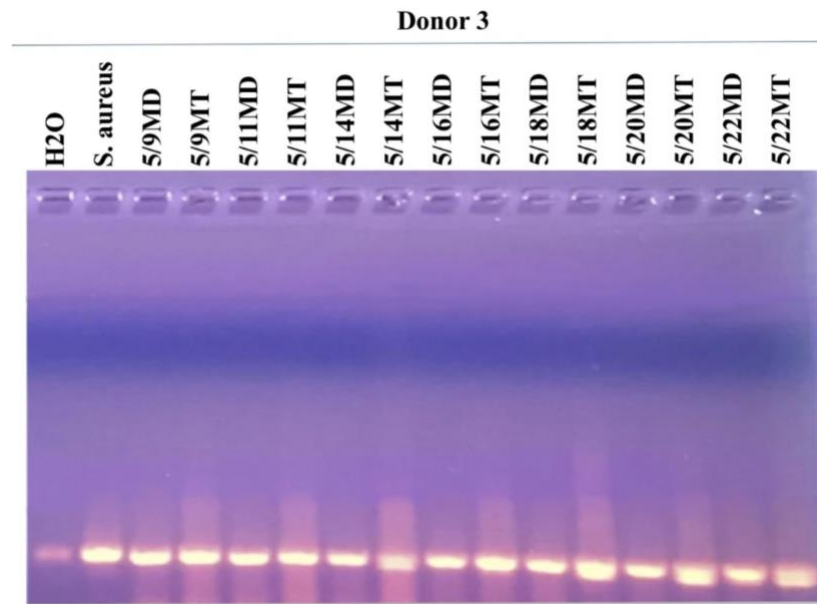


Figure 7: Polymerase chain reaction and gel electrophoresis results for donor 3. PCR and gel electrophoresis results for the muscle tissue samples collected from donor 3. Water was used as a negative control and *S. aureus* was used as a positive control (no muscle tissue present in these samples). The samples were named based on the location of the muscle tissue sample (MD indicates muscle from the deltoid and MT indicates muscle from the thigh) and the number of days following donor placement the sample was collected.

Next Generation 16s rRNA Sequencing

Since bacterial DNA was detected in the muscle samples and buccal samples by PCR, the extracted DNA samples were sent to Michigan State University (MSU) for analysis using next generation 16S sequencing. Bioinformatic analysis was completed at MSU using R (30) to sort the data into graphical formats to show the necrobiome composition at various time points.

Figure 8 shows A total of 6,784,236 paired end reads were obtained from 123 samples. The mean reads per sample was 55,608. Based on the alpha rarefaction plots, a rarefaction depth of 3,000 reads was chosen. This depth resulted in the loss of one sample (FR180, 952 reads before filtering). After filtering and rarefaction, 120 samples remained with 366 Amplicon sequencing variants (ASVs).

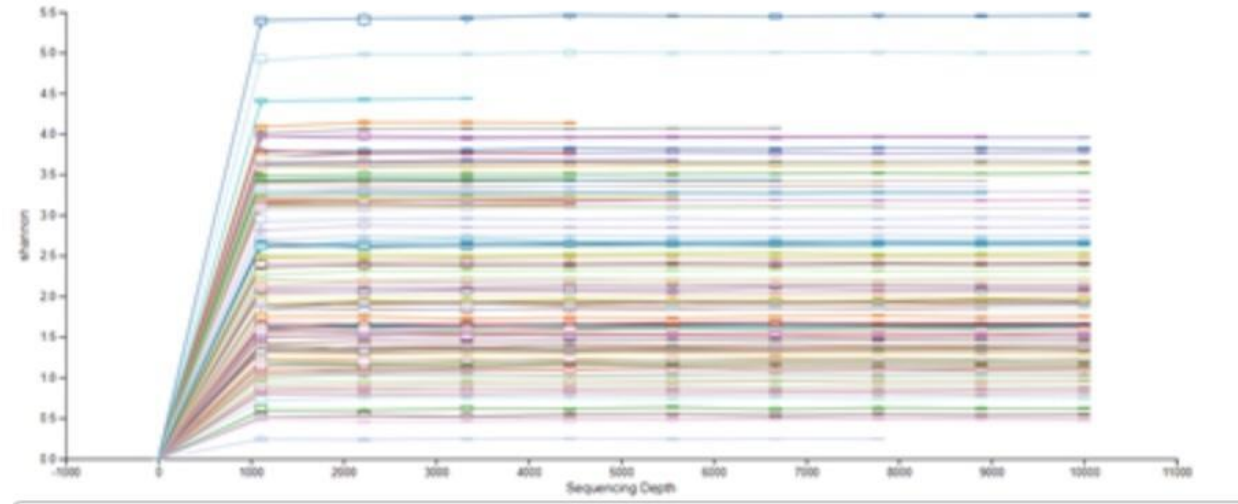


Figure 8: Sample Overview. From 123 samples, 6,784,236 paired end reads were obtained with a mean reads per sample of 55,608.

The richness of species observed in each data set was variable depending on the location of the sample site, as well as by donor. In general, the number of species observed in deltoid samples remained fairly constant over time and temperature (ADD) with the exception of samples taken from donor 2, where the observed number of species tended to increase over ADD. Buccal swabs taken from donor 2 showed a sharp increase in the number of observed species. Samples taken from the thigh for all three donors all showed a decrease in the number of observed species over increasing ADD (figure 9).

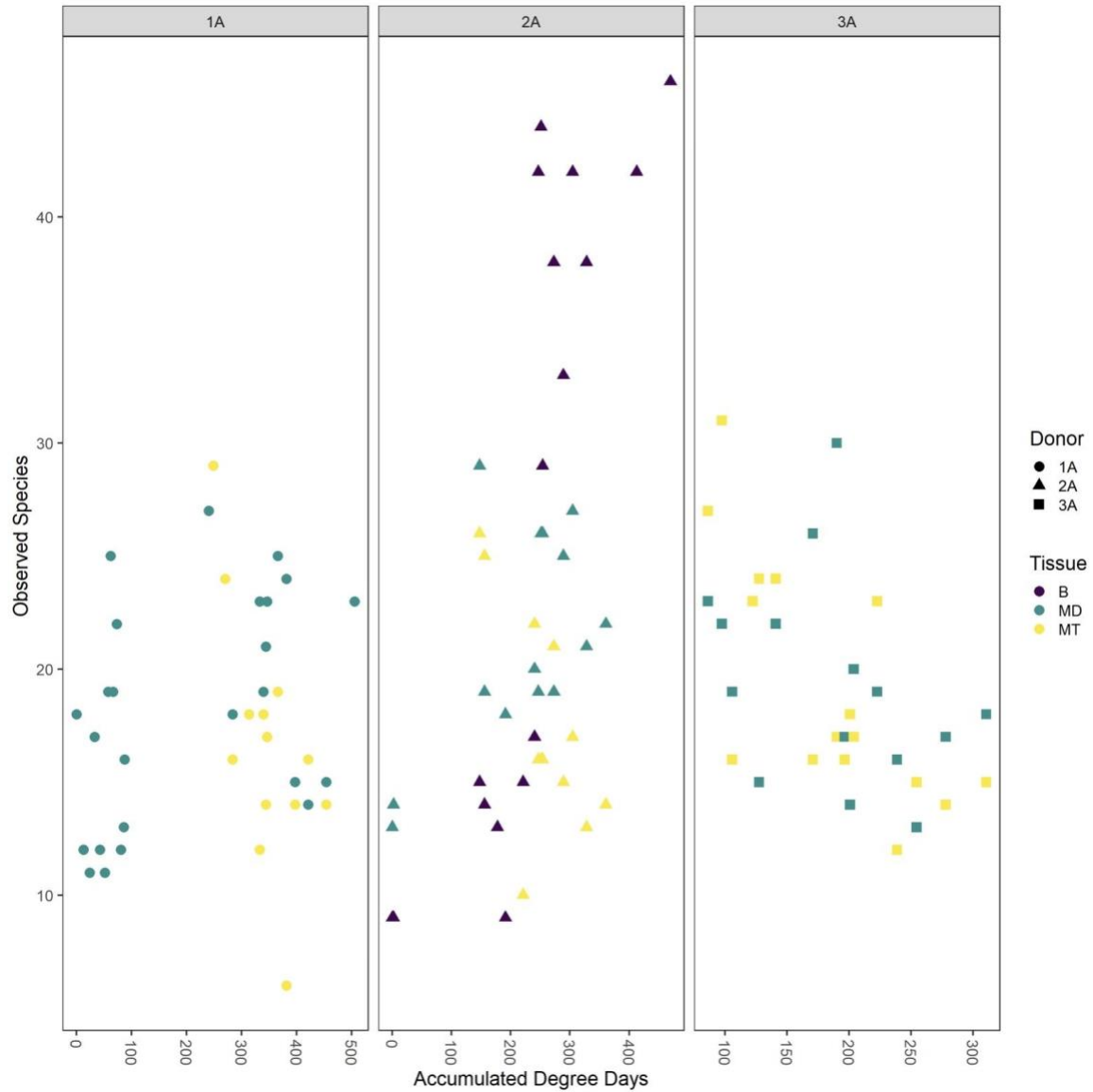


Figure 9: Richness of bacterial species over ADD. The number of observed species per type of sample was graphed in accordance with accumulated degree-days. Each box represents a donor as well as each shape used to pinpoint the sample (A circle indicates donor 1 (1A), triangle indicates donor 2 (2A), and a square indicates donor 3 (3A)). The color of each data point indicates the site the sample was taken from.

Figure 10 represents the relative abundance of bacteria represented under the phylum level in accordance with ADD. In general, the relative abundance of Bacteroidota was variable between donor and sample site, but tended to increase later in decomposition. The relative abundance of Firmicutes drastically increased and became one of the most abundant bacteria over increasing ADD. The relative abundance of Proteobacteria tended to initially increase and then decrease as decomposition progressed. Samples taken from the oral cavity showed a significantly increased relative abundance of Proteobacteria compared to samples taken from muscle tissue. Finally, DNA that was unable to be categorized as bacterial DNA was labeled and graphed as unassigned. This DNA was only present in the muscle tissue samples trending as having an initially high relative abundance which decreased over ADD. In some sample sets, the unassigned phylum stayed relatively stable throughout the decomposition process.

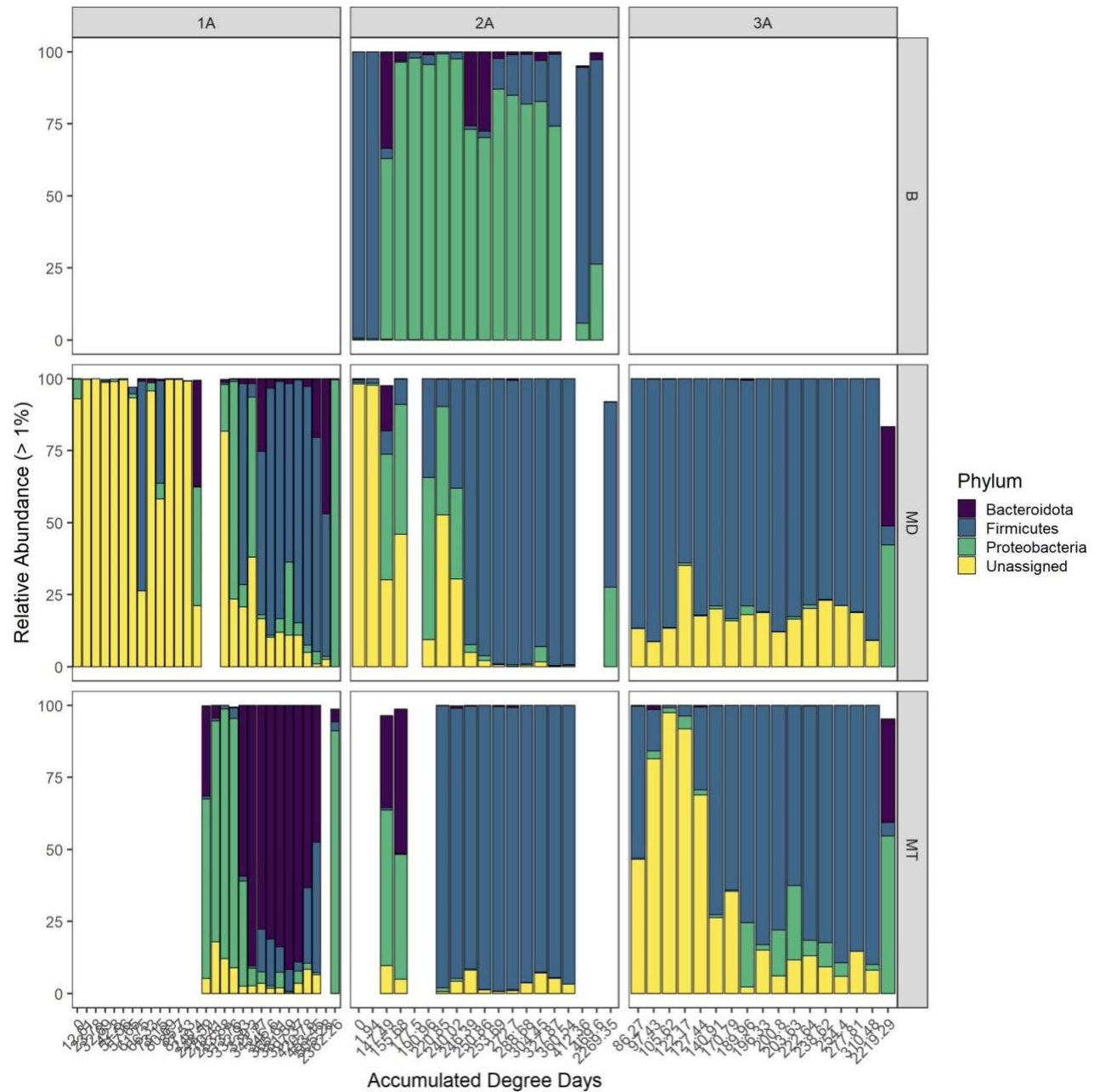


Figure 10: Taxa plot - phylum level. The relative abundance of each represented phylum (Bacteroidota, Firmicutes, Proteobacteria, and unassigned) were graphed in terms of accumulated degree-days. Each column represents a donor and each row represents the sample site. The color of the bars is indicative of the phylum that represents the bacteria classified under that category.

Figure 11 represents the relative abundance of bacteria represented under the family level in accordance with ADD. *Carnobacteriaceae* was almost exclusively found in donor 2 muscle tissue samples during mid to late decomposition. Similarly, *Clostridiaceae* was mostly found in donor 2 muscle tissue samples, with some being seen in the earlier and later stages of decomposition in donor 3 thigh muscle tissue samples. *Dysgomonadaceae* tended to appear in middle to late decomposition in a relatively low abundance in the buccal samples (donor 2) and in deltoid samples from donor 1. In thigh muscle samples from donor 1, *Dysgomonadaceae* had a very high relative abundance (sustained over 70%) throughout middle to late decomposition.

Lactobacillaceae was most prominently and abundantly seen in both muscle tissue sample locations from donor 3 throughout decomposition; a relatively low abundance can be seen in early buccal samples from donor 2 and in middle ADD in deltoid samples from donor 1.

Peptostreptococcaceae were most abundant in deltoid samples from donor 2 and found in a relatively low abundance at various time points in thigh muscle samples from donors 2 and 3.

Pseudomonadaceae abundance was quite variable between donors and by sample locations. From donor 1, it is found in a variable abundance (ranging from <10% to >50%) in mid to late deltoid samples and in a greater than 50% abundance in early thigh muscle samples.

Pseudomonadaceae is seen in a relatively high abundance in early buccal swab samples from donor 2. From the same donor, it is seen in a lower abundance in early deltoid and thigh samples. Finally, *Pseudomonadaceae* had a very low abundance in deltoid and thigh samples taken from donor 3 with a very small read (<5%) in deltoid samples at 189.96 ADD and in thigh muscle samples at 2219.29 ADD.

DNA that was unable to be assigned to a specific family of bacteria were exclusively found in muscle tissue samples from all three donors. The general trend indicated an inverse relationship between relative abundance and increasing ADD. *Wohlfahrtiimonadaceae* was almost exclusively found in increasing relative abundance in buccal swab samples taken from donor 2. Lastly, *Yersiniaceae* abundance was variable, most commonly being seen in small spikes around 200 - 250 ADD. However, there are some instances of low abundance being seen in later decomposition as well.

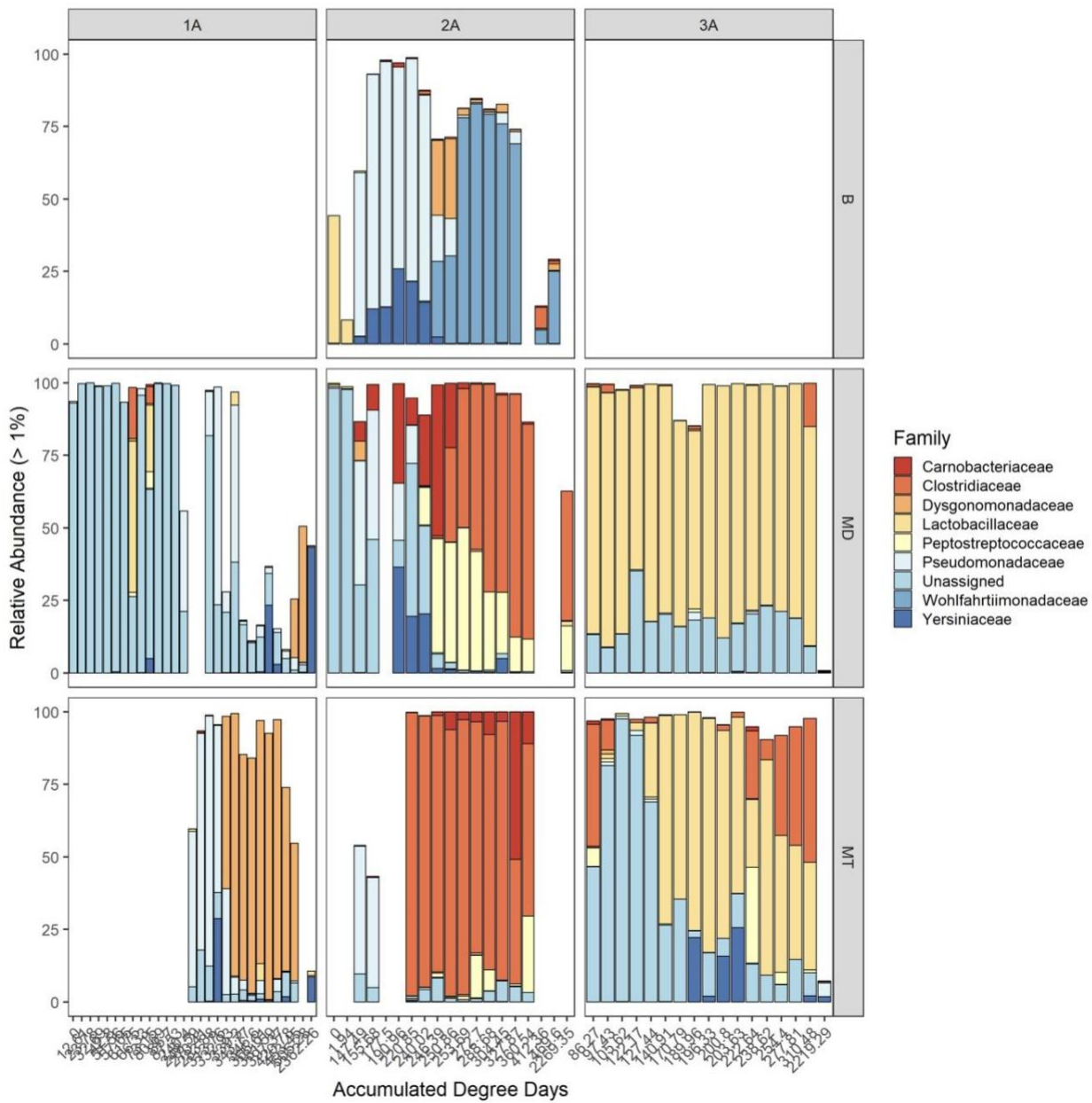


Figure 11: Taxa plot - family level. The relative abundance of each represented family (*Carnobacteriaceae*, *Clostridiaceae*, *Dysgonomonadaceae*, *Lactobacillaceae*, *Peptostreptococcaceae*, *Pseudomonadaceae*, unassigned, *Wohlfahrtiimonadaceae*, and *Yersiniaceae*) were graphed in terms of accumulated degree-days. Each column represents a donor and each row represents the sample site. The color of the bars is indicative of the family that represents the bacteria classified under that category.

Figure 12 represents the relative abundance of bacteria that fall under the genus level in terms of ADD, donor, and sample site. The relative abundance pattern of the genus level matches that of the higher order family level discussed in figure 11, so I will provide a brief overview here.

Carnobacterium was only seen in muscle tissue samples from donor 2, as well as *Clostridium*.

However, *Clostridium* also makes an appearance in thigh muscle tissue samples in donor 3.

Dysgonomonas is seen at a relatively high abundance in thigh muscle samples from donor 1 and in a relatively low abundance in deltoid samples taken from donor 1 and buccal samples from donor 2. *Dysgonomonas* was seen in a low relative abundance in late buccal samples (donor 2) and deltoid samples (donor 1) and at a high relative abundance in mid to late ADD thigh muscle samples from donor 1.

Ignatzschineria was exclusively found in buccal samples starting around 250 ADD and remained at a relatively high abundance for the remainder of the decomposition process. *Lactobacillus* was mainly seen in muscle samples taken from donor 3 and early buccal samples. The highest abundance of *Paeniclostridium* was found in deltoid samples from donor 2. *Pseudomonas* was found in differing abundance depending on the donor and the sample site. In general, it was found in its highest abundance in early samples and decreasing with progressing ADD. Finally, DNA that was not assigned to a specific bacterial genus was seen only in muscle tissue samples and followed a similar, but more extreme, pattern as *Pseudomonas* where it has an initially high relative abundance (sometimes ~99%) and decreases with increasing ADD.

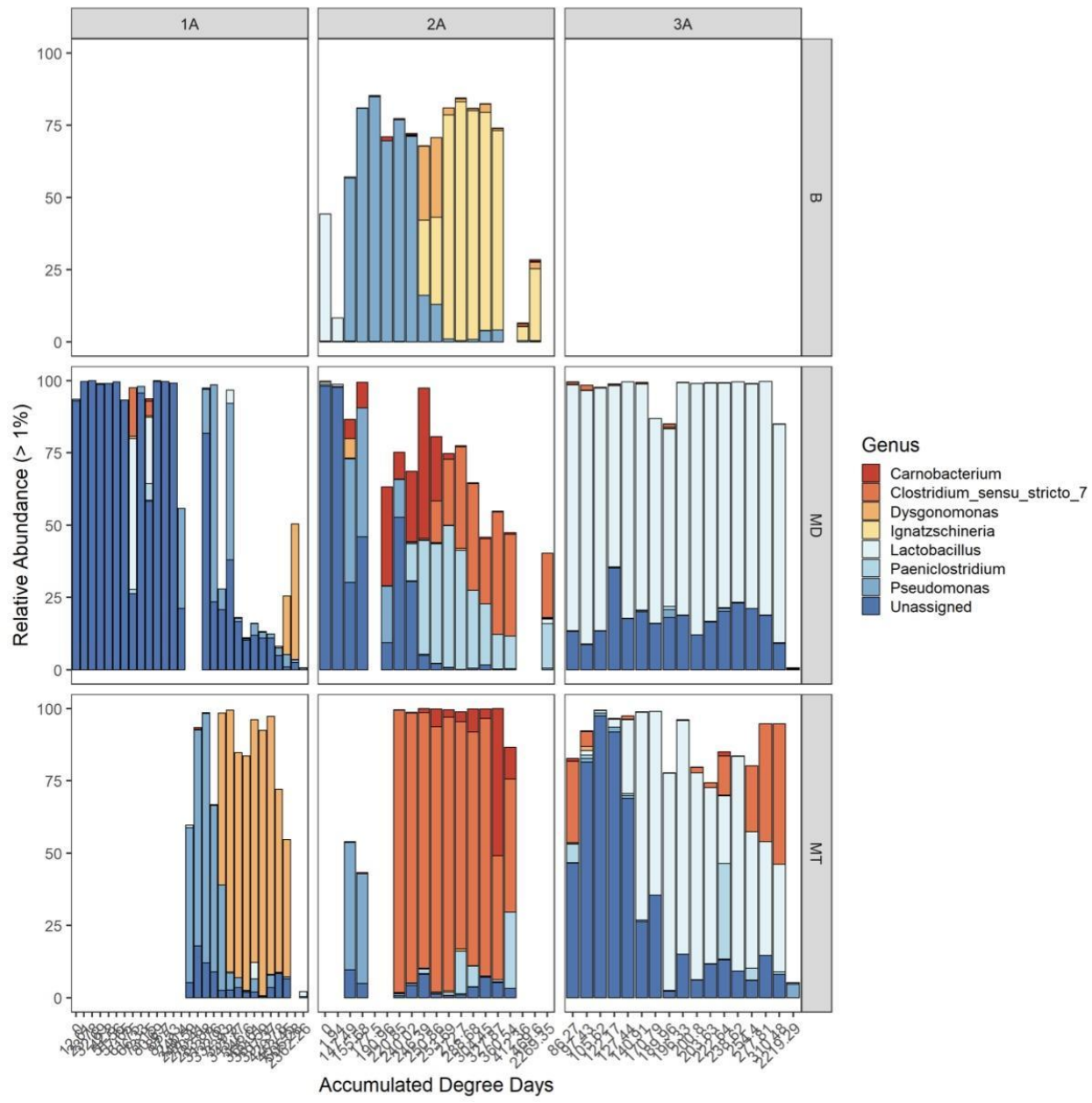


Figure 12: Taxa plot - genus level. The relative abundance of each represented genus (*Carnobacterium*, *Clostridium*, *Dysgonomonas*, *Ignatzschineria*, *Lactobacillus*, *Paeniclostridium*, *Pseudomonas*, and unassigned) were graphed in terms of accumulated degree-days. Each column represents a donor and each row represents the sample site. The color of the bars is indicative of the genus that represents the bacteria classified under that category.

Figure 13 details the relative abundance of four major phyla by date and by sample location. Since no thigh muscle samples were taken in 2019, it was omitted from this figure. The buccal samples were taken from donor 2 and the deltoid sample information was compiled from both donors 1 and 2. The most striking result is that of the unassigned DNA, seen only in muscle tissue samples and not at all in buccal samples. The other prominent result is that of *Firmicutes*; found in early November in buccal samples and in late October in deltoid samples. It is also worthy to note the lack of specific types of bacterial phyla in these samples. In buccal and deltoid samples taken in 2019, we do not see *Bacteriodota* and we see a very low abundance of *Proteobacteria* in deltoid samples.

However, when compared to figure 14, which details the relative abundance of the same four major bacterial phyla in samples taken from the oral cavity, deltoid, and the thigh in 2020, we see a drastic increase of *Proteobacteria* in buccal swab samples and a smaller, yet significant increase in deltoid and thigh muscle tissue samples. We also see the same finding of Unassigned DNA only in muscle tissue samples. *Bacteriodota* abundance varied with little discernible pattern, however, it was most abundantly found in thigh muscle samples. Finally, *Firmicutes* had a general trend of increasing as time progressed, but was most abundant in muscle tissue samples from the thigh and deltoid.

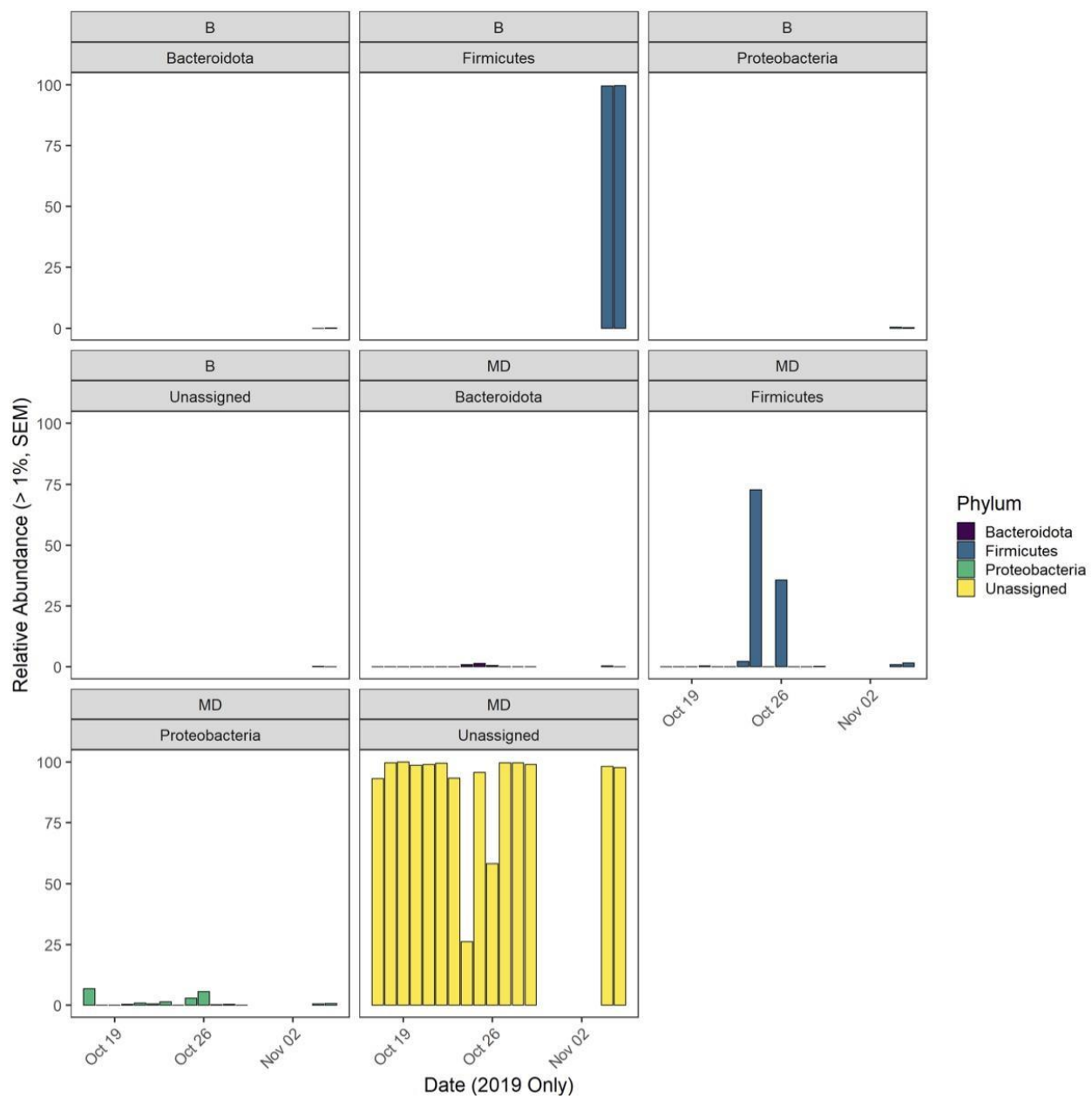


Figure 13: Relative abundance of major phyla by sample location (2019). The relative abundance of four major phyla (*Bacteroidata*, *Firmicutes*, *Proteobacteria*, and unassigned) found in specific sample locations (buccal or deltoid samples) for samples obtained in 2019. Buccal sample information is exclusively from donor 2 and the deltoid sample information is obtained and compiled from both donors 1 and 2.

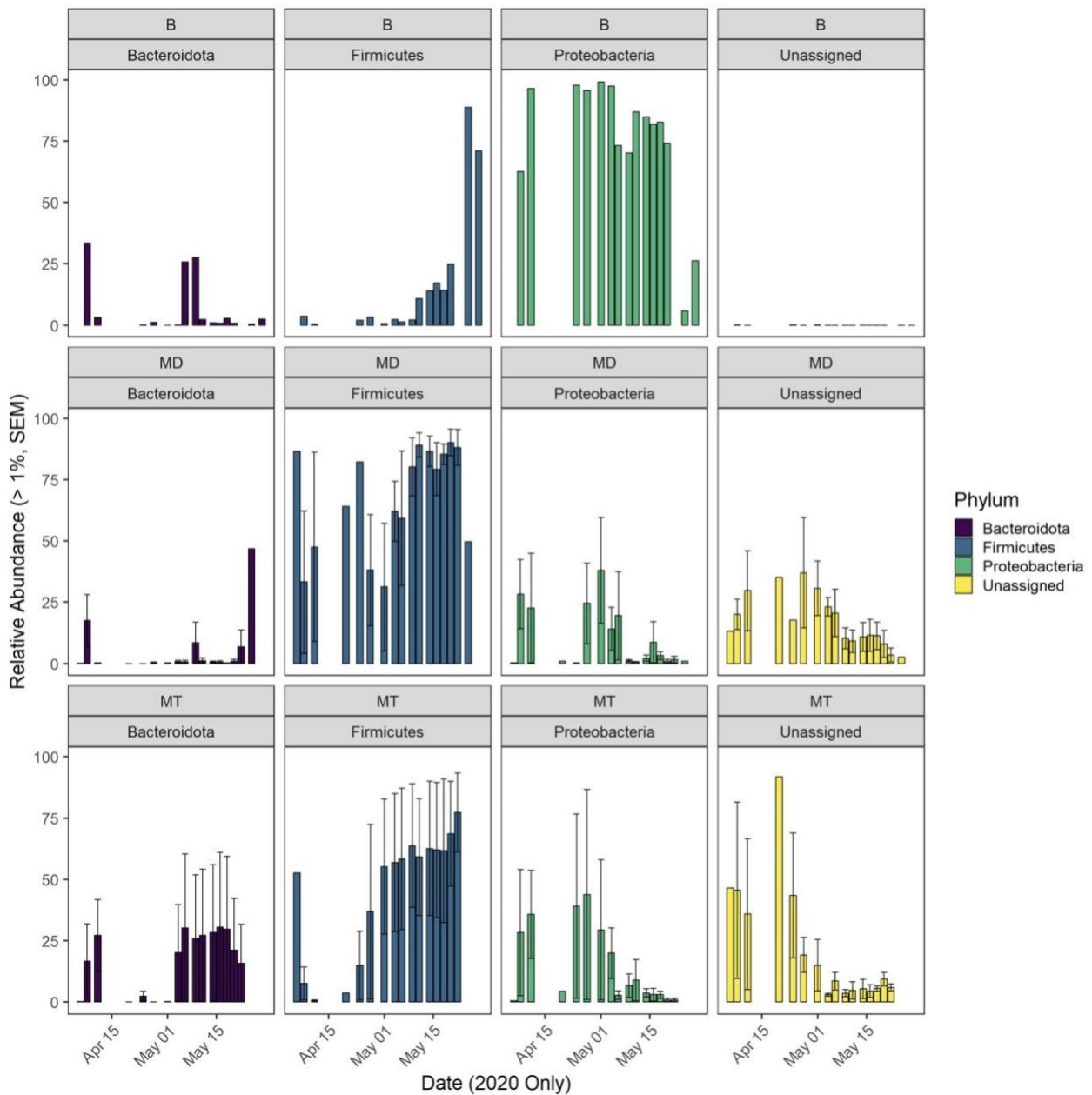


Figure 14: Relative abundance of major phyla by sample location (2020). The relative abundance of four major phyla (*Bacteroidata*, *Firmicutes*, *Proteobacteria*, and unassigned) found in specific sample locations (buccal, deltoid, and thigh muscle samples) for samples obtained in 2020. Buccal sample information is exclusively from donor 2 and deltoid and thigh muscle sample information is obtained and compiled from donors 1, 2, and 3.

Figure 15 details the relative variance of bacterial families by sample location using a beta dispersion plot. The beta dispersion plot assesses the diversity of the bacterial families in terms of sample location by using a spatial median (centroid) set by the amalgamation of all sample data generated from this study. The closer the median falls to the centroid, the less diverse the bacterial population. Conversely, the further the data points are from the centroid, the more diverse. The smaller the box, the less diversity within the interquartile range (IQR); the bigger the box, the more diversity within the IQR. Outliers are signified by a single dot above or below the maximum or minimum values, respectively (more than 1.5 X IQR above or below the 25th percentile).

Figure 15 shows the most bacterial diversity appearing in muscle tissue samples taken from the deltoid as evidenced by the relatively large IQR and the mean furthest from the centroid. Following deltoid samples, thigh muscle tissue samples were the next most variable in terms of bacterial family diversity, followed by buccal swab samples.

Similarly, figure 16 uses the same means to determine bacterial community diversity, however, it is measuring variance at the genus level. Here, we see a high variance among buccal swab samples, and low variance among deltoid and thigh muscle tissue samples, with thigh muscle samples being slightly more diverse than deltoid samples.

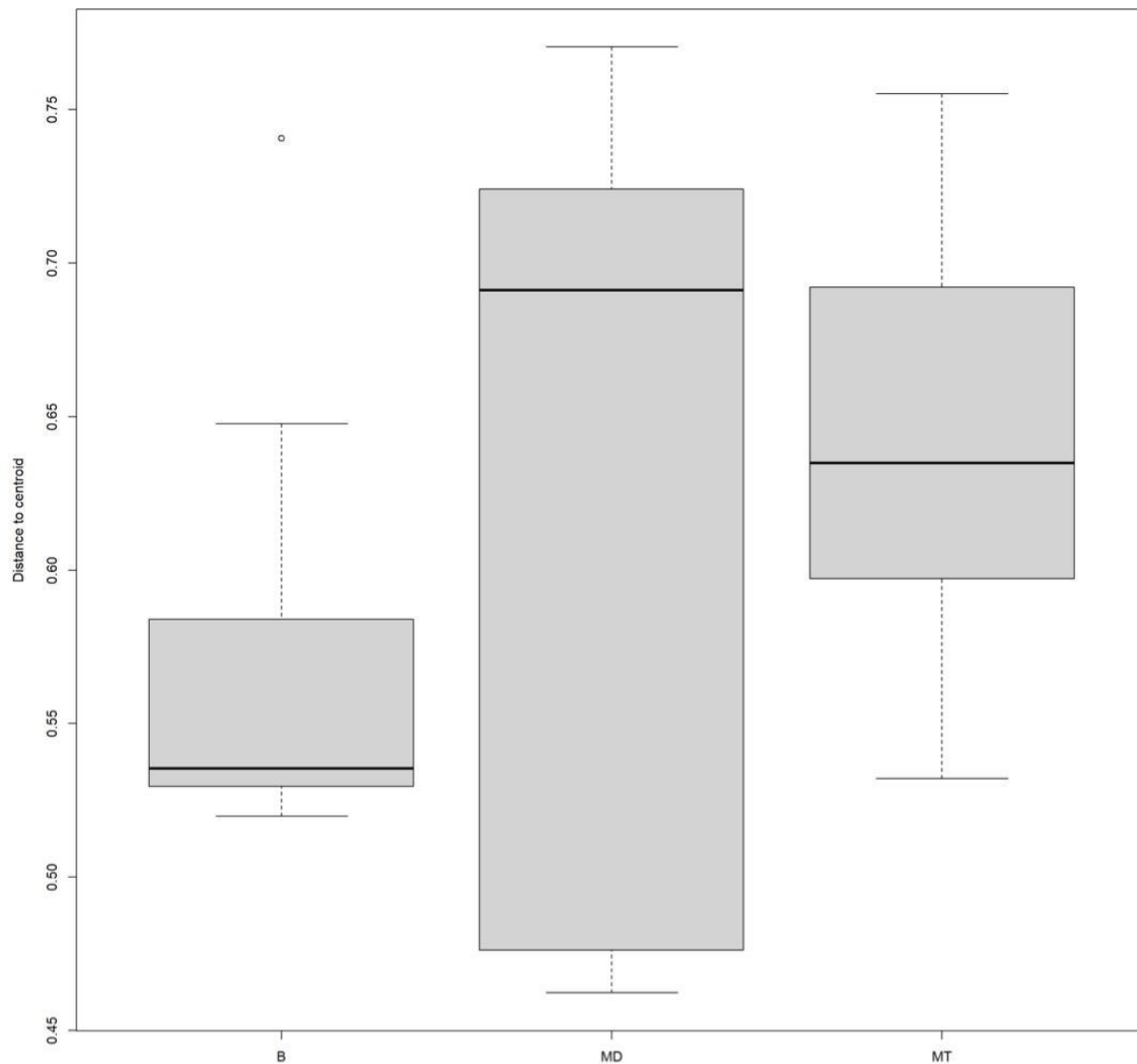


Figure 15: Relative variation of bacterial organisms at the family level by sample location.
All family-level information from all samples and from all time points was collated into a single data set. The sequencing information from specific sample sites (buccal swab, deltoid, and thigh muscle tissue samples) was then compared to the entire data set by means of a non-metric dissimilarity coefficient (the distance to centroid).

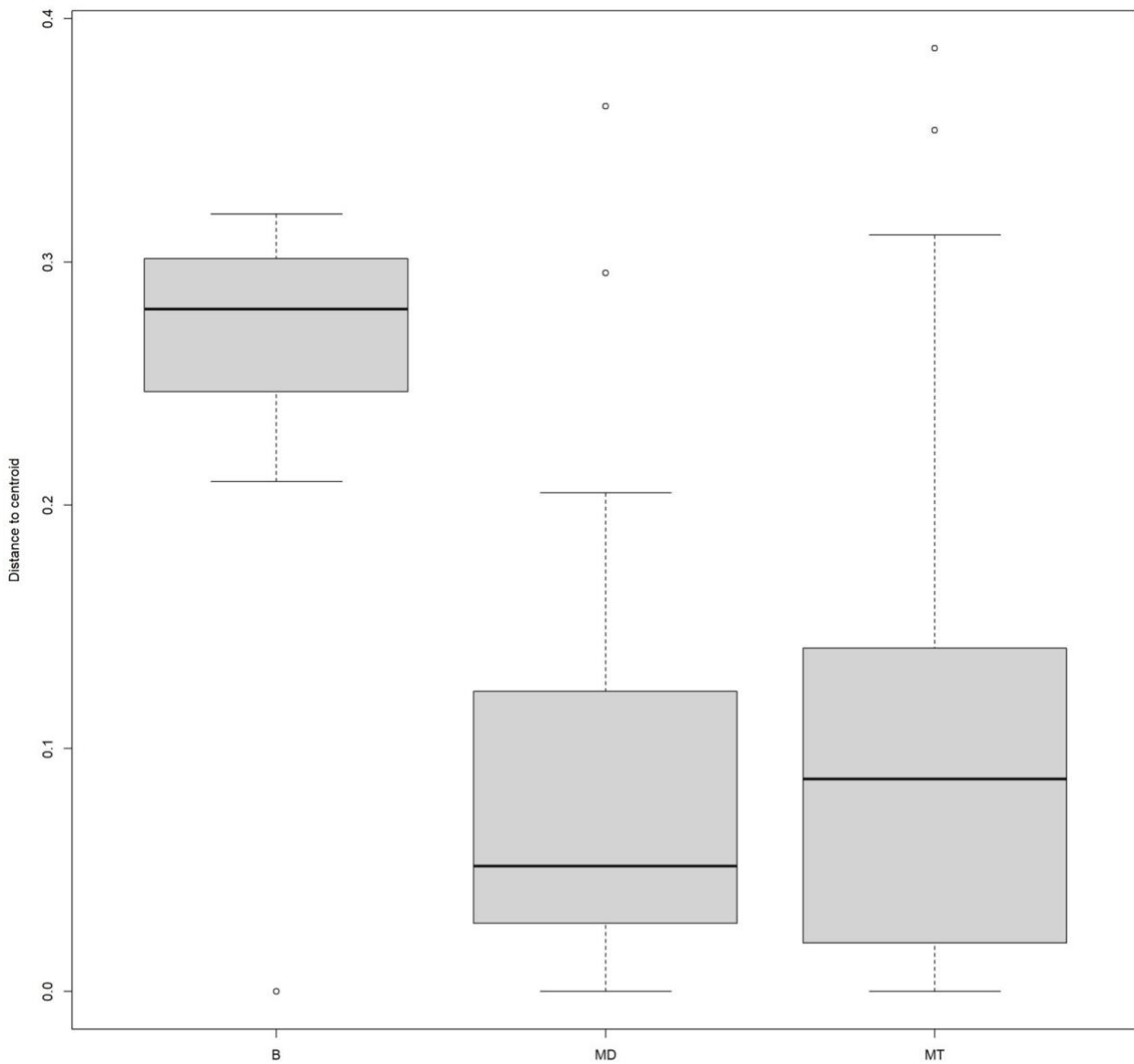


Figure 16: Relative variation of bacterial organisms at the genus level by sample location.
 All genus-level information from all samples and from all time points was collated into a single data set. The sequencing information from specific sample sites (buccal swab, deltoid, and thigh muscle tissue samples) was then compared to the entire data set by means of a non-metric dissimilarity coefficient (the distance to centroid).

Figure 17 explains the relative variance of bacterial families by donor using a beta dispersion plot. As mentioned previously, all sequencing information was compiled to form a spatial median or centroid used to measure variance of specific data sets off of. In this particular figure, donor 3 had a relatively large IQR and maximum values, however, the majority of the bacterial family diversity fell close to the centroid (specified by the mean value) indicating that the majority of the families sequenced from donor 3 were of relatively low diversity compared to the entire data set. Donor 2 had the most variance in diversity, closely followed by donor 3.

Figure 18 details the relative variance of bacterial genera by donor using the beta dispersion plot. Similar to the family level, donor 2 had the most variance in diversity, followed by donor 1 and donor 3.

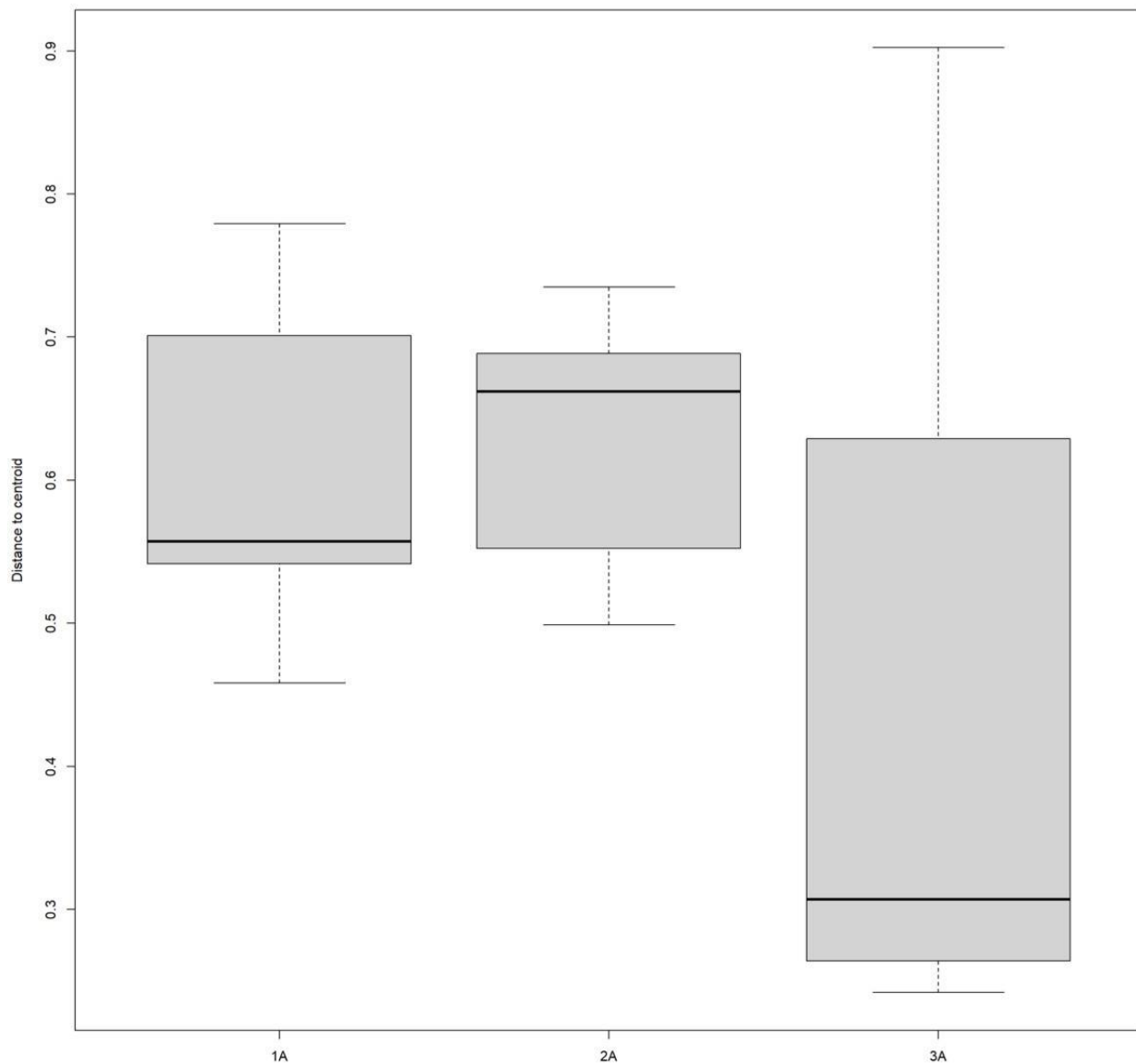


Figure 17: Relative variation of bacterial organisms at the family level by donor. All family-level information from all samples and from all time points was collated into a single data set. The sequencing information from specific donors (1A, 2A, and 3A) was then compared to the entire data set by means of a non-metric dissimilarity coefficient (the distance to centroid).

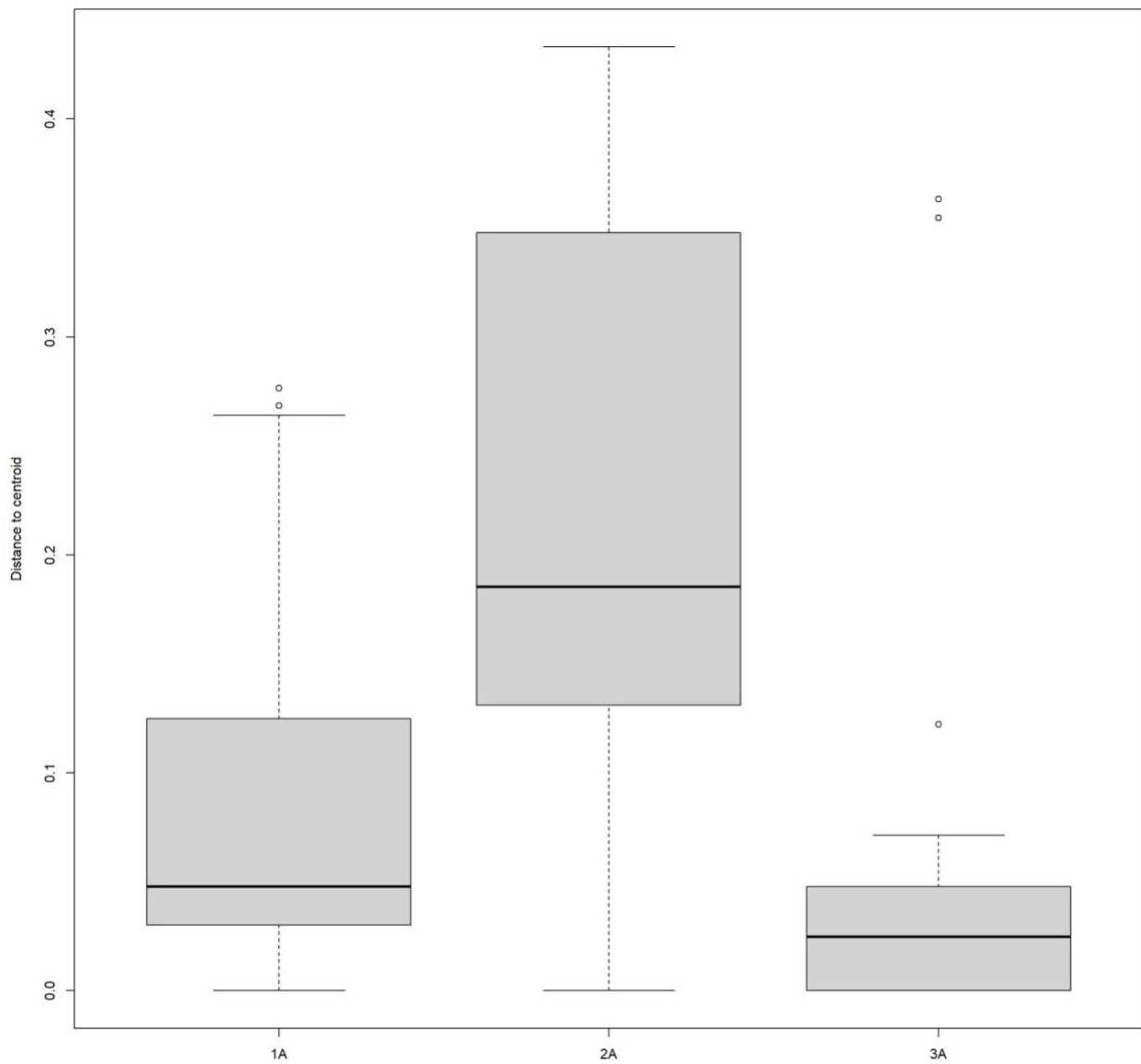


Figure 18: Relative variation of bacterial organisms at the genus level by donor. All genus-level information from all samples and from all time points was collated into a single data set. The sequencing information from specific donors (1A, 2A, and 3A) was then compared to the entire data set by means of a non-metric dissimilarity coefficient (the distance to centroid).

Figure 19 explains the relative variance of bacterial families by date using a beta dispersion plot. As mentioned previously, all sequencing information was compiled to form a spatial median or centroid used to measure variance of specific data sets off of. In this data set, all sequencing information from a specific date was compiled from all three donors and compared to the entire data set for all donors, sample sites, and dates.

From April 11th to August 30th, there was little variation in the diversity of the bacterial families present during that time frame. Outliers include dates around April 6th, April 19th, May 25th, and May 28th. For each of these samples, there was very little diversity in the bacterial species found in the samples as indicated by a non-existent IQR and maximum and minimum values. However, the variance of the bacterial species found in the samples ranged from being a relatively common occurring bacterial family to being slightly more common than the rest of the data set, as indicated by the mean value in relation to the distance to centroid.

Figure 20 explains the relative variance of bacterial genera by date using a beta dispersion plot. As mentioned previously, all sequencing information was compiled to form a spatial median or centroid used to measure variance of specific data sets off of.

Similar to results seen in figure 19, bacterial genera variation was relatively consistent over time with slightly more variation in genus level sequencing data, comparatively. The same dates mentioned above (April 6th, April 19th, May 25th, and May 28th) all show similar results in the diversity and variation of bacterial genera present during those dates. One interesting finding from samples taken very late in decomposition (August 30th) showed that there was a significant increase in the variance of bacterial genera present in samples taken on that date. This is signified by the increased distance to centroid compared to the rest of the data set.

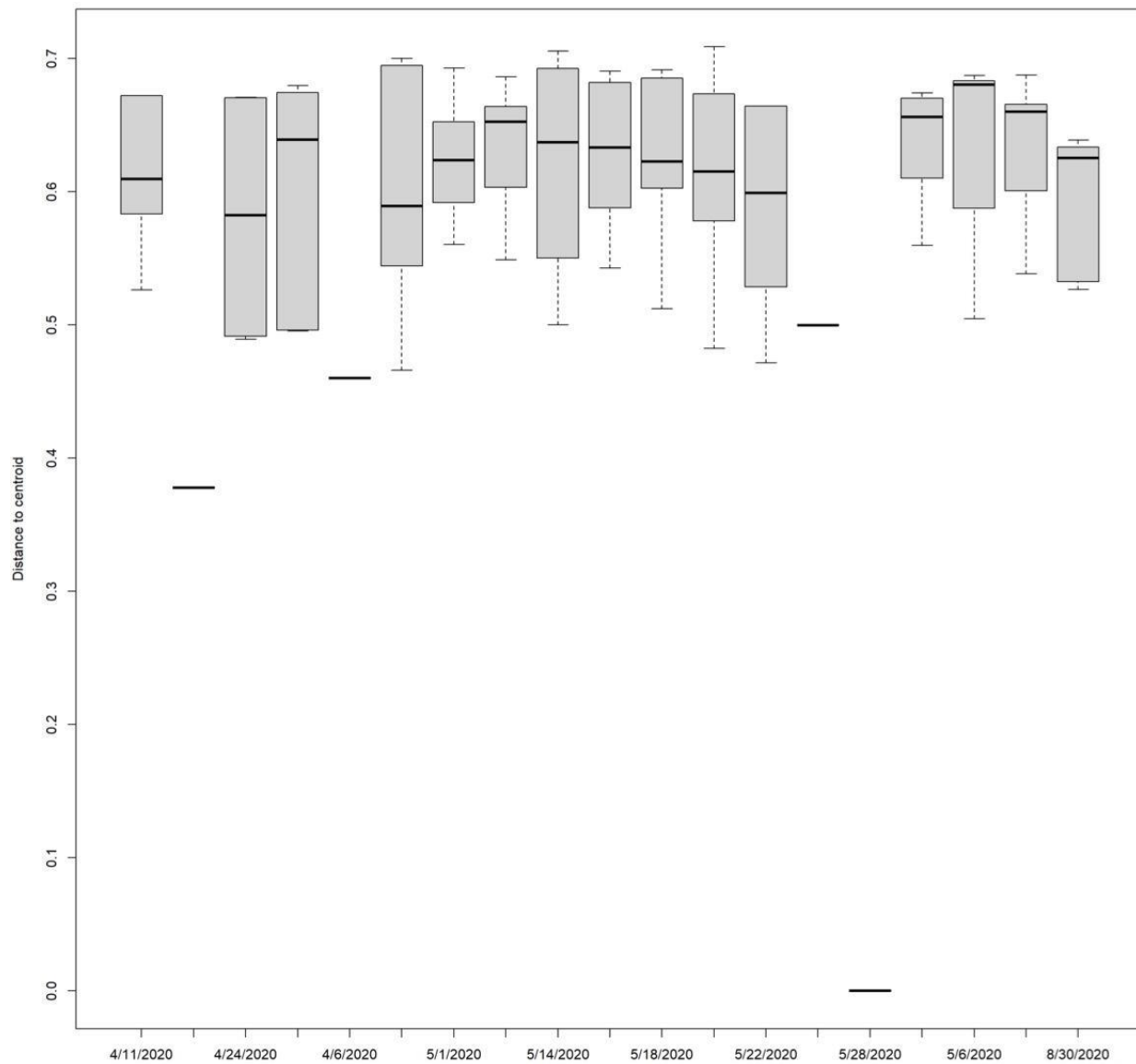


Figure 19: Relative variation of bacterial organisms at the family level by date. All family-level information from all samples and from all time points was collated into a single data set. The sequencing information from specific dates was then compared to the entire data set by means of a non-metric dissimilarity coefficient (the distance to centroid).

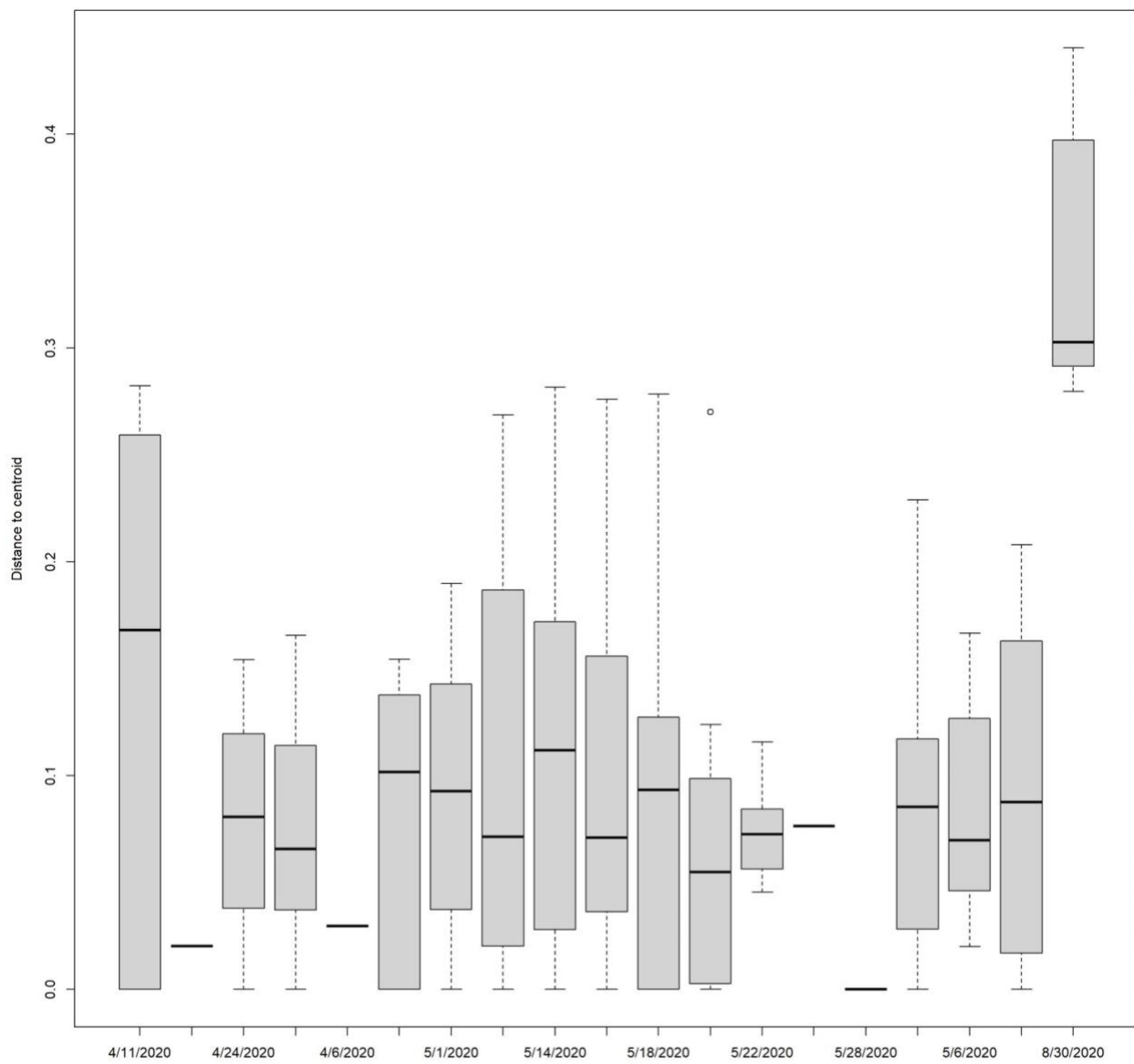


Figure 20: Relative variation of bacterial organisms at the genus level by date. All genus-level information from all samples and from all time points was collated into a single data set. The sequencing information from specific dates was then compared to the entire data set by means of a non-metric dissimilarity coefficient (the distance to centroid).

Figure 21 is a principal coordinates analysis plot (PCoA plot) detailing the variance in bacterial family composition by date and tissue type. The distance between data points in both axis directions is indicative of the percent variance between samples. The percent variance was calculated and generated via R and is a non-Euclidean means to measure the variance between samples.

As seen in figure 21, groups of samples can be parsed from this data set. For example, groups of thigh muscle tissue samples taken in May can be seen in the upper and lower left hand corners of the graph. Groups of deltoid samples taken in May can be seen in the middle left side of the graph as well as the middle right side of the graph. Finally, groups of buccal swab samples taken in May can be found in the middle left of the graph. While it is important to note the groupings of specific samples, it is also important to note the outliers. The majority of the outliers are samples taken of thigh muscle tissue; seen as a scattering of data points throughout the graph. A smaller number of outliers consist of deltoid samples.

Interestingly, very little pattern can be discerned from figure 22 showing a PCoA plot detailing the variance of bacterial genera composition in terms of sample site and date. There are small groupings of buccal swab samples noted in the middle top and middle left of the graph and a larger grouping of deltoid and thigh muscle tissue samples seen in the very middle of the graph. However, most data points appear to be randomly scattered throughout the graph, indicating that the sequencing data for the genus level is more varied between samples, especially muscle tissue samples.

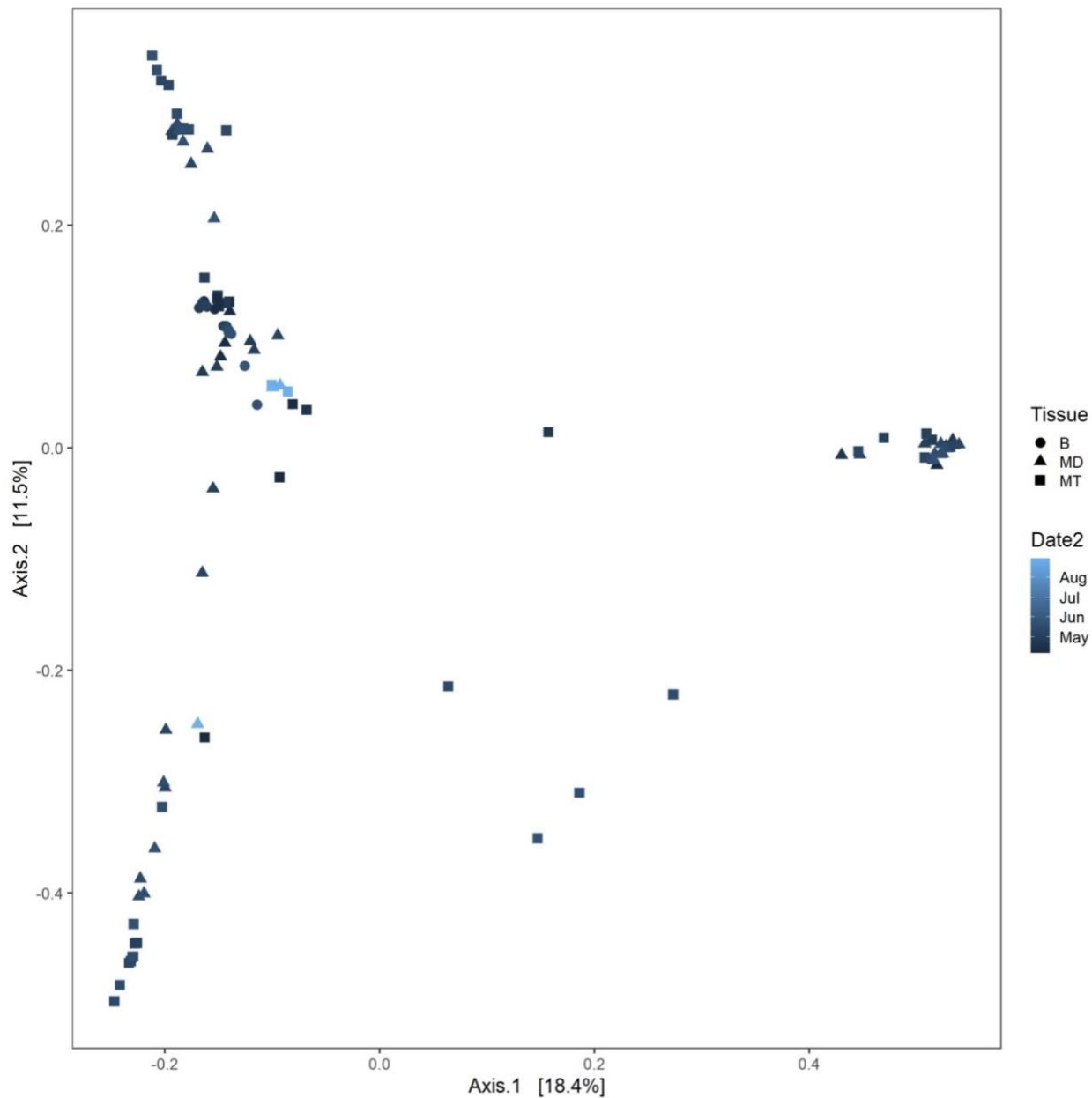


Figure 21: Principal coordinates analysis plot (PCoA plot) of samples by date and tissue type (family level). Sequencing information from specific sample sites (buccal swab, deltoid, and thigh muscle tissue samples) was correlated to the date the sample was taken (May through August) and graphed into a coordinate plane based on the percent variance between the samples.

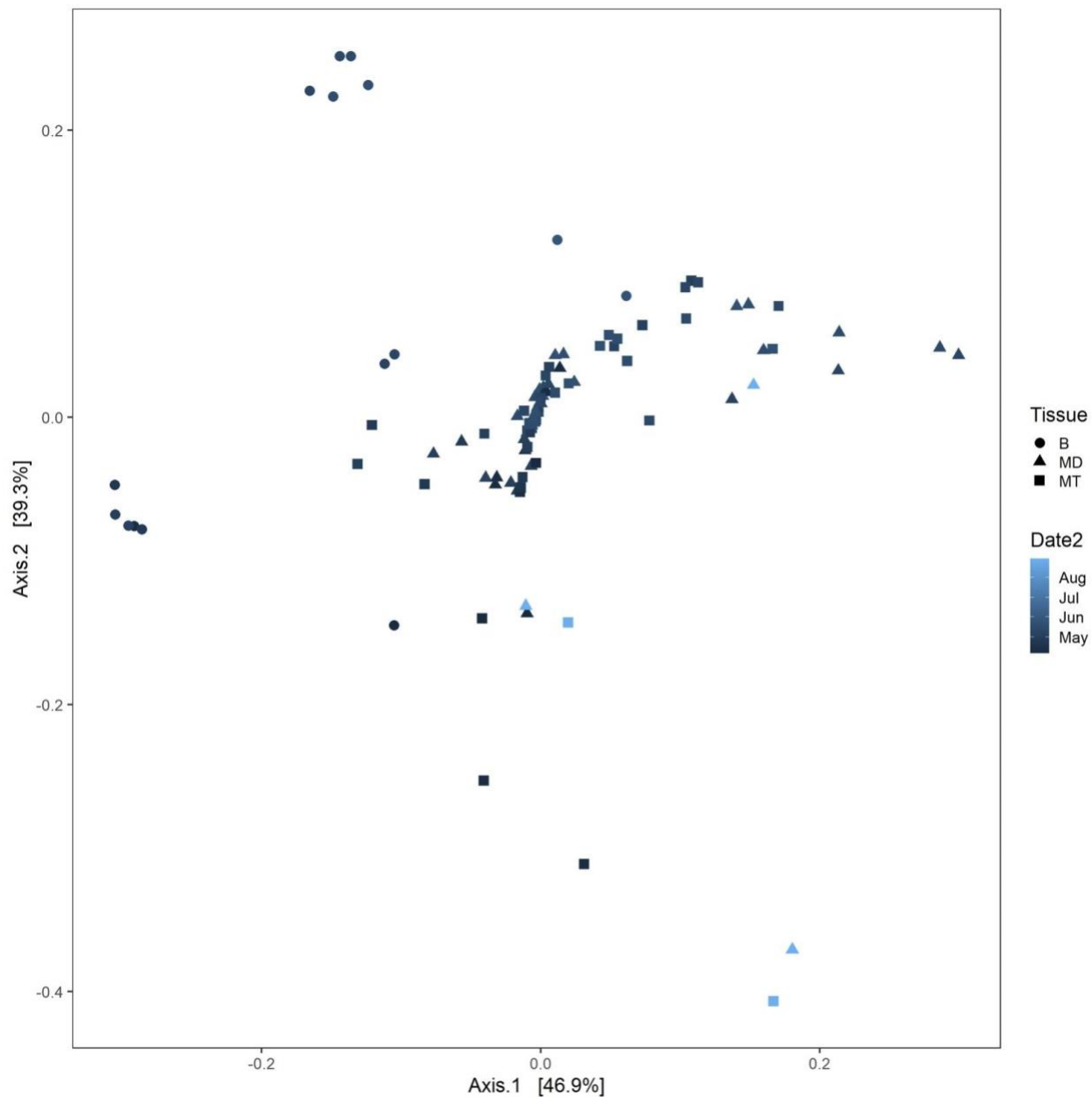


Figure 22: Principal coordinates analysis plot (PCoA plot) of samples by date and tissue type (genus level). Sequencing information from specific sample sites (buccal swab, deltoid, and thigh muscle tissue samples) was correlated to the date the sample was taken (May through August) and graphed into a coordinate plane based on the percent variance between the samples.

Figures 23 and 24 use the Random Forest™ data analysis algorithm from R to select the most important bacterial genus for predicting sample site location (figure 23) or donor (figure 24). All of the sequencing information generated from this study was amassed and the sample site location data or the donor data was compared to the entire data set and used for this evaluation. This data analysis tool uses mean decrease accuracy or permutation importance to quantitate the importance of each prediction; the higher the mean decrease accuracy, the better the prediction.

Figure 23 details the most important genus in determining sample site location or which tissue the sample came from. The most important predictor for this series is the DNA considered unassigned followed by *Clostridium sensu stricto* 7, *Dysgonomonas*, and *Streptococcus*; all other genera were very similar in importance.

Figure 24 details the most important genus in determining which donor a sample came from. In this case, *Lactobacillus* was the most important predictor followed by *Carnobacterium*, *Clostridium sensu stricto* 7, Unassigned, and *Leuconostoc*; all other genera were very similar in importance.

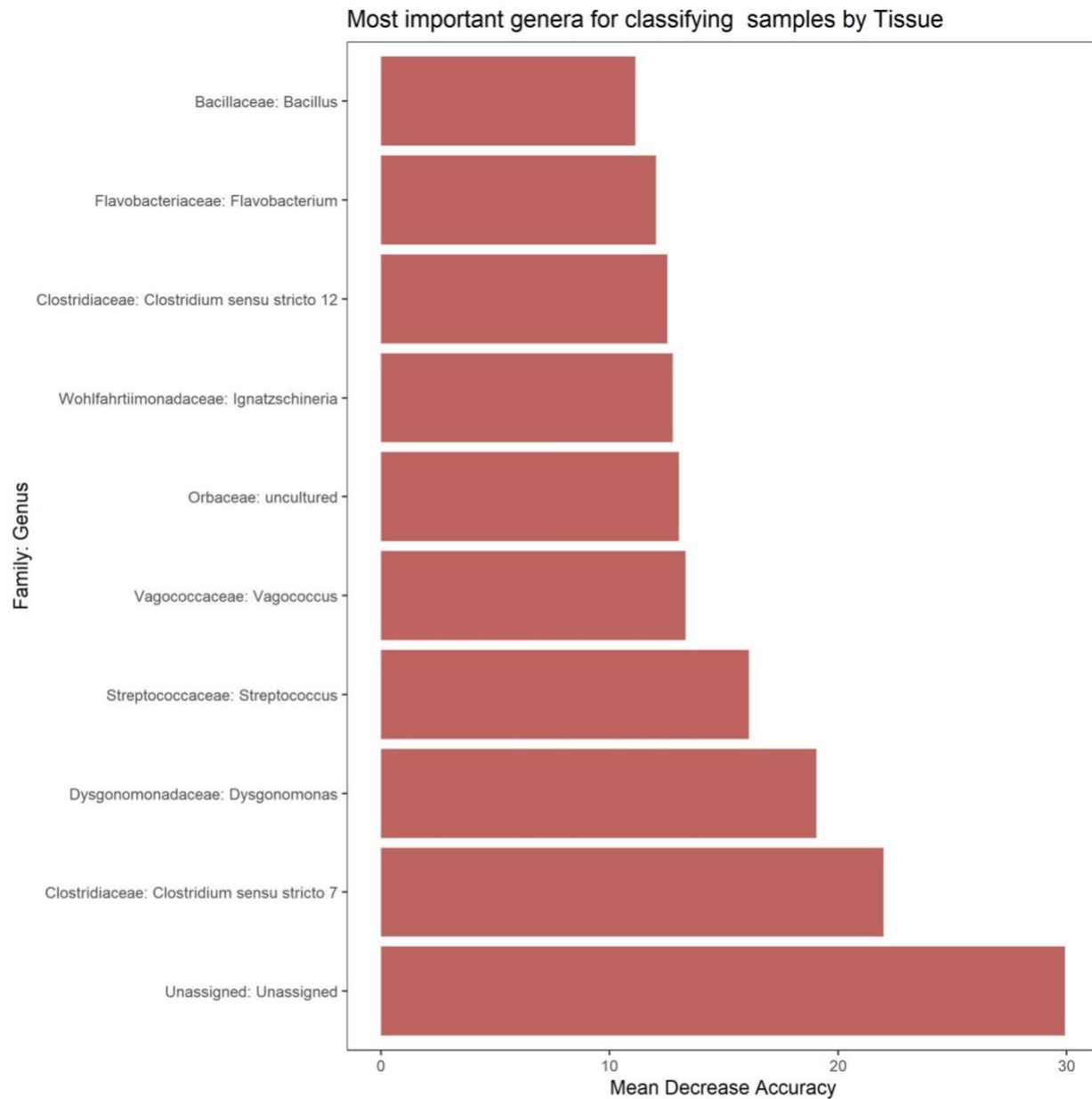


Figure 23: Most important genera for classifying samples by tissue type. Using the “Random Forest™” data analysis algorithm from R, aggregates of sequencing information were sampled and selected based on the ability of the bacterial genus to predict sample site location. The importance of the bacterial genus in predicting sample location was measured using mean decrease accuracy (permutation importance); how much the accuracy of the model decreases when the specific variable is discarded.

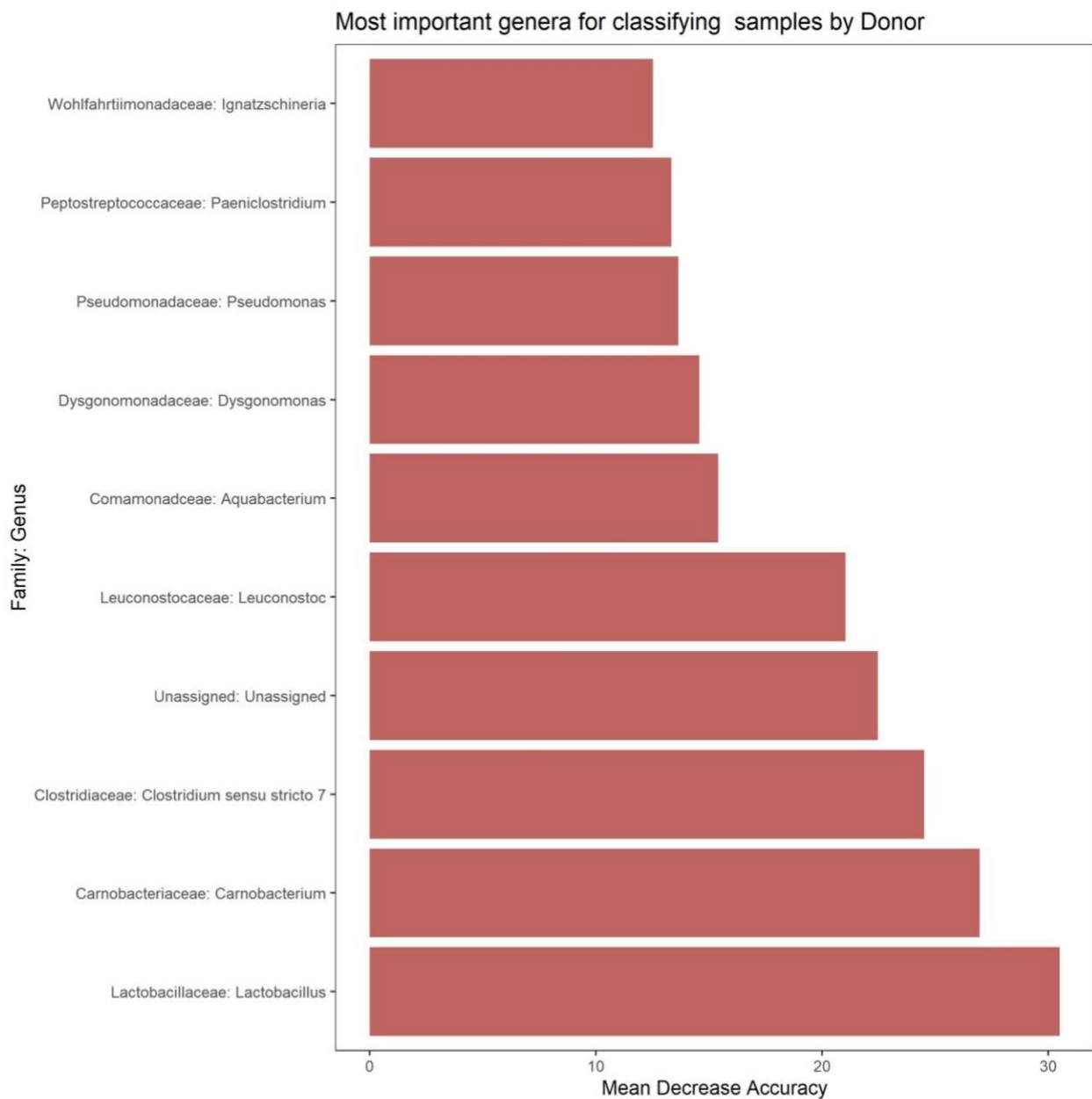


Figure 24: Most important genera for classifying samples by donor. Using the “Random Forest™” data analysis algorithm from R, aggregates of sequencing information were sampled and selected based on the ability of the bacterial genus to predict donors. The importance of the bacterial genus in determining donor was measured using mean decrease accuracy (permutation importance); how much the accuracy of the model decreases when the specific variable is discarded.

Figure 25 details the relative abundance of specific bacterial genera in terms of tissue sample location. All sequencing information from each sample site and from all donors was compiled together to form the standard that these specific values were then compared to. Note that the Y axis value ranges vary between each genus sequencing information based on the abundance of the species in relation to the entire data set.

Genera indicative of buccal swab samples include *Ignatzschineria* (~28% relative abundance), *Streptococcus* (~3.5% relative abundance), uncultured (~1.25% relative abundance), and *Vagococcus* (~1.5% relative abundance). When compared to the other sample site locations (deltoid and thigh muscle tissue samples), the aforementioned bacterial genera were not found.

Genera indicative of deltoid muscle tissue samples include *Clostridium sensu stricto 12* (~2% relative abundance), *Flavobacterium* (~0.75% relative abundance), *Hathewaya* (~0.4% relative abundance), and unassigned (~35% relative abundance). When compared to other sample types, *Clostridium sensu stricto 12* was not found in major abundance in buccal samples or thigh muscle samples. *Flavobacterium* was not found in buccal samples, but was found in thigh muscle tissue samples at about 0.25% relative abundance compared to 0.75% relative abundance in the deltoid samples. *Hathewaya* was not found in buccal samples, but was found at a low abundance in thigh samples (~0.1% relative abundance) compared to about 0.4% in deltoid samples. DNA in the unassigned category was not found in buccal samples, but was found at a relatively high abundance in thigh muscle samples (~15% relative abundance) compared to about 35% relative abundance in deltoid samples.

Finally, genera indicative of thigh muscle tissue samples include *Clostridium sensu stricto 7* (~22% relative abundance) and *Dysgonomonas* (~15% relative abundance). When compared to

the other sample locations, *Clostridium sensu stricto* 7 was not found in buccal swab samples, but was found at about 4% relative abundance in deltoid muscle tissue samples. *Dysgonomonas* was found at a ~4% relative abundance in buccal samples and at about a 2% relative abundance in deltoid muscle tissue samples.

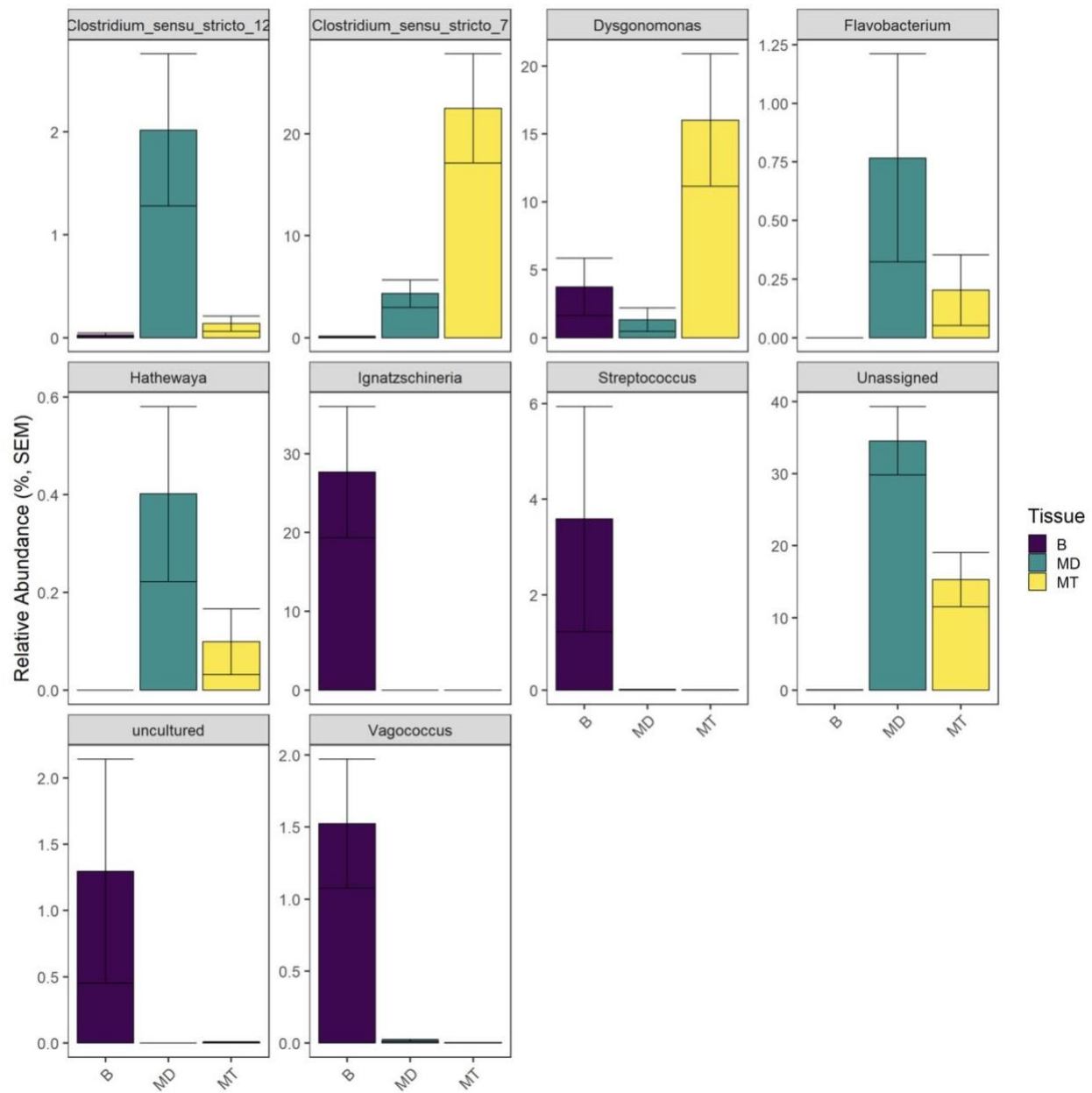


Figure 25: Relative abundance of bacterial genera by tissue type. The relative abundance of each bacterial genera (*Clostridium_sensu_stricto_12*, *Clostridium_sensu_stricto_7*, *Dysogomononas*, *Flavobacterium*, *Hathewaya*, *Ignatzschineria*, *Streptococcus*, *Unassigned*, *Uncultured*, *Vagococcus*) were measured and aggregated from all donors in terms of sample location (buccal swab (B) [purple], deltoid (MD) [green], and thigh muscle (MT) [yellow] tissue samples).

Figure 26 details the relative abundance of specific bacterial genera in terms of donor. All sequencing information from each sample site and from all donors was compiled together to form the standard that these specific values were then compared to. Note that the Y axis value ranges vary between each genus sequencing information based on the abundance of the species in relation to the entire data set.

Genera indicative of donor 1 (1A) include *Dysgonomonas* (~18% relative abundance), *Pseudomonas* (~14% relative abundance), and DNA falling under the unassigned category (~35% relative abundance). When compared to the other donors, *Dysgonomonas* was found at a very low relative abundance in donor 2 (<2%) and not found in donor 3. *Pseudomonas* was found in a similar abundance in donor 2 (~15%) and in a very low abundance in donor 3 (<1%). DNA under the unassigned category was found in all three donors: donor 2 (~10% relative abundance) and donor 3 (~25% relative abundance).

Genera indicative of donor 2 (2A) includes *Carnobacterium* (~5% relative abundance), *Clostridium sensu stricto* 7 (~23% relative abundance), *Ignatzschineria* (~10% relative abundance), *Paeniclostridium* (~7.5% relative abundance), *Pseudomonas* (~15% relative abundance), and unassigned (~10% relative abundance). When compared to other donors, *Carnobacterium* and *Ignatzschineria* were not found in other donors. *Clostridium sensu stricto* 7 was not found in donor 1, but was found in a low relative abundance in donor 3 (~4%). *Paeniclostridium* was not found in donor 1, but was found in a relatively low abundance in donor 3 (~1%). *Pseudomonas* and unassigned DNA were found in all three donors, mentioned above.

Genera indicative of donor 3 (3A) includes *Aquabacterium* (~0.075% relative abundance), *Lactobacillus* (~58% relative abundance), *Leuconostoc* (~1.5% relative abundance), and

unassigned (~25% relative abundance). When compared to other donors, *Aquabacterium*, *Lactobacillus*, and *Leuconostoc* were not found at a significant abundance in donors 1 or 2 and DNA in the unassigned category was found in all three donors, mentioned above.

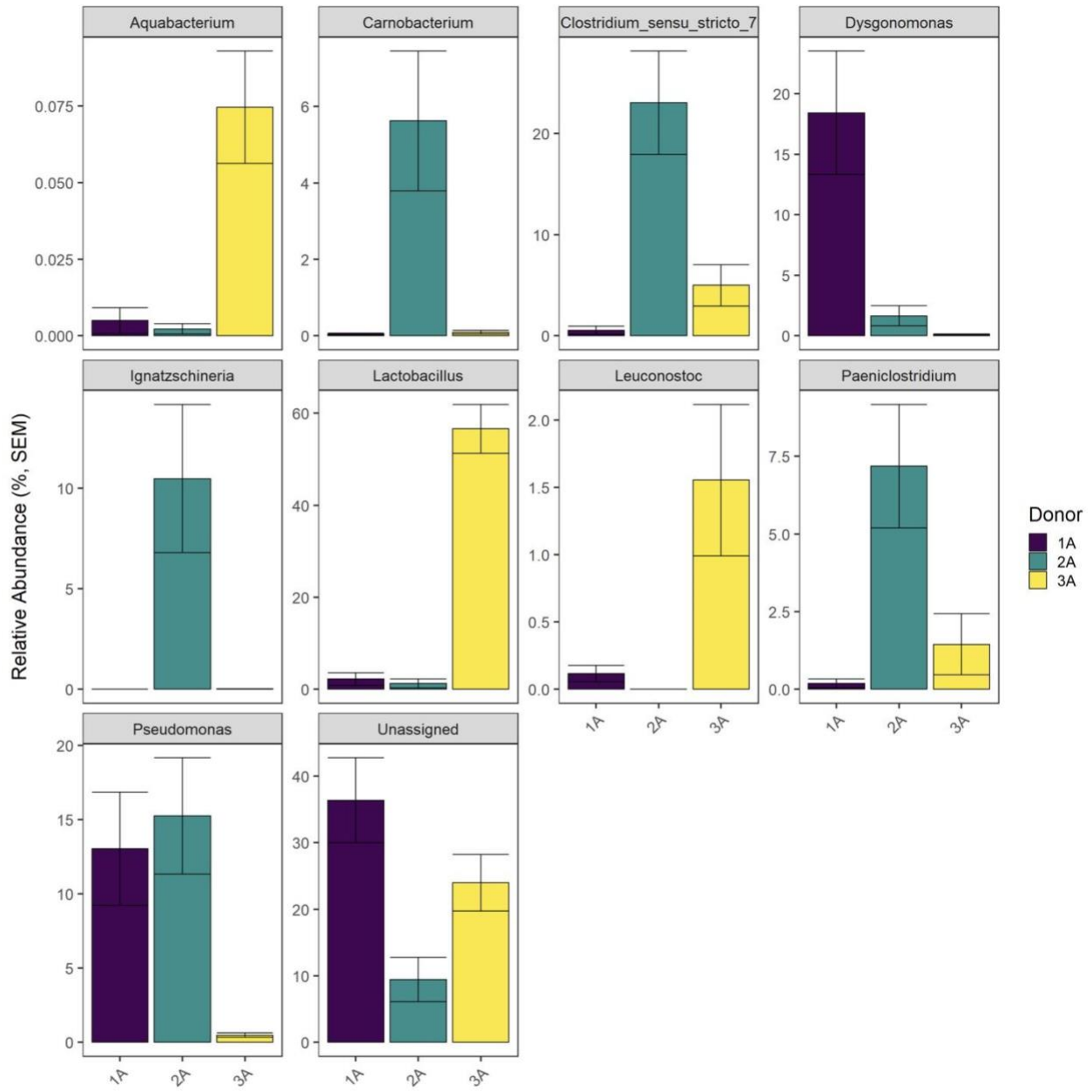


Figure 26: Relative abundance of bacterial genera by donor. The relative abundance of each bacterial genera (*Aquabacterium*, *Carnobacterium*, *Clostridium_sensu_stricto_7*, *Dysgonomonas*, *Ignatzschineria*, *Lactobacillus*, *Leuconostoc*, *Paeniclostridium*, *Pseudomonas*, and unassigned) were measured and aggregated from all sample sites in terms of donors (donor 1 (1A) [purple], donor 2 (2A) [green], and donor 3 (3A) [yellow]).

Chapter 6: Discussion

DNA Isolation and Purification

Based on the NanoDrop concentration and purity results, both the proof-of-concept and the preliminary testing of the samples show very similar results. The concentration of DNA in the samples did not show a trend based on the sample site, likely because DNA isolation was not specific to prokaryotic DNA, rather any DNA, whether prokaryotic or eukaryotic, was extracted. The 260/280 ratio results indicated that the purity of the extracted nucleic acids was within the normal range of about 1.8, while the 260/230 ratio indicated that there was possible contamination of muscle tissue proteins that were not adequately filtered out during the purification step.

Polymerase Chain Reaction and Gel Electrophoresis

PCR and gel electrophoresis results for the muscle tissue samples all showed evidence of successful prokaryotic DNA amplification based on the presence of a band at 360 bp. The results also showed an interesting trend in the strength of the bands as time progressed. Shortly after death, one would expect that there would be very little, if any, bacteria present in the muscle tissue. As decomposition progresses, bacteria from the skin, gut, insects, scavengers, and the environment are introduced into the tissues. This would account for the strengthening of the bands as decomposition progressed, indicating that there are relatively little bacteria present in early samples and progressively more as decomposition ensues.

The results for the buccal swabs showed that there was a consistent amount of prokaryotic DNA detection based on visual assessment of the gel. In contrast to the muscle tissue samples, the oral

cavity is home to many different species of bacteria, the mouth is also unrestricted to environmental and insect-associated bacteria, validating the results seen in figure 6.

Next Generation 16s rRNA Sequencing

By Time, Temperature, and ADD

Donors one and two were placed within two weeks of one another in mid-October and early-November, respectively, just a few weeks before freezing temperatures set in. During the few weeks before freezing, the weather conditions ranged between 10 °C to -10 °C; mostly staying around refrigeration temperatures. Once freezing temperatures and snowfall set in, it was around five months before temperatures reached above freezing and sample collection could be resumed.

Donor three was placed in the middle of winter (late-January) and was not able to be accessed for sampling until the spring thaw in early April. Between January and April, the temperature remained below freezing and no sample collection took place.

The bacterial community variance remained relatively consistent over time with the exception of a few specific outliers mentioned previously. However, samples taken at a very late time point (August 30th; ~2220 ADD) showed a significant increase in bacterial diversity as seen in the beta dispersion plots and a lack of any significantly abundant bacteria as seen in the taxa plots. This could be due to the fact that the muscle tissue at this time was fully exposed to the environment, allowing insect, scavenger, air, and environmental microbes access to the sample site.

By Sample Site Location

In general, buccal swabs showed the most significant increase in bacterial community diversity and richness with increasing ADD as well as the presence of a few bacterial genera exclusively found here. *Ignatzschineria*, a bacterial genus associated with insects (4), was exclusively found in buccal samples starting at an initially low relative abundance and rising over increasing ADD. *Pseudomonas*, an environmental microbe (31), was also found in its highest abundance in early buccal samples.

The presence of mainly insect-associated microbes and environmental-associated microbes in the oral cavity is easily explained by the exposure of the oral cavity to the environment compared to the muscle tissue samples which were protected from environmental and insect exposure with surgical dressings. Insects transfer bacteria from their microbiome to decaying tissues as well as bacteria picked up from the environment. When these bacterial organisms are introduced, they also become a part of the necrobiome and influence decomposition.

Relative variance in the number of bacterial genera did not differ significantly in deltoid and thigh muscle tissue samples between donors or between themselves. Thigh muscle samples had slightly more variance compared to deltoid samples. However, one specific finding in muscle tissue samples became quite interesting: sequenced DNA that was unable to be assigned to a specific bacterial origin.

The unassigned DNA was likely DNA that was amplified from human mitochondria, which is abundantly present in muscle and has DNA sequences originating from ancient prokaryotic organisms (32). This notion is further supported by the fact that none of the four major databases used to categorize the sequenced DNA could match these sequences to a particular bacterium and it is unlikely that we have discovered a new and highly abundant bacterial genus. Finally,

these DNA reads only came from muscle tissue samples and not from buccal samples, supporting the idea that this is a mitochondrial DNA sequence that is being detected.

Another interesting finding is the elevated presence of gut-associated microbes specifically in thigh muscle tissue samples. Gut-associated microbes such as *Dysgonomonas*, *Carnobacterium*, *Lactobacillus* and *Clostridium* (*Clostridium* is considered both an environmental and a gut-associated microbe (33)) were largely found in thigh muscle tissue samples in all three donors.

The presence of gut-associated microbes in the thigh muscle samples is explained by the purging process just following the bloat stage and the positioning of the donors when placed. First, the purging process expels fluids from the abdomen. Some of the fluids travel through blood vessel and nerve tracts into the tissues of the thigh. Secondly, the donors are placed on a slight incline, positioning the head slightly higher than the feet. Gravity also allows the fluids from the abdomen to travel into the lower extremities.

By Donor

The richness of bacterial species did not differ significantly between donors. In general, the diversity and variability between samples taken from each donor followed a relatively similar pattern, with donor 1 having slightly more diversity in bacterial species than donor 3; possibly due to the placement timing (donor one had a few weeks where bacterial growth could occur before freezing, donor 3 did not). However, donor 2 had a significantly increased bacterial community diversity resulting from buccal sample information, only done for donor 2 due to situational factors.

It is important to note that diet, lifestyle, medical history, and many other factors can influence an individual's microbiome, which can drastically affect the initial microbial community following death. Hence, the initial results of this study. Medical information for each donor, found in Appendix A can be useful in determining the reason behind the individual necrobiome variances mentioned below.

There were a few bacterial genera that were exclusively found in a specific donor which is postulated to be from individual innate microbiome variances between different people with different lifestyles and causes of death. For example, *Dysgonomonas* was mainly found in samples taken from donor 1, more specifically, mainly from thigh muscle samples with a small abundance found in deltoid samples. *Dysgonomonas* is an anaerobic genus that can cause gastroenteritis in immunocompromised patients (34). This donor had multiple procedures done in the abdominal region that could be responsible for this finding.

Paeniclostridium was almost exclusively found in deltoid samples from donor 2. Some *Paeniclostridium* species are potentially pathogenic bacteria associated with a number of severe infections in humans such as gastrointestinal (GI) infections, toxic shock, and soft tissue infection. Other species are benign, but not normally found in the human GI tract (35). This donor did not have any outwardly appearing medical conditions that could be responsible for this finding, however, medical history could be an important factor in this case as well.

Carnobacterium was exclusively found in donor 2 muscle tissue samples. *Carnobacterium* is a microbe associated with food products; mainly dairy, meat, and fish (36). It is possible that this individual's diet could have introduced this microbe into their gut microbiota.

General Sample Information

When samples were graphed at the family level based on their similarity or dissimilarity to each other, groups of samples could be parsed from the entire data set. In theory, these samples could be categorized as hailing from a specific donor due to the similarity in bacterial DNA sequencing information. The bacterial families present in the samples would be relatively similar over time, especially coming from the same sample site, so it would be expected that a PCoA plot would show these samples grouped together. At the genus level, very little grouping patterns could be discerned, possibly due to the wider diversity of genus-level sequencing information.

Being able to parse sample information and match it to a specific donor or sample site is a crucial factor in identifying bacterial markers.

When analyzed for bacterial markers for sample site location, predictably, unassigned DNA was the most important predictor; the presence indicating a muscle tissue sample. Looking closer, unassigned DNA was a better predictor of deltoid samples than thigh muscle samples, most likely due to a higher abundance of bacterial species present in the thigh muscle samples presumably from purging events.

The second-best predictor for sample site location was *Clostridium sensu stricto* 7, mostly found in thigh muscle samples. As mentioned previously, *Clostridium* is a microbe associated with both the human gut and the environment. In this case, it is expected to be a gut-associated microbe because of the location and the timing of when it appeared and became most abundant.

The terminology referring to *Clostridium* species (ie: sensu stricto) arises from the fact that this family is composed of a very large and complex grouping of bacteria. Based on 16s rRNA

sequencing, the genera are roughly categorized, however, the categorization still varies drastically. “Sensu stricto” translates from Latin as “strictly speaking or in a narrow sense (37).” In this application, sensu stricto refers to true members of the genus *Clostridium*, not the genera that are loosely categorized using phylogenetic analysis (38).

Although considered less important, *Ignatzschineria* was an important predictor of buccal samples and *Clostridium sensu stricto* 12 was an important predictor of deltoid samples.

When analyzed for bacterial markers for donor identification, *Lactobacillus* was the most important predictor. *Lactobacillus* was almost exclusively found in donor 3, likely due to the diet and lifestyle of that specific donor. *Lactobacillus* is a lactic acid bacterium, normally a part of a healthy gut microbiome. As noted in Appendix A, donor 3’s cause of death was due to acute trauma and not because of an illness which likely kept the gut flora intact. The general appearance of donor 3 also indicated that they lived a healthy and active lifestyle, also bolstering the premise of finding beneficial gut microbiota.

In further support of this argument, *Leuconostoc* is another lactic acid bacterium associated with a healthy gut microbiome and healthy diet and lifestyle. *Leuconostoc* was another important indicator of donor 3; although it was the fourth most important predictor.

The second most important bacterial marker for donor identification was *Carnobacterium*. *Carnobacterium* was most indicative of donor 2. As mentioned previously, this bacterium could have been present due to a specific diet.

Although considered less important, *Dysgonomonas* was an important predictor of donor 1.

In Conclusion

The aforementioned relates necrobiome succession throughout the decomposition process to patterns in time, temperature, ADD, bacterial markers for sample site location and donor identification and, in all, PMI. Using this information, some key points can be conveyed.

Determining individual microbiome/necrobiome differences could be useful for sample identification in medicolegal death investigations. Further, knowing and understanding the succession patterns within specific tissues could further help indicate PMI.

The ability to parse sample sequencing information and match it to a specific donor or sample site is a crucial factor in identifying bacterial markers. Specific bacterial markers, whether unique to the subject or in general, could be critical in subject identification or timeline identification.

Specific bacterial species only present during illness (ie: bacterial infections) can be detected using these means, which could provide information about the subject. These species could also be used as important markers for medical history or possibly lifestyle factors.

Lastly, we have gained a glimmer of understanding of when specific environmental microbes appear in muscle tissue samples during the process of cold weather decomposition as it relates to ADD, arguably the most important factor in relation to PMI.

Future Directions

Further research in this field is needed to bolster the sample size and gain more generalized information on bacterial community composition during specific time points and the necrobiome succession throughout decomposition in cold weather environments.

Samples taken immediately after death could give a better insight to the initial innate microbiome of specific individuals. These differences could be used to advance our understanding of how specific bacterial species influence the process of decomposition.

Finally, further research into how cold weather affects the microbial community at any point in the decomposition process helps to better predict PMI based on necrobiome changes that occur throughout the decomposition process.

APPENDICES

Appendix A: General Donor Information

Donor 1

Date-of-Death	10/11/2019
Date-of-Placement	10/17/2019
Sex	Female
Age-at-Death	65
Height	5'5"
Weight	185 lbs
Cause of Death	COPD, DVT/BC Lower Extremities
Manner of Death	Natural
Hospitalized	Yes: more than one week prior to death
Medical Interventions	Tracheostomy, colostomy, three IVs (2 in Left arm, 1 in Right arm)
Antibiotics (Immediately prior to death)	No Information
Buccal Samples	Fluid from digestive tract in oral cavity precluded ability to collect samples
Cecum Samples	Fluid in abdomen precluded ability to collect samples
Muscle Samples (Deltoid/Thigh)	Collected consistently from 10/17/2019 through 05/25/2020 (except for months when donor was frozen due to winter weather conditions); one late-stage sample collected on 08/30/2020

Donor 2

Date-of-Death	11/02/2019
Date-of-Placement	11/04/2019
Sex	Female
Age-at-Death	67
Height	5'4"
Weight	170 lbs
Cause of Death	Lewy Body Dementia
Manner of Death	Natural
Hospitalized	No Information
Medical Interventions	None
Antibiotics (Immediately prior to death)	No Information
Buccal Samples	Collected consistently from 11/04/2019 through 05/25/2020 (except for months when donor was frozen due to winter weather conditions); one late-stage sample collected on 08/30/2020

Cecum Samples	Freezing conditions precluded ability to collect samples
Muscle Samples (Deltoid/Thigh)	Collected consistently from 11/04/2019 through 05/25/2020 (except for months when donor was frozen due to winter weather conditions); one late-stage sample collected on 08/30/2020

Donor 3

Date-of-Death	01/17/2020
Date-of-Placement	01/24/2020
Sex	Female
Age-at-Death	80
Height	5'6"
Weight	110 lbs
Cause of Death	Multiple Blunt Force Injuries/Motor Vehicle Accident
Manner of Death	Accident
Hospitalized	No
Medical Interventions	None
Antibiotics (Immediately prior to death)	No
Buccal Samples	Head trauma precluded ability to collect samples
Cecum Samples	Freezing conditions precluded ability to collect samples
Muscle Samples (Deltoid/Thigh)	Collected consistently from 04/06/2020 through 05/22/2020; one late-stage sample collected on 08/30/2020

Appendix B: Full Sample Data Sheets

Donor 1

Donor 1		Placement Date: 10/17/2019		Incision site: R deltoid & R thigh														
Sampling						Storage		DNA Extraction		NanoDrop				PCR		Sample		
Sample	Date collected	Size of punch	Time taken?	Pictures taken?	TBS	Weather condition	Special notes	Temp of storage	Weight (mg)	Date of DNA extraction	Temp of storage (°C)	Concentration (ng/μL)	260/280 ratio	260/230 ratio	16s rRNA PCR positive?			
1-MD-1A	10/17/2019	8mm	11:00 AM	yes	yes	Slight rain	Donor placed. Start of skin slippage.	-80	32.8	6/10/2020	-20	112.4	1.8	1.89	none	1-MD-1A		
2-MD-1A	10/18/2019	8mm	9:00 AM	yes	yes	partial cloudy		-80	30.8	6/10/2020	-20	111.1	1.83	2.91	low	2-MD-1A		
3-MD-1A	10/19/2019	8mm	9:15 AM	yes	yes	Sunny		-80	22.5	6/10/2020	-20	179.3	1.82	2.38	low	3-MD-1A		
4-MD-1A	10/20/2019	8mm	9:00 AM	yes	yes	Sunny	Less swelling in fingers & toes	-80	29.6	6/10/2020	-20	222	1.82	2.23	none/low	4-MD-1A		
5-MD-1A	10/21/2019	8mm	9:00 AM	yes	yes	partial cloudy	More skin slippage under breast & on R wrist	-80	24	6/11/2020	-20	45.3	1.82	0.19	low	5-MD-1A		
6-MD-1A	10/22/2019	8mm	11:00 AM	yes	yes	Rain	adipose between toes?	-80	27	6/11/2020	-20	43.9	1.81	0.59	low	6-MD-1A		
7-MD-1A	10/23/2019	8mm	10:30 AM	yes	yes	partial cloudy	Significant slippage under breast. Slippage on shoulder, arm, wrist, clavical area.	-80	24	6/11/2020	-20	46.8	1.81	0.59	low	7-MD-1A		
8-MD-1A	10/24/2019	8mm	9:00 AM	yes	yes	partial cloudy/sunny	R hand degloving starting	-80	26	6/24/2020	-20	57.3	1.79	2.19	medium	8-MD-1A		
9-MD-1A	10/25/2019	8mm	11:30 AM	yes	yes	Sunny		-80	27	6/11/2020	-20	34.9	1.81	0.36	low	9-MD-1A		
10-MD-1A	10/26/2019	8mm	10:00 AM	yes	yes	Sunny		-80	25	6/24/2020	-20	28.7	1.8	2.73	low	10-MD-1A		
11-MD-1A	10/27/2019	8mm	10:00 AM	yes	yes	Sunny		-80	20	6/11/2020	-20	37.8	1.82	0.25	medium	11-MD-1A		
12-MD-1A	10/28/2019	8mm	9:30 AM	yes	yes	Sunny		-80	29	6/11/2020	-20	44.6	1.82	0.23	medium	12-MD-1A		
13-MD-1A	10/29/2019	8mm	11:00 AM	yes	yes	Snow	First snowfall.	-80	21	6/11/2020	-20	38.2	1.83	0.09	low	13-MD-1A		
Post Freezing		Post Freezing		Post Freezing		Post Freezing		Post Freezing		Post Freezing		Post Freezing		Post Freezing		Post Freezing		
174-MD-1A	4/8/2020	8mm	9:30	yes	OC	Sunny	Partially covered with snow	-80	22	6/11/2020	-20	45.2	1.85	0.5	low	174-MD-1A		
174-MT-1A RIPA	4/8/2020	Punch	9:30	yes	OC	no	Sunny	-20	For Austrian Group							174-MT-1A RIPA		
177-MD-1A	4/11/2020	8mm	9:30	yes	OC	Sunny		-80	22	6/11/2020	-20	185.6	1.82	0.85	low	177-MD-1A		
177-MT-1A	4/11/2020	8mm	9:30	yes	OC	no	Sunny	-80	22	6/24/2020	-20	238.8	1.81	1.04	medium	177-MT-1A		
177-MT-1A RIPA	4/11/2020	8mm	9:30	yes	OC	no	Sunny	-20	For Austrian Group							177-MT-1A RIPA		
190-MT-1A	4/24/2020	punch	9:30	yes	OC	no	Sunny	After another frozen period	-80	23	6/15/2020	-20	85.4	1.82	2.11	low	190-MT-1A	
190-MT-1A RIPA	4/24/2020	punch	9:30	yes	OC	no	Sunny	-20	For Austrian Group							190-MT-1A RIPA		
193-MD-1A	4/27/2020	6mm	9:30	yes	OC	no	Sunny	-80	23	6/15/2020	-20	144.5	1.83	1.55	low	193-MD-1A		
193-MT-1A	4/27/2020	punch	9:30	yes	OC	no	Sunny	-80	29	6/15/2020	-20	136.4	1.82	1.73	low/medium	193-MT-1A		
193-MT-1A RIPA	4/27/2020	Punch	9:30	yes	OC	no	Sunny	-20	For Austrian Group							193-MT-1A RIPA		
197-MD-1A	5/1/2020	6mm	9:30	yes	OC	no	Sunny	-80	30	6/15/2020	-20	187.3	1.83	1.36	low/medium	197-MD-1A		
197-MT-1A	5/1/2020	punch	9:30	yes	OC	no	Sunny	-80	27	6/15/2020	-20	109.8	1.83	2.41	medium	197-MT-1A		
197-MT-1A RIPA	5/1/2020	punch	9:30	yes	OC	no	Sunny	-20	For Austrian Group							197-MT-1A RIPA		
200-MD-1A	5/4/2020	6mm	9:30	yes	OC	no	cloudy	-80	26	6/15/2020	-20	66.5	1.83	2.55	medium	200-MD-1A		
200-MD-1A	5/4/2020	punch	9:30	yes	OC	no	cloudy	-80	22	6/15/2020	-20	82.8	1.83	1.82	medium	200-MD-1A		
200-MT-1A RIPA	5/4/2020	punch	9:30	yes	OC	no	cloudy	-20	For Austrian Group							200-MT-1A RIPA		
202-MD-1A	5/6/2020	punch	1:30	yes	yes	sunny		-80	27	6/15/2020	-20	132.8	1.83	1.84	low/medium	202-MD-1A		
202-MD-1A	5/6/2020	punch	1:30	yes	yes	sunny		-80	24	6/15/2020	-20	103.8	1.81	0.28	medium	202-MD-1A		
202-MT-1A RIPA	5/6/2020	punch	1:30	yes	yes	sunny		-20	For Austrian Group							202-MT-1A RIPA		
205-MD-1A	5/9/2020	punch	9:30	no	no	sunny		-80	21	6/15/2020	-20	90	1.81	1.17	medium	205-MD-1A		
205-MT-1A	5/9/2020	punch	9:30	no	no	sunny		-80	24	6/15/2020	-20	130.6	1.83	2.42	medium/high	205-MT-1A		
205-MT-1A RIPA	5/9/2020	punch	9:30	no	no	sunny		-20	For Austrian Group							205-MT-1A RIPA		
207-MD-1A	5/11/2020	punch	9:30	no	no	sunny		-80	21	6/15/2020	-20	64.8	1.8	0.27	medium	207-MD-1A		
207-MT-1A	5/11/2020	punch	9:30	no	no	sunny		-80	23	6/16/2020	-20	78.3	1.82	0.66	medium/high	207-MT-1A		
207-MT-1A RIPA	5/11/2020	punch	9:30	no	no	sunny		-20	For Austrian Group							207-MT-1A RIPA		
210-MD-1A	5/14/2020	punch	2:50	no	no	sunny		-80	23	6/16/2020	-20	139.2	1.83	1.14	medium	210-MD-1A		
210-MT-1A	5/14/2020	punch	2:50	no	no	sunny		-80	25	6/16/2020	-20	81.5	1.82	1.58	medium/high	210-MT-1A		
210-MT-1A RIPA	5/14/2020	punch	2:50	no	no	sunny		-20	For Austrian Group							210-MT-1A RIPA		
212-MD-1A	5/16/2020	punch	9:30	no	no	sunny		-80	23	6/16/2020	-20	134.4	1.83	1.08	medium/high	212-MD-1A		
212-MT-1A	5/16/2020	punch	9:30	no	no	sunny		-80	22	6/16/2020	-20	47.3	1.79	0.26	high	212-MT-1A		
212-MT-1A RIPA	5/16/2020	punch	9:30	no	no	sunny		-20	For Austrian Group							212-MT-1A RIPA		
214-MD-1A	5/18/2020	punch	9:30	no	no	sunny		-80	24	6/16/2020	-20	109.4	1.83	1.92	high	214-MD-1A		
214-MT-1A	5/18/2020	punch	9:30	no	no	sunny		-80	24	6/24/2020	-20	128.8	1.81	2.45	high	214-MT-1A		
214-MT-1A RIPA	5/18/2020	punch	9:30	no	no	sunny		-20	For Austrian Group							214-MT-1A RIPA		
216-MD-1A	5/20/2020	punch	9:30	no	no	sunny		-80	21	6/16/2020	-20	151	1.83	1.69	high	216-MD-1A		
216-MD-1A	5/20/2020	punch	9:30	no	no	sunny		-80	25	6/16/2020	-20	172.2	1.83	2.11	high	216-MD-1A		
216-MT-1A RIPA	5/20/2020	punch	9:30	no	no	sunny		-20	For Austrian Group							216-MT-1A RIPA		
218-MD-1A	5/22/2020	punch	9:30	no	no	sunny		-80	29	6/16/2020	-20	62.3	1.8	0.41	high	218-MD-1A		
218-MT-1A	5/22/2020	punch	9:30	no	no	sunny		-80	22	6/16/2020	-20	271.5	1.83	2.35	high	218-MT-1A		
218-MT-1A RIPA	5/22/2020	punch	9:30	no	no	sunny		-20	For Austrian Group							218-MT-1A RIPA		
221-MD-1A	5/25/2020	punch	9:30	no	no	sunny		-80	28	6/16/2020	-20	68.8	1.8	0.4	high	221-MD-1A		

Donor 2

Donor 2		Placement Date: 11/4/2019		Incision site: R deltoid f		Storage	DNA Extraction		NanoDrop		PCR		Sample			
Sampling	Date	Size of punch	Pictures TBS	Time taken?	Weather	Special notes	Temp of storage (°C)	Weight (mg) [muscle samples]	Date of DNA extraction	Temp of storage (°C)	Concentration (ng/µL)	260/280 ratio	260/230 ratio	16s rRNA PCR positive?		
1-MD-2A	11/4/2019	8mm	9:30 yes	yes	Clear & cold	Donor placed. No signs of decomp.	-80		27 6/17/2020	-20	50.6	1.79	0.31	none	1-MD-2A	
1-B-2A	11/4/2019	NA	9:30 yes	yes	Clear & cold		-80	*250	6/26/2020	-20	5	1.72	1.28	medium/high	1-B-2A	
1-B-2B	11/4/2019	NA	9:30 yes	yes	Clear & cold		-80	NA	NA	-20	NA	NA	NA	NA	1-B-2B	
2-MD-2A	11/5/2019	8mm	9:30 yes	yes	snow		-80	28	6/17/2020	-20	61	1.8	1.61	none	2-MD-2A	
2-B-2A	11/5/2019	NA	9:30 yes	yes	snow		-80	*250	6/26/2020	-20	3	1.53	0.92	medium/high	2-B-2A	
2-B-2B	11/5/2019	NA	9:30 yes	yes	snow		-80	NA	NA	-20	NA	NA	NA	NA	2-B-2B	
Post Freezing																
156-MD-2A	4/8/2020	8mm	9:30 no	no	Sunny	significant skin damage from freezing	-80		23 6/17/2020	-20	108.2	1.83	1.15	none/low	156-MD-2A	
156-MT-2A	4/8/2020	punch	9:30 no	no	Sunny	mold/fungus growth	-80		22 6/17/2020	-20	79.6	1.8	1.96	low	156-MT-2A	
156-MT-2A RIPA	4/8/2020	punch	9:30 no	no	Sunny		-20	For Austrian Group	NA	NA	-20	NA	NA	NA	NA	156-MT-2A RIPA
156-B-2A	4/8/2020	NA	9:30 no	no	Sunny		-80	*250	6/26/2020	-20	16.3	1.76	1.39	high	156-B-2A	
156-B-2B	4/8/2020	NA	9:30 no	no	Sunny		-80	NA	NA	-20	NA	NA	NA	NA	156-B-2B	
159-MD-2A	4/11/2020	6mm	9:30 yes OC	no	Sunny		-80		24 6/17/2020	-20	89.5	1.81	0.65	none/low	159-MD-2A	
159-MT-2A RIPA	4/11/2020	6mm	9:30 yes OC	no	Sunny		-80		24 6/17/2020	-20	84.7	1.82	1.21	medium	159-MT-2A RIPA	
159-B-2A	4/11/2020	NA	9:30 yes OC	no	Sunny		-80	*250	6/26/2020	-20	12.1	1.62	0.88	high	159-B-2A	
159-B-2B	4/11/2020	NA	9:30 yes OC	no	Sunny		-80	NA	NA	-20	NA	NA	NA	NA	159-B-2B	
172-B-2A	4/24/2020	NA	9:30 yes OC	no	Sunny		-80	*250	6/26/2020	-20	15.6	1.74	1.18	high	172-B-2A	
172-B-2B	4/24/2020	NA	9:30 yes OC	no	Sunny		-80	NA	NA	-20	NA	NA	NA	NA	172-B-2B	
175-MD-2A	4/27/2020	6mm	9:30 yes OC	no	Sunny		-80		28 6/17/2020	-20	73.8	1.83	1.45	medium	175-MD-2A	
175-B-2A	4/27/2020	NA	9:30 yes OC	no	Sunny		-80	*250	6/26/2020	-20	11.3	1.65	1.27	high	175-B-2A	
175-B-2B	4/27/2020	NA	9:30 yes OC	no	Sunny		-80	NA	NA	-20	NA	NA	NA	NA	175-B-2B	
179-MD-2A	5/1/2020	punch	9:30 yes OC	no	Sunny		-80		20 6/17/2020	-20	92.1	1.83	1.63	low/medium	179-MD-2A	
179-MT-2A	5/1/2020	punch	9:30 yes OC	no	Sunny		-80		24 6/17/2020	-20	107.3	1.82	1.07	high	179-MT-2A	
179-MT-2A RIPA	5/1/2020	punch	9:30 yes OC	no	Sunny		-80	For Austrian Group							179-MT-2A RIPA	
179-B-2A	5/1/2020	NA	9:30 yes OC	no	Sunny		-80	*250	6/26/2020	-20	7.5	1.58	0.9	high	179-B-2A	
179-B-2B	5/1/2020	NA	9:30 yes OC	no	Sunny		-80	NA	NA	-20	NA	NA	NA	NA	179-B-2B	
182-MD-2A	5/4/2020	6mm	9:30 yes OC	no	cloudy		-80		26 6/17/2020	-20	69.7	1.81	1.77	low/medium	182-MD-2A	
182-MT-2A RIPA	5/4/2020	punch	9:30 yes OC	no	cloudy		-80		25 6/17/2020	-20	96.4	1.82	1.06	high	182-MT-2A RIPA	
182-B-2A	5/4/2020	NA	9:30 yes OC	no	cloudy		-80	*250	6/26/2020	-20	8.4	1.59	1	high	182-B-2A	
182-B-2B	5/4/2020	NA	9:30 yes OC	no	cloudy		-80	NA	NA	-20	NA	NA	NA	NA	182-B-2B	
184-MD-2A	5/6/2020	punch	1:30 yes	yes	sunny		-80		24 6/17/2020	-20	128.3	1.83	1.06	high	184-MD-2A	
184-MT-2A	5/6/2020	punch	1:30 yes	yes	sunny		-80		25 6/19/2020	-20	151	1.83	2.44	high	184-MT-2A	
184-MT-2A RIPA	5/6/2020	punch	1:30 yes	yes	sunny		-80	For Austrian Group							184-MT-2A RIPA	
184-B-2A	5/6/2020	NA	1:30 yes	yes	sunny		-80	*250	6/26/2020	-20	12.1	1.71	1	high	184-B-2A	
184-B-2B	5/6/2020	NA	1:30 yes	yes	sunny		-80	NA	NA	-20	NA	NA	NA	NA	184-B-2B	
187-MD-2A	5/9/2020	punch	9:30 no	no	sunny		-80		28 6/19/2020	-20	190.5	1.82	1.09	high	187-MD-2A	
187-MT-2A	5/9/2020	punch	9:30 no	no	sunny		-80		26 6/19/2020	-20	164.2	1.79	0.43	high	187-MT-2A	
187-MT-2A RIPA	5/9/2020	punch	9:30 no	no	sunny		-80	For Austrian Group							187-MT-2A RIPA	
187-B-2A	5/9/2020	NA	9:30 no	no	sunny		-80	*250	6/26/2020	-20	6.6	1.62	0.88	high	187-B-2A	
187-B-2B	5/9/2020	NA	9:30 no	no	sunny		-80	NA	NA	-20	NA	NA	NA	NA	187-B-2B	
189-MD-2A	5/11/2020	punch	9:30 no	no	sunny		-80		23 6/19/2020	-20	130.7	1.83	1.43	high	189-MD-2A	
189-MT-2A	5/11/2020	punch	9:30 no	no	sunny		-80		24 6/19/2020	-20	157.5	1.78	0.33	high	189-MT-2A	
189-MT-2A RIPA	5/11/2020	punch	9:30 no	no	sunny		-80	For Austrian Group							189-MT-2A RIPA	
189-B-2A	5/11/2020	NA	9:30 no	no	sunny		-80	*250	6/26/2020	-20	5.3	1.46	0.96	high	189-B-2A	
189-B-2B	5/11/2020	NA	9:30 no	no	sunny		-80	NA	NA	-20	NA	NA	NA	NA	189-B-2B	
192-MD-2A	5/14/2020	punch	2:50 no	no	sunny		-80		25 6/19/2020	-20	78.4	1.82	1.67	high	192-MD-2A	
192-MT-2A RIPA	5/14/2020	punch	2:50 no	no	sunny		-80		28 6/19/2020	-20	154.1	1.82	1.87	high	192-MT-2A RIPA	
192-B-2A	5/14/2020	NA	2:50 no	no	sunny		-80	For Austrian Group							192-B-2A RIPA	
192-B-2B	5/14/2020	NA	2:50 no	no	sunny		-80	*250	6/26/2020	-20	5	1.33	0.75	high	192-B-2A	
192-B-2B	5/14/2020	NA	2:50 no	no	sunny		-80	NA	NA	-20	NA	NA	NA	NA	192-B-2B	
194-MD-2A	5/16/2020	punch	9:30 no	no	sunny		-80		22 6/26/2020	-20	12.4	1.79	0.9	high	194-MD-2A	
194-MT-2A	5/16/2020	punch	9:30 no	no	sunny		-80		20 6/19/2020	-20	115.8	1.78	1.84	high	194-MT-2A	
194-MT-2A RIPA	5/16/2020	punch	9:30 no	no	sunny		-80	For Austrian Group							194-MT-2A RIPA	
194-B-2A	5/16/2020	NA	9:30 no	no	sunny		-80	*250	6/26/2020	-20	9.6	1.71	1.22	high	194-B-2A	
194-B-2B	5/16/2020	NA	9:30 no	no	sunny		-80	NA	NA	-20	NA	NA	NA	NA	194-B-2B	
196-MD-2A	5/18/2020	punch	9:30 no	no	sunny		-80		20 6/19/2020	-20	27.9	1.79	0.15	high	196-MD-2A	
196-MT-2A	5/18/2020	punch	9:30 no	no	sunny		-80		26 6/19/2020	-20	125.3	1.82	1.33	high	196-MT-2A	
196-MT-2A RIPA	5/18/2020	punch	9:30 no	no	sunny		-80	For Austrian Group							196-MT-2A RIPA	
196-B-2A	5/18/2020	NA	9:30 no	no	sunny		-80	*250	6/26/2020	-20	9.9	1.62	0.99	high	196-B-2A	
196-B-2B	5/18/2020	NA	9:30 no	no	sunny		-80	NA	NA	-20	NA	NA	NA	NA	196-B-2B	
198-MD-2A	5/20/2020	punch	9:30 no	no	sunny		-80		28 6/26/2020	-20	9.2	1.71	0.34	high	198-MD-2A	
198-MT-2A	5/20/2020	punch	9:30 no	no	sunny		-80		30 6/22/2020	-20	69.1	1.79	0.21	high	198-MT-2A	
198-MT-2A RIPA	5/20/2020	punch	9:30 no	no	sunny		-80	For Austrian Group							198-MT-2A RIPA	
198-B-2A	5/20/2020	NA	9:30 no	no	sunny		-80	*250	6/26/2020	-20	4.4	1.5	0.78	high	198-B-2A	
198-B-2B	5/20/2020	NA	9:30 no	no	sunny		-80	NA	NA	-20	NA	NA	NA	NA	198-B-2B	
200-MD-2A	5/22/2020	punch	9:30 no	no	sunny	significant fly/maggot activity; strong odor	-80		28 6/26/2020	-20	10.5	1.58	0.07	high	200-MD-2A	
200-MT-2A	5/22/2020	punch	9:30 no	no	sunny	significant fly/maggot activity; strong odor	-80		25 6/22/2020	-20	76.1	1.81	0.84	high	200-MT-2A	
200-MT-2A RIPA	5/22/2020	punch	9:30 no	no	sunny	significant fly/maggot activity; strong odor	-80	For Austrian Group							200-MT-2A RIPA	
203-B-2A	5/25/2020	NA	9:30 no	no	sunny		-80	*250	6/26/2020	-20	4.3	1.46	0.59	high	203-B-2A	
203-B-2B	5/25/2020	NA	9:30 no	no	sunny		-80	NA	NA	-20	NA	NA	NA	NA	203-B-2B	
206-B-2A	5/28/2020	NA	9:30 no	no	sunny		-80	*250	6/26/2020	-20	2.3	1.05	0.25	high	206-B-2A	
206-B-2B	5/28/2020	NA	9:30 no	no	sunny		-80	NA	NA	-20	NA	NA	NA	NA	206-B-2B	

Donor 3

Sampling							Storage	DNA Extraction			NanoDrop			PCR		Sample
Sample	Date collected	Size of punch	Time taken?	TBS taken?	Weather condition	Special notes	Temp of storage (°C)	Weight (mg)	Date of DNA extraction	Temp of storage (°C)	Concentration (ng/µL)	260/280 ratio	260/230 ratio	16s rRNA	PCR positive?	Sample
4/6-MD-3A	4/6/2020	8mm	8:30	Yes OC	no	Rain	-80	22	6/22/2020	-20	100.5	1.82	0.95	medium		4/6-MD-3A
4/6-MT-3A	4/6/2020	8mm	8:30	Yes OC	no	Rain	-80	24	6/22/2020	-20	117.8	1.82	1.99	none		4/6-MT-3A
4/6-MT-3A RIPA (m)	4/6/2020	8mm	8:30	Yes OC	no	Rain										4/6-MT-3A RIPA
4/8-MD-3A	4/8/2020	8mm	9:30	Yes OC	no	Sunny	-80	20	6/22/2020	-20	96.7	1.8	0.4	medium		4/8-MD-3A
4/8-MT-3A	4/8/2020	punch	9:30	Yes OC	no	Sunny	-80	28	6/22/2020	-20	187.4	1.81	0.87	none		4/8-MT-3A
4/8-MT-3A RIPA	4/8/2020	punch	9:30	Yes OC	no	Sunny										4/8-MT-3A RIPA
4/11-MD-3A	4/11/2020	6mm	9:30	Yes OC	no	Sunny	-80	28	6/22/2020	-20	120	1.81	0.62	medium		4/11-MD-3A
4/11-MT-3A	4/11/2020	6mm	9:30	Yes OC	no	Sunny	-80	25	6/22/2020	-20	198.9	1.81	0.66	none		4/11-MT-3A
4/11-MT-3A RIPA	4/11/2020	6mm	9:30	Yes OC	no	Sunny										4/11-MT-3A RIPA
4/20-MD-3A	4/20/2020	6mm	9:30	Yes OC	no	Sunny	-80	23	6/22/2020	-20	98.2	1.82	0.94	low		4/20-MD-3A
4/20-MT-3A	4/20/2020	punch	9:30	Yes OC	no	Sunny	-80	24	6/22/2020	-20	154.2	1.8	0.88	low		4/20-MT-3A
4/20-MT-3A RIPA	4/20/2020	punch	9:30	Yes OC	no	Sunny										4/20-MT-3A RIPA
4/24-MD-3A	4/24/2020	6mm	9:30	Yes OC	no	Sunny	-80	27	6/23/2020	-20	109.4	1.83	1.49	medium/high		4/24-MD-3A
4/24-MT-3A	4/24/2020	punch	9:30	Yes OC	no	Sunny	-80	20	6/22/2020	-20	141.1	1.8	1.35	low		4/24-MT-3A
4/24-MT-3A RIPA	4/24/2020	punch	9:30	Yes OC	no	Sunny										4/24-MT-3A RIPA
4/27-MD-3A	4/27/2020	6mm	9:30	no	no	Sunny	-80	26	6/23/2020	-20	102.8	1.81	0.51	high		4/27-MD-3A
4/27-MT-3A	4/27/2020	punch	9:30	no	no	Sunny	-80	22	6/23/2020	-20	217.2	1.82	2.17	low		4/27-MT-3A
4/27-MT-3A RIPA	4/27/2020	punch	9:30	no	no	Sunny										4/27-MT-3A RIPA
5/1-MD-3A	5/1/2020	6mm	9:30	no	no	Sunny	-80	28	6/23/2020	-20	43.1	1.75	0.37	high		5/1-MD-3A
5/1-MT-3A	5/1/2020	punch	9:30	no	no	Sunny	-80	20	6/23/2020	-20	162.2	1.82	0.94	low		5/1-MT-3A
5/1-MT-3A RIPA	5/1/2020	punch	9:30	no	no	Sunny										5/1-MT-3A RIPA
5/4-MD-3A	5/4/2020	6mm	9:30	no	no	cloudy	-80	23	6/23/2020	-20	82.1	1.81	1.1	high		5/4-MD-3A
5/4-MT-3A	5/4/2020	punch	9:30	no	no	cloudy	-80	22	6/23/2020	-20	57.2	1.79	0.4	high		5/4-MT-3A
5/4-MT-3A RIPA	5/4/2020	punch	9:30	no	no	cloudy										5/4-MT-3A RIPA
5/6-MD-3A	5/6/2020	6mm	1:30	Yes	yes	sunny	-80	21	6/23/2020	-20	91.5	1.82	0.92	high		5/6-MD-3A
5/6-MT-3A	5/6/2020	punch	1:30	yes	yes	sunny	-80	21	6/23/2020	-20	97.5	1.83	1.95	high		5/6-MT-3A
5/6-MT-3A RIPA	5/6/2020	punch	1:30	yes	yes	sunny										5/6-MT-3A RIPA
5/9-MD-3A	5/9/2020	6mm	9:30	no	no	sunny	-80	26	6/23/2020	-20	55.5	1.81	1.76	high		5/9-MD-3A
5/9-MT-3A	5/9/2020	punch	9:30	no	no	sunny	-80	27	6/23/2020	-20	86.8	1.8	0.81	high		5/9-MT-3A
5/9-MT-3A RIPA	5/9/2020	punch	9:30	no	no	sunny										5/9-MT-3A RIPA
5/11-MD-3A	5/11/2020	6mm	9:30	no	no	sunny	-80	22	6/23/2020	-20	38.7	1.77	0.99	high		5/11-MD-3A
5/11-MT-3A	5/11/2020	punch	9:30	no	no	sunny	-80	23	6/24/2020	-20	71.3	1.89	1.77	high		5/11-MT-3A
5/11-MT-3A RIPA	5/11/2020	punch	9:30	no	no	sunny										5/11-MT-3A RIPA
5/14-MD-3A	5/14/2020	punch	2:50	no	no	sunny	-80	22	6/24/2020	-20	47	1.78	0.51	high		5/14-MD-3A
5/14-MT-3A	5/14/2020	punch	2:50	no	no	sunny	-80	27	6/24/2020	-20	94	1.83	2.03	medium/high		5/14-MT-3A
5/14-MT-3A RIPA	5/14/2020	punch	2:50	no	no	sunny										5/14-MT-3A RIPA
5/16-MD-3A	5/16/2020	punch	9:30	no	no	sunny	-80	22	6/24/2020	-20	60.6	1.81	0.5	high		5/16-MD-3A
5/16-MT-3A	5/16/2020	punch	9:30	no	no	sunny	-80	28	6/24/2020	-20	70.4	1.8	1.47	high		5/16-MT-3A
5/16-MT-3A RIPA	5/16/2020	punch	9:30	no	no	sunny										5/16-MT-3A RIPA
5/18-MD-3A	5/18/2020	punch	9:30	no	no	sunny	-80	26	6/24/2020	-20	72.5	1.77	0.72	high		5/18-MD-3A
5/18-MT-3A	5/18/2020	punch	9:30	no	no	sunny	-80	25	6/24/2020	-20	75.6	1.79	0.3	high		5/18-MT-3A
5/18-MT-3A RIPA	5/18/2020	punch	9:30	no	no	sunny										5/18-MT-3A RIPA
5/20-MD-3A	5/20/2020	punch	9:30	no	no	sunny	-80	26	6/24/2020	-20	40.5	1.78	0.4	high		5/20-MD-3A
5/20-MT-3A	5/20/2020	punch	9:30	no	no	sunny	-80	25	6/24/2020	-20	25.8	1.69	0.27	high		5/20-MT-3A
5/20-MT-3A RIPA	5/20/2020	punch	9:30	no	no	sunny										5/20-MT-3A RIPA
5/22-MD-3A	5/22/2020	punch	9:30	no	no	sunny										5/22-MD-3A
5/22-MT-3A	5/22/2020	punch	9:30	no	no	sunny										5/22-MT-3A
5/22-MT-3A RIPA	5/22/2020	punch	9:30	no	no	sunny										5/22-MT-3A RIPA

Appendix C: DNA Isolation and Purification Sample Data Sheets

Donor 1

Sampling		DNA Extraction			Concentration (n	260/280	260/230	16s rRNA	PCR
		Date collected	Weight (mg)	Date of DNA extraction					
Sample									
1-MD-1A	SMD101	10/17/2019	32.8	6/10/2020	112.4		1.8	1.89	none
2-MD-1A	SMD102	10/18/2019	30.8	6/10/2020	111.1		1.83	2.91	low
3-MD-1A	SMD103	10/19/2019	22.5	6/10/2020	179.3		1.82	2.38	low
4-MD-1A	SMD104	10/20/2019	29.6	6/10/2020	222		1.82	2.23	none/low
5-MD-1A	SMD105	10/21/2019	24	6/11/2020	45.3		1.82	0.19	low
6-MD-1A	SMD106	10/22/2019	27	6/11/2020	43.9		1.81	0.59	low
7-MD-1A	SMD107	10/23/2019	24	6/11/2020	46.8		1.81	0.59	low
8-MD-1A	SMD108	10/24/2019	26	6/24/2020	57.3		1.79	2.19	medium
9-MD-1A	SMD109	10/25/2019	27	6/11/2020	34.9		1.81	0.36	low
10-MD-1A	SMD110	10/26/2019	25	6/24/2020	28.7		1.8	2.73	low
11-MD-1A	SMD111	10/27/2019	20	6/11/2020	37.8		1.82	0.25	medium
12-MD-1A	SMD112	10/28/2019	29	6/11/2020	44.6		1.82	0.23	medium
13-MD-1A	SMD113	10/29/2019	21	6/11/2020	38.2		1.83	0.09	low
174-MD-1A	SMD114	4/8/2020	22	6/11/2020	45.2		1.85	0.5	low
177-MD-1A	SMD115	4/11/2020	22	6/11/2020	185.6		1.82	0.85	low
177-MT-1A	SMT115	4/11/2020	22	6/24/2020	238.8		1.81	1.04	medium
190-MT-1A	SMT116	4/24/2020	23	6/15/2020	85.4		1.82	2.11	low
193-MD-1A	SMD117	4/27/2020	23	6/15/2020	144.5		1.83	1.55	low
193-MT-1A	SMT117	4/27/2020	29	6/15/2020	136.4		1.82	1.73	low/medium
197-MD-1A	SMD118	5/1/2020	30	6/15/2020	187.3		1.83	1.36	low/medium
197-MT-1A	SMT118	5/1/2020	27	6/15/2020	109.8		1.83	2.41	medium
200-MD-1A	SMD119	5/4/2020	26	6/15/2020	66.5		1.83	2.55	medium
200-MT-1A	SMT119	5/4/2020	22	6/15/2020	82.8		1.83	1.82	medium
202-MD-1A	SMD120	5/6/2020	27	6/15/2020	132.8		1.83	1.84	low/medium
202-MT-1A	SMT120	5/6/2020	24	6/15/2020	103.8		1.81	0.28	medium
205-MD-1A	SMD121	5/9/2020	21	6/15/2020	90		1.81	1.17	medium
205-MT-1A	SMT121	5/9/2020	24	6/15/2020	130.6		1.83	2.42	medium/high
207-MD-1A	SMD122	5/11/2020	21	6/15/2020	64.8		1.8	0.27	medium
207-MT-1A	SMT122	5/11/2020	23	6/16/2020	78.3		1.82	0.66	medium/high
210-MD-1A	SMD123	5/14/2020	23	6/16/2020	139.2		1.83	1.14	medium
210-MT-1A	SMT123	5/14/2020	25	6/16/2020	81.5		1.82	1.58	medium/high
212-MD-1A	SMD124	5/16/2020	23	6/16/2020	134.4		1.83	1.08	medium/high
212-MT-1A	SMT124	5/16/2020	22	6/16/2020	47.3		1.79	0.26	high
214-MD-1A	SMD125	5/18/2020	24	6/16/2020	109.4		1.83	1.92	high
214-MT-1A	SMT125	5/18/2020	24	6/24/2020	128.8		1.81	2.45	high
216-MD-1A	SMD126	5/20/2020	21	6/16/2020	151		1.83	1.69	high
216-MT-1A	SMT126	5/20/2020	25	6/16/2020	172.2		1.83	2.11	high
218-MD-1A	SMD127	5/22/2020	29	6/16/2020	62.3		1.8	0.41	high
218-MT-1A	SMT127	5/22/2020	22	6/16/2020	271.5		1.83	2.35	high
221-MD-1A	SMD128	5/25/2020	28	6/16/2020	68.8		1.8	0.4	high
318-MD-1A	SMD129	8/30/2020	30	9/3/2020	9.3		1.27	0.03	NA
318-MT-1A	SMT129	8/30/2020	33	9/3/2020	9.9		0.74	0	NA

Donor 2

Sampling		DNA Extraction		NanoDrop		260/280	260/230	PCR
		Date collected	Weight (mg) [muscle samples] *Volume (µL) [buccal swabs]	Date of DNA extraction	Concentration (ng/µL)			16s rRNA PCR positive?
1-MD-2A	SMD201	11/4/2019		27	6/17/2020	50.6	1.79	0.31 none
1-B-2A	SBS201	11/4/2019		*250	6/26/2020	5	1.72	1.28 medium/high
2-MD-2A	SMD202	11/5/2019		28	6/17/2020	61	1.8	1.61 none
2-B-2A	SBS202	11/5/2019		*250	6/26/2020	3	1.53	0.92 medium/high
156-MD-2A	SMD203	4/8/2020		23	6/17/2020	108.2	1.83	1.15 none/low
156-MT-2A	SMT203	4/8/2020		22	6/17/2020	79.6	1.8	1.96 low
156-B-2A	SBS203	4/8/2020		*250	6/26/2020	16.3	1.76	1.39 high
159-MD-2A	SMD204	4/11/2020		24	6/17/2020	89.5	1.81	0.65 none/low
159-MT-2A	SMT204	4/11/2020		24	6/17/2020	84.7	1.82	1.21 medium
159-B-2A	SBS204	4/11/2020		*250	6/26/2020	12.1	1.62	0.88 high
172-B-2A	SBS205	4/24/2020		*250	6/26/2020	15.6	1.74	1.18 high
175-MD-2A	SMD206	4/27/2020		28	6/17/2020	73.8	1.83	1.45 medium
175-B-2A	SBS206	4/27/2020		*250	6/26/2020	11.3	1.65	1.27 high
179-MD-2A	SMD207	5/1/2020		20	6/17/2020	92.1	1.83	1.63 low/medium
179-MT-2A	SMT207	5/1/2020		24	6/17/2020	107.3	1.82	1.07 high
179-B-2A	SBS207	5/1/2020		*250	6/26/2020	7.5	1.58	0.9 high
182-MD-2A	SMD208	5/4/2020		26	6/17/2020	69.7	1.81	1.77 low/medium
182-MT-2A	SMT208	5/4/2020		25	6/17/2020	96.4	1.82	1.06 high
182-B-2A	SBS208	5/4/2020		*250	6/26/2020	8.4	1.59	1 high
184-MD-2A	SMD209	5/6/2020		24	6/17/2020	128.3	1.83	1.06 high
184-MT-2A	SMT209	5/6/2020		25	6/19/2020	151	1.83	2.44 high
184-B-2A	SBS209	5/6/2020		*250	6/26/2020	12.1	1.71	1 high
187-MD-2A	SMD210	5/9/2020		28	6/19/2020	190.5	1.82	1.09 high
187-MT-2A	SMT210	5/9/2020		26	6/19/2020	164.2	1.79	0.43 high
187-B-2A	SBS210	5/9/2020		*250	6/26/2020	6.6	1.62	0.88 high
189-MD-2A	SMD211	5/11/2020		23	6/19/2020	130.7	1.83	1.43 high
189-MT-2A	SMT211	5/11/2020		24	6/19/2020	157.5	1.78	0.33 high
189-B-2A	SBS211	5/11/2020		*250	6/26/2020	5.3	1.46	0.96 high
192-MD-2A	SMD212	5/14/2020		25	6/19/2020	78.4	1.82	1.67 high
192-MT-2A	SMT212	5/14/2020		28	6/19/2020	154.1	1.82	1.87 high
192-B-2A	SBS212	5/14/2020		*250	6/26/2020	5	1.33	0.75 high
194-MD-2A	SMD214	5/16/2020		22	6/26/2020	12.4	1.79	0.9 high
194-MT-2A	SMT214	5/16/2020		20	6/19/2020	115.8	1.78	1.84 high
194-B-2A	SBS214	5/16/2020		*250	6/26/2020	9.6	1.71	1.22 high
196-MD-2A	SMD215	5/18/2020		20	6/19/2020	27.9	1.79	0.15 high
196-MT-2A	SMT215	5/18/2020		26	6/19/2020	125.3	1.82	1.33 high
196-B-2A	SBS215	5/18/2020		*250	6/26/2020	9.9	1.62	0.99 high
198-MD-2A	SMD216	5/20/2020		28	6/26/2020	9.2	1.71	0.34 high
198-MT-2A	SMT216	5/20/2020		30	6/22/2020	69.1	1.79	0.21 high
198-B-2A	SBS216	5/20/2020		*250	6/26/2020	4.4	1.5	0.78 high
200-MD-2A	SMD217	5/22/2020		28	6/26/2020	10.5	1.58	0.07 high
200-MT-2A	SMT217	5/22/2020		25	6/22/2020	76.1	1.81	0.84 high
203-B-2A	SBS218	5/25/2020		*250	6/26/2020	4.3	1.46	0.59 high
206-B-2A	SBS219	5/28/2020		*250	6/26/2020	2.3	1.05	0.25 high
300-MD-2A	SMD220	8/30/2020		29	9/3/2020	153.7	1.15	0.04 NA
300-MT-2A	SMT220	8/30/2020		29	9/3/2020	23.6	1.49	0.05 NA

Donor 3

Sampling	Sample	DNA Extraction			Concentration (ng/µL)	260/280 ratio	260/230 ratio	16s rRNA PCR positive?
		Date collected	Weight (mg)	Date of DNA extraction				
4/6-MD-3A	SMD301	4/6/2020	22	6/22/2020	100.5	1.82	0.95	medium
4/6-MT-3A	SMT301	4/6/2020	24	6/22/2020	117.8	1.82	1.99	none
4/8-MD-3A	SMD302	4/8/2020	20	6/22/2020	96.7	1.8	0.4	medium
4/8-MT-3A	SMT302	4/8/2020	28	6/22/2020	187.4	1.81	0.87	none
4/11-MD-3A	SMD303	4/11/2020	28	6/22/2020	120	1.81	0.62	medium
4/11-MT-3A	SMT303	4/11/2020	25	6/22/2020	198.9	1.81	0.66	none
4/20-MD-3A	SMD304	4/20/2020	23	6/22/2020	98.2	1.82	0.94	low
4/20-MT-3A	SMT304	4/20/2020	24	6/22/2020	154.2	1.8	0.88	low
4/24-MD-3A	SMD305	4/24/2020	27	6/23/2020	109.4	1.83	1.49	medium/high
4/24-MT-3A	SMT305	4/24/2020	20	6/22/2020	141.1	1.8	1.35	low
4/27-MD-3A	SMD306	4/27/2020	26	6/23/2020	102.8	1.81	0.51	high
4/27-MT-3A	SMT306	4/27/2020	22	6/23/2020	217.2	1.82	2.17	low
5/1-MD-3A	SMD307	5/1/2020	28	6/23/2020	43.1	1.75	0.37	high
5/1-MT-3A	SMT307	5/1/2020	20	6/23/2020	162.2	1.82	0.94	low
5/4-MD-3A	SMD308	5/4/2020	23	6/23/2020	82.1	1.81	1.1	high
5/4-MT-3A	SMT308	5/4/2020	22	6/23/2020	57.2	1.79	0.4	high
5/6-MD-3A	SMD309	5/6/2020	21	6/23/2020	91.5	1.82	0.92	high
5/6-MT-3A	SMT309	5/6/2020	21	6/23/2020	97.5	1.83	1.95	high
5/9-MD-3A	SMD310	5/9/2020	26	6/23/2020	55.5	1.81	1.76	high
5/9-MT-3A	SMT310	5/9/2020	27	6/23/2020	86.8	1.8	0.81	high
5/11-MD-3A	SMD311	5/11/2020	22	6/23/2020	38.7	1.77	0.99	high
5/11-MT-3A	SMT311	5/11/2020	23	6/24/2020	71.3	1.89	1.77	high
5/14-MD-3A	SMD312	5/14/2020	22	6/24/2020	47	1.78	0.51	high
5/14-MT-3A	SMT312	5/14/2020	27	6/24/2020	94	1.83	2.03	medium/high
5/16-MD-3A	SMD313	5/16/2020	22	6/24/2020	60.6	1.81	0.5	high
5/16-MT-3A	SMT313	5/16/2020	28	6/24/2020	70.4	1.8	1.47	high
5/18-MD-3A	SMD314	5/18/2020	26	6/24/2020	72.5	1.77	0.72	high
5/18-MT-3A	SMT314	5/18/2020	25	6/24/2020	75.6	1.79	0.3	high
5/20-MD-3A	SMD315	5/20/2020	26	6/24/2020	40.5	1.78	0.4	high
5/20-MT-3A	SMT315	5/20/2020	25	6/24/2020	25.8	1.69	0.27	high
5/22-MD-3A	SMD316	5/22/2020	24	6/24/2020	31.6	1.71	0.08	high
5/22-MT-3A	SMT316	5/22/2020	26	6/26/2020	43	1.82	0.69	high
8/30-MD-3A	SMD317	8/30/2020	29	9/3/2020	80	1.35	0.37	NA
8/30-MT-3A	SMT318	8/30/2020	33	9/3/2020	65.8	1.2	0.3	NA

References

1. Damann FE, Carter DO. Human decomposition ecology and postmortem microbiology [internet]. In: Manual of Forensic Taphonomy. (Boca Raton: CRC Press, 2014) [cited 2021 February 10]; 37-45. Available from <https://drive.google.com/file/d/1uCrz6VX4shuxRSMawIrxjp2ixJDqnina/view?usp=drivesdk>
2. Cardozo HFV, Santos A, Dias R, Garcia C, Pinto M, Sérgio C, Magalhães T. Establishing a minimum postmortem interval of human remains in an advanced state of skeletonization using the growth of bryophytes and plant roots. International Journal of Legal Medicine 2010;124:451-456.
3. Hauther KA, Cobaugh KL, Jantz LM, Sparer TE, DeBruyn, JM. Estimating time since death from postmortem human gut microbial communities. Journal of Forensic Sciences 2015;60(5):1234-1240.
4. Hyde ER, Haarmann DP, Lynne AM, Bucheli SR, Petrosino JF. The living dead: bacterial community structure of a cadaver at the onset and end of the bloat stage of decomposition. PLOS One 2013;8(10):1-10.
5. DeBruyn JM, Hauther KA. Postmortem succession of gut microbial communities in deceased human subjects. PeerJ 2017;5 e3437.
6. Yatsunenko T, Rey FE, Manary MJ, Trehan I, Dominguez-Bello MG, Contreras M, Magris M, Hidalgo G, Baldassano RN, Anokhin AP, Heath AC, Warner B, Reeder J, Kuczynski J, Caporaso JG, Lozupone CA, Lauber C, Clemente JC, Knights D, Knight R, Gordon JI . Human gut microbiomes are viewed across age and geography. Nature 2012;486:222-227.
7. Pechal JL, Crippen TL, Benbow ME, Tarone AM, Dowd S, Tomberlin JK. The potential use of bacterial community succession in forensics as described by high throughput metagenomic sequencing. International Journal of Legal Medicine 2014;128:193-205.
8. Pinheiro J. Decay process of a cadaver. Forensic Anthropology and medicine. 2006;85-116.
9. Hyde ER, Haarmann DP, Petrosino JF, Lynne AM, Bucheli SR. Initial insights into bacterial succession during human decomposition. International Journal of Legal Medicine 2015;129:661-671.
10. Lovley DR, Coates JD. Novel forms of anaerobic respiration of environmental relevance. ScienceDirect 2000;3(3):252-256.
11. Connor M, Baigent C, Hansen ES. Measuring desiccation using qualitative changes: A step toward determining regional decomposition sequences. Journal of Forensic Sciences 2019;64(4):1004-1011. doi: 10.1111/1556-4029.14003

12. Dibner H, Valdez CM, Carter OC. An experiment to characterize the decomposer community associated with carcasses (*Sus scrofa domesticus*) on Oahu, Hawaii. *Journal of Forensic Sciences*. 2019;64(5):1412-1420.
13. Smets W, Moretti S, Denys S, Lebeur S. Airborne bacteria in the atmosphere: Presence, purpose, and potential. *Atmospheric Environment*. 2016;139:214-221.
14. Womack AM, Bohannan BJM, Green JL. Biodiversity and biogeography of the atmosphere. *Philosophical Transactions of the Royal Society B*. 2010;365:3645-3653 doi:10.1098/rstb.2010.0283
15. Polymenakou PN. Atmosphere: A source of pathogenic or beneficial microbes? *Atmosphere*. 2012;3:87-102 doi:10.3390/atmos3010087
16. Pechal JL, Schmidt CJ, Jordan HR, Benbow ME. Frozen: thawing and its effect on the postmortem microbiome in two pediatric cases. *Journal of Forensic Sciences*. 2017;64(5):1399-1405.
17. Ehrenfellner B, Zissler A, Steinbacher P, Monticello FC, Pittner S. Are animal models predictive for human postmortem muscle protein degradation? *International Journal of Legal Medicine*. 2017;131:1615-1621.
18. Pittner S, Ehrenfellner B, Monticello FC, Zissler A, Sanger AM, Stoiber W, Steinbacher P. Postmortem muscle protein degradation in humans as a tool for PMI delimitation. *International Journal of Legal Medicine*. 2016;130(6):1547-1555. doi: 10.1111/1556-4029.14003
19. Damann FE, Williams DE, Layton AC. Potential use of bacterial community succession in decaying human bone for estimating postmortem interval. *Journal of Forensic Sciences*. 2015;60(4):844-850. doi: 10.1111/1556-4029.12744
20. Dibner H, Valdez CM, Carter DO. An experiment to characterize the decomposer community associated with carcasses (*Sus scrofa domesticus*) on Oahu, Hawaii. *Journal of Forensic Sciences*. 2019; doi: 10.1111/1556-4029.14009
21. Burcham ZM, Cowick CA, Baugher CN, Pechal JL, Schmidt CJ, Rosch JW, Benbow E, Jordan HR. Total RNA analysis of bacterial community structural and functional shifts throughout vertebrate decomposition. *Journal of Forensic Sciences*. 2019; doi: 10.1111/1556-4029.14083
22. Myburgh J, L'Abbe EN, Steyn M, Becker PJ. Estimating the postmortem interval (PMI) and using accumulated degree-days (ADD) in a temperate region of South Africa. *Forensic Science International*. 2013;229(1-3):165.el-165.e6. <https://doi.org/10.1016/j.forsciint.2013.03.037>
23. Megyesi MS, Nawrocki SP, Haskell NH. Using accumulated degree-days to estimate the postmortem interval from decomposed human remains. *Journal of Forensic Sciences*. 2005;50(3):618-626.

24. Dabbs GR. How should forensic anthropologists correct National Weather Service temperature data for use in estimating the postmortem interval? *Journal of Forensic Sciences*. 2015;60(3):581-587.
25. Knights D. Microbiome discovery 3: 16S variable regions. 2016: Accessed on May 21, 2020 from https://www.youtube.com/watch?v=8Aa_mnyXm70
26. Anahtar MN, Bowman BA, Kwon DS. Efficient nucleic acid extraction and 16S rRNA gene sequencing for bacterial community characterization. *Journal of Visualized Experiments* 2016: e53939.
27. Finley SJ, Benbow EM, Javan GT. Microbial communities associated with human decomposition and their potential use as postmortem clocks. *International Journal of Legal Medicine*. 2015;129:623-632 DOI 10.1007/s00414-014-1059-0
28. Metcalf JL, Parfrey LW, Gonzalez A, Lauber CL, Knights D, Ackermann G, Humphrey GC, Gebert MJ, Treuren WV, Berg-Lyons D, Keepers K, Guo Y, Bullard J, Fierer N, Carter DO, Knights R. A microbial clock provides an accurate estimate of the postmortem interval in a mouse model system. *ELife*. 2013: e01104. doi:<https://doi.org/10.7554/elife.01104>
29. Michigan Public Health Code (excerpt) act 368 of 1997, part 1: Revised Uniform Anatomical Gift Law. [Online reference] accessed March 21, 2021. <http://legislature.mi.gov/doc.aspx?mcl-368-1978-10-101>
30. R Core Team. R: A language and environment for statistical computing. R Foundation for Statistical Computing, Vienna, Austria. (2020) URL <https://www.R-project.org/>.
31. Iglewski BH. *Pseudomonas*. Medical Microbiology. 4th edition. Galveston (TX): University of Texas Medical Branch at Galveston; 1996. Chapter 27.
32. Boguszewska K, Szewczuk M, Kazmierczak-Baranska J, Karwowski BT. The similarities between human mitochondria and bacteria in the context of structure, genome, and base excision repair system. 2020;25(2857)1-30. <https://doi.org/10.3390/molecules25122857>
33. The Editors of Encyclopaedia, Britannica. *Clostridium*. Encyclopedia Britannica, 3 Nov. 2017, <https://www.britannica.com/science/Clostridium>. Accessed 5 April 2021.
34. Hofstad T, Olsen I, Eribe ER, Falsen E, Collins MD, Lawson PA. *Dysgonomonas* gen. nov. to accommodate *Dysgonomonas* gadei sp. nov., an organism isolated from a human gallbladder, and *Dysgonomonas* capnocytophagooides (formerly CDC group DF-3). *International Journal of Systematic and Evolutionary Microbiology*. 2000;50(6):2189-2195. <https://doi.org/10.1099/00207713-50-6-2189>
35. Kim JY, Kim YB, Song HS, Chung WH, Lee C, Ahn SW, Lee SH, Jung MY, Kim TW, Nam YD, Roth SW. Genomic analysis of a pathogenic bacterium, *Paeniclostridium sordellii* CBA7122 containing the highest number of rRNA operons, isolated from a

human stool sample. *Frontiers in Pharmacology*. 2017;8(840)1-5.
<https://doi.org/10.3389/fphar.2017.00840>

36. Leisner JJ, Laursen BG, Prevost H, Drider D, Dalgaard P. *Carnobacterium*: positive and negative effects in the environment and in foods. *FEMS Microbial Review*. 2007;Sep;31(5):592-613. doi: 10.1111/j.1574-6976.2007.00080.x
37. Oxford Languages. “Sensu stricto” Oxford University Press 2021; accessed April 6th from:
https://www.google.com/search?q=what+does+sensu+stricto+mean&rlz=1C9BKJA_enUS938US938&oq=what+does+sensu+stricto+mean&aqs=chrome..69i57j0i22i30j0i10i22i30j0i22i30.6069j0j7&hl=en-US&sourceid=chrome-mobile&ie=UTF-8
38. Wiegel J, Tanner R, Rainey FA. An introduction to the family Clostridiaceae. *The Prokaryotes*. 2006; Springer, New York, NY. https://doi.org/10.1007/0-387-30744-3_20